Naval Command,
Control and Ocean
Surveillance Center RDT&E Division San Diego, CA
92152-5001

Technical Report 1624
September 1993

HF Sky-Wave Field Strength Predictions

D. B. Sailors
R. B. Rose

Technical Report 1624
September 1993

HF Sky-Wave Field Strength Predictions

D. B. Sailors
R. B. Rose

NAVAL COMMAND, CONTROL AND OCEAN SURVEILLANCE CENTER
RDT&E DIVISION
San Diego, California 92152–5001

K. E. EVANS, CAPT, USN
Commanding Officer

R. T. SHEARER
Executive Director

ADMINISTRATIVE INFORMATION

Work for this report was performed by members of the Ionospheric Branch, Code 542, in the Ocean and Atmospheric Sciences Division of NCCOSC, RDT&E Division, San Diego, California, during the period of March through June 1993. The work was funded by Naval Security Group Command, Washington, DC, under Program Element 0603013N.

Released by
J. A. Ferguson, Head
Ionospheric Branch

Under authority of
J. H. Richter, Head
Ocean and Atmospheric
Sciences Division

ACKNOWLEDGMENTS

The technical report was compiled through the contribution of J. Camuna of the Australian Ionospheric Prediction Service (IPS) who provided documentation for the Advanced Stand-Alone Prediction System (ASAPS) and T. Damboldt of the Forschungsinstitut der Deutschen Bundespost who provided the FTZ4 model.

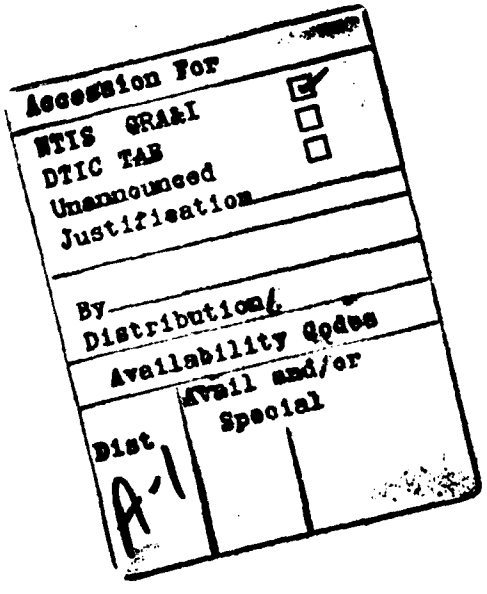

RV

EXECUTIVE SUMMARY

OBJECTIVES

Describe how the field strength of an HF signal, expressed in decibels (dB) above or below 1 microvolt per meter reference, is calculated in different HF propagation prediction programs and how the accuracy of the predicted field strength values from these programs can be determined and presented.

RESULTS

All of these prediction programs produce median predictions of the rms field strength. Seven HF propagation prediction programs have been reviewed for the Polar, Equatorial, Near vertical incidence Experiment (PENEX) project. These include three empirical based programs (Medusa PROPHET, FTZ, and FTZ4), and four analytical programs (HFTDA, IONCAP, ASAPS, and AMBCOM). AMBCOM is the only ray tracing program included.

The implementation of a data screening program DASCR3 allows the development and generation of a powerful statistical description of the characteristics of the measured field strength and of how well the seven candidate programs predict observations. It offers all the statistical requirements suggested by the Comité Consultatif International des Radiocommunications (CCIR) for the determination of the accuracy of a field strength prediction program. (The CCIR is the International Radio Consultation Committee in English.) Useful statistical parameters produced by DASCR3 that can describe the accuracy of a predicted field strength value include the following: average residual (bias), root-mean-square residual (or standard deviation), average relative residual (relative bias), root-mean-square relative residual, average absolute relative residual (magnitude of the error in the model), correlation coefficient between observed and predicted values, standard error of the estimate of linear regression, and the constants necessary to represent the residual distribution by a Johnson distribution and its corresponding test of fit information. DASCR3's ability to allow and store up to 40 different auxiliary variables allows the comparison to be subdivided into many subcategories. DASCR3 usage also allows the determination of possible improvements that might be made to these field strength prediction programs.

RECOMMENDATIONS

1. The accuracy of the field strength predictions from the seven HF predictions described herein be determined using PENEX data.

2. For comparison to other accuracy determinations, these same seven programs be compared to CCIR Data Base D.1 using DASCR3.

3. The accuracy of these programs be determined as a function of the following auxiliary variables: the month; year; sunspot number; circuit identifier (name and path transmitter and receiver coordinates); frequency; great-circle distance; 24 predicted hourly values (always monthly median values) of sky-wave field strength in dB relative to 1 μV/m, of path basic MUF, of the percentage of the days per month when the frequency is below the path basic MUF, of solar zenith angle and cosine of the solar zenith angle at path midpoint, of E-layer MUF; 24 predicted hourly values at each reflection point (control point) of E-layer critical frequency, secant of the angle of incidence on the D-layer, critical frequency of the sporadic-E layer f_oEs, and the sporadic-E layer blanketing frequency f_bEs; and the eight 3-hour magnetic index K_p values.

4. The Johnson distribution parameters be determined for each value of auxiliary variable used to determine the accuracy of each program.

5. The results of the accuracy studies of these programs be used to make recommendations on how each program might be improved.

CONTENTS

FIGURES

TABLES

INTRODUCTION

This report describes how the field strength of an HF signal, expressed in dB above or below a 1 microvolt per meter reference, is derived in different HF prediction programs, particularly the ones that will be evaluated in Project PENEX. HF sky-wave field strength is a measure of the signal intensity as it appears at the receiver antenna. Field strength is one of the least understood parameters characterizing HF signals and is one of the most difficult parameters to measure by calibration techniques. The report will present a general discussion of HF prediction programs and their differences; it will also provide a detailed discussion of how each program develops their field strength numbers. A substantial amount of text is devoted to the development of the basic transmission loss equations used in each program to show the difference between the models.

The final section will present how the observed and predicted data will be compared in the analytical studies and will describe a special data screening program used for that purpose at the Naval Command, Control and Ocean Surveillance Center, Research, Development, Test and Evaluation Division (NRaD).

HF PREDICTION TECHNIQUES

The following section is taken from AGARDograph No. 326 (pp. 69–72, 1990). To determine the performance of an ionospheric-dependent radio system, more than just an ionospheric model is needed. The ionospheric model must be tied to a set of equations or a formulation that enables the simulation of the propagation of radio waves through the ionospheric model. The set of equations, or the formulation chosen, together with the ionospheric model, are often termed an *ionospheric propagation model.* When the ionospheric model that is contained in the propagation model can be used for making predictions of the ionospheric structure, the propagation model is termed an *ionospheric propagation prediction model.* The propagation model must provide the method for calculating the geometry pertinent to the radio system, as well as methods for handling information about required performance levels: transmitter power, signal level and modulation, antenna characteristics, receiver location, and noise environment. The degree that each of these is incorporated into the propagation model often determines the complexity of the model.

Most of the HF propagation models available assume that signals are reflected from the ionospheric E- and F-regions according to strict geometrical considerations. The ionospheric parameters at the reflection points are estimated from the ionospheric model and are used as input to the formulation relating to the reflection process. The details of the method used to evaluate the reflection of HF signals from the ionospheric regions (i.e., the evaluation of modes) vary with different propagation models.

Performance predictions are made for many purposes, such as system design, frequency management, and operational improvements. Most of the propagation methods were originally intended to provide information of a long-term predictive nature by using monthly median predictions of ionospheric structure; however, a trend has emerged in recent years to utilize propagation predictions on much shorter time scales. The complexity of the long-term and short-term propagation prediction methods is generally as different as the approaches used.

The best known long-term performance prediction methods involve the used of large-scale computer programs. The work of Lucas and Haydon (1966) was the first long-term,

computer-based program of its sort. The concepts of service probability and reliability were introduced in this program, HFMUFS, and was subsequently replaced by that of Barghausen et al. (1969). There were four distinct versions of these programs, dubbed ITS78. Each was given a slightly different name and was color coded (Red Deck, Blue Deck, Yellow Deck, Buff Deck) according to the color of the cards on which it was sent out.

The final version, HFMUFES4, (Haydon et al., 1976) gained international usage. Since its introduction, the IONCAP program (Teters et al., 1983) has also become widely used. These programs provide the means to calculate HF propagation parameters at any location on the earth. Field strength, mode reliability, and Maximum Usable Frequency (MUF) are but a few of the parameters that are obtained from these programs. They enable the program user to specify antenna gains as a function of take-off angle and to specify required systems performance, in terms of the signal-to-noise ratio evaluated at the receiving point of the circuit. Both programs have common features, such as use of the same sets of numerical coefficients to represent the morphological behavior of the ionospheric structure and the atmospheric noise expected at the reception point. There are, however, significant differences among HFMUFS, HFMUFES4, and IONCAP. The major changes from HFMUFS in HFMUFES4 are as follows:

1. All numerical coefficients representing the ionospheric characteristics were calculated as functions of universal time.
2. E-layer propagation characteristics were calculated from numerical coefficients representing E-layer critical frequencies (Leftin, 1976).
3. Numerical coefficients, representing the minimum virtual height of the F-region, were included for calculating the semi-thickness of the F-layer (Leftin, Ostrow & Preston, 1967).
4. Revised values of manmade noise and its frequency dependence were included.
5. A method for combining two, or more, noise sources of nearly equal amplitudes was added.
6. A new formula for estimating absorption, including a winter anomaly effect, was derived (Schultz & Gallet, 1970).
7. The chi-square distribution was used to evaluate all distributions (Zacharisen & Crow, 1970).
8. Revised excess system losses were included.
9. System performance predictions could be made for sporadic E-propagation.
10. The numerical maps of f_oF2 were continuous in month and sunspot number.
11. Numerical coefficients representing atmospheric noise, as a function of universal time, were included (Zacharisen & Jones, 1970).
12. Numerical maps of the continents, for use in ground loss calculations, were added (Zacharisen, 1972).
13. Provision was made to use up to three different transmitting and receiving antennas over the HF band.
14. Modifications were made to allow antenna patterns to be read into the program.

The ionospheric loss term in IONCAP differs significantly from that used in either HFMUFS or HFMUFES4. The IONCAP uses the same set of f_oF2 coefficients as does the HFMUFS.

The original version of IONCAP used the same 1-MHz representation of atmospheric noise. The current IONCAP uses a 1-MHz representation of atmospheric noise due to Spaulding and Washburn (1985). The various modes in these three programs are computed in different manners; consequently, the signal-to-noise ratio that is calculated by each of the programs for the circuit conditions is different. The IONCAP program has a distinct advantage of the Barghausen et al. (1969) program by enabling the user to incorporate into the calculation specific knowledge about the ionosphere, such as, an electron density profile obtained from independent information.

In utilizing a propagation prediction method, the user must specify the particulars of the circuit, such as the transmitter and receiver location, transmitter power, transmitter and receiver antenna, and the quality of service required. In addition, the universal time, month, and sunspot number that are appropriate for the period for which calculations are to be performed must be specified. There are numerous output options that are available, including Maximum Usable Frequency (MUF) for the circuit, the Lowest Useful Frequency (LUF), and the field strength for any frequency that has been indicated by the user. The mode, signal-to-noise ratio, predicted signal reliability, and take-off angle for each mode are likewise available.

The three prediction programs discussed above are complete HF propagation performance prediction programs. There is an existing class of programs that can be considered a subset of these. These programs are concerned primarily with evaluating the field strength of an ionospheric-dependent radio system. Models of this type are given in CCIR report 252-2 (CCIR, 1970a), the supplement to CCIR Report 252-2 (CCIR, 1980) and CCIR Report 894 (CCIR, 1982); CCIR Report 894-2 (CCIR, 1990a). The field strength calculations given in Report 252-2 (CCIR, 1970a) are consistent with the method used in HFMUFS. On the other hand, the field strength calculations that are given in the Supplement to Report 252-2 (CCIR, 1980) are more complex than the method of calculation of field strength used in ITS78 or HFMUFES4. The complexity is due to a significant difference in the manner in which the ionospheric modes are evaluated. In the CCIR Report 252-2 approach to ionospheric reflection estimations and mode evaluation, the pertinent calculations are performed at specific points, called control points, along the propagation path determined by the path length. No account is taken of the change, or gradient, in electron density along, or transverse to, the propagation path. These gradients are accounted for in the Supplement to Report 252-2. It thus provides a more physically appealing calculation at an increase in computational time by a factor of 10 to 30.

The field strength prediction method given in CCIR Report 894 had as its roots: work performed by CCIR Interim Working Party 6/12 to develop a sky-wave propagation prediction program for use in planning the HF broadcasting service (ITU, 1984). This field strength model is actually a combination of two field strength programs: a simplified version of CCIR Report 252-2 is used for path lengths of less that 7000 km, and the field strength model developed by Deutsche Bundespost (FTZ) (Damboldt, 1976) is used for distances of greater than 9000 km. A linear interpolation scheme is employed for distances between 7000 and 9000 km. More recent revisions to this method are described in CCIR Reports 894-1 (CCIR, 1986) and 894-2 (CCIR, 1990).

For the propagation models given above, the field strength is evaluated for each mode that is determined according to the geometry incorporated into the program. The selection of the modes that are chosen to determine the overall field strength for a given frequency is not the same for each of the programs. Generally, however, three or four of the modes that are associated with the

least amount of loss are chosen; then, the antenna gain is incorporated into the field strength calculation for each mode.

The FTZ propagation program (Damboldt, 1976; Damboldt & Suessmann, 1989) employs an empirical field strength calculation that is based upon observations collected over a number of HF circuits, most of which terminate in Germany. The data that have been gathered for more than 10 years for certain circuits are related to predicted ionospheric critical frequencies to obtain an empirical method for determining field strength. In particular, the field strength recordings revealed a steady increase in signal strength from the LUF to a maximum value, following approximately an inverse frequency dependence. This frequency is called the *LUF* in this method; a formula for its calculation is provided. It is different than the classical LUF calculation. After the maximum value is reached, the field strength decreases until it reaches the operational *MUF*, which is higher than the classical MUF. This is the consequence of several mechanisms that are not taken into account by the other prediction techniques. Because of its simplicity, the FTZ method was adopted in the mid-1970s for propagation prediction programs designed for computers with limited memory in the early desktop models, such as PROPHET and early versions of Medusa. The weakness in FTZ models is that the peak of the field is dependent on how the operational *MUF* and *LUF* are used to determine the field strength. If these frequencies are well chosen, then the field strength is for the minimum hop mode, and the antenna gain can be determined for it. Otherwise, the field strength prediction will be inaccurate at any given frequency, and the mode, for which the field strength is represented, will be unknown. How the MUF and LUF are chosen for the FTZ model will be discussed in some detail later.

Report 894 (CCIR, 1982) provides the basis of yet another propagation model that was developed at the First Session of the HF Broadcasting Conference (ITU, 1984). This model, referred to as the HFBC84, was developed specifically for planning the use of the HF spectrum for broadcasting proposes. The primary difference between HFBC84 and the Report 894 model is in the manner that the antenna gain is taken into account in the computation of field strength. Before the selection of the modes, which are to be combined to determine field strength of a given frequency on paths of less than 7000 km, the antenna gain at the appropriate take-off angle for each mode is added to the field strength. The resultant field strength is determined by using the strongest E-mode and the two strongest F-modes for paths up to 4000 km. Between 4000 and 7000 km, only the two strongest F-modes are considered. For paths greater than 9000 km, the maximum antenna gain that occurs between 0- and 8-degrees elevation angle is used in the field strength computation. The inclusion of the antenna gain in the field strength calculation, prior to the selection of the modes that are combined to form the resultant field strength, leads to a much improved field strength prediction. The HFBC84 program provides an efficient means to determine the area serviced by the HF broadcast transmitter and to assess the likely interference.

Yet another prediction program was produced by the International Working Part (IWP) 6/1 of the CCIR in response to Recommendation No. 514 (HFBC-87), which invites the CCIR to "...undertake studies of the propagation prediction method adopted by the Conference and to recommend both improvements in the method and later, if necessary, an improved method to be used in the future." An interim report was produced by the CCIR as Report 894-2 (CCIR, 1990). In 1991, a final report (CCIR, 1991) presented eight elements of the HFBC-87 propagation method for which improvements were recommended.

There is a class of prediction programs that differs considerably from those discussed in previous paragraphs. These programs are concerned primarily with tracing the signal rays

through the ionosphere. The one program of this type to be considered in the PENEX evaluations is called Ambient Ionospheric Communication Predictions at HF Program AMBCOM (Hatfield, 1980; Hatfield et al., 1987; Smith & Hatfield, 1987). AMBCOM was born out of work done by Stanford Research Institute in the 1960s to develop computer codes, called NUCOM Codes, that would simulate ionospheric changes after above ground nuclear explosions.

In AMBCOM, the ionosphere is modeled in three parabolic layers. Ionospheric tilts and initial frequency gradients are taken into account by specifying the parabolic parameters at as many as 41 points along the path. These parameters were initially derived from the Institute for Telecommunications Sciences coefficients used in HFMUFES. Then they were modified to incorporate a high-latitude ionospheric model (Elkins & Rush, 1973a and 1973b; Vondrak et al., 1978), an auroral absorption model (Vondrak et al., 1978), and a sporadic-E model (Phillips, 1963; Sinno, Kam, & Kirukawa, 1976; Kolawole, 1978). If desired, actual measurements may be used in place of parameters. The propagation analysis consists of a rapid, semi-analytic, two-dimensional, ray tracing routine based on the Kift-Fooks method (Westover & Roben, 1963). Both topside and bottomside reflections from the normal ionospheric layers are allowed. AMBCOM computes propagation losses with a homing feature for evaluation of specific point-to-point communication circuits, along with binary error rates and signal-to-noise ratio.

EMPIRICAL HF FIELD STRENGTH MODELING—1976 TO PRESENT

INTRODUCTION

In 1976, the original development of the MINIMUF model (Levine, 1976) provided simple formulation to calculate the HF MUF using minicomputer and emerging microcomputer technology. Empirical HF oblique sounder data provided the basis of the MINIMUF and QLOF, a simple LUF model. At the same time, work in Germany by Deutsche Bundespost produced a simplified empirical field strength (Damboldt, 1976). This model, called Nachrichtentechische Zeitschrift (FTZ), used data that, for the most part, had been collected over long paths (i.e., greater than 7000 km). Because the model was simple and easy to use, this last fact was just ignored. Given that the LUF and MUF boundaries could be estimated, it was generally felt that FTZ gave a reasonable estimate of predicted field strength. The field strength model, coupled with a noise model that was developed later, led to predictions of signal-to-noise. In 1976, the first PROPHET system was developed on an AN/UYK-3 militarized minicomputer that had 32-Kbytes (KB) of RAM. Over the years, literally dozens of versions of PROPHET were developed by using the MINIMUF, QLOF and FTZ models as the heart of the predictions. Traditional methods to calculate these parameters were just too cumbersome; however, computer technology over the last several years has made that a moot point. The question of how good these predictions were has lingered throughout this period, and the issue has largely remained unresolved.

It should be remembered that in 1976, MINIMUF, the genesis of these simple models, was developed, such that MUF calculations could be done in less that 32 KB of RAM. The original MINIMUF was 80 Basic statements in length. The approach is untraditional because MINIMUF is an emulation on how the MUF boundary fluctuates as a function of time of day, season, and sunspot cycle. Simply put, it is an empirically calibrated, dual RC lag circuit. Its developers were engineers. As a result of scientists in the HF propagation field taking every opportunity to discredit MINIMUF, the accuracy of MINIMUF itself has been well documented by its

developing organization (Sailors, Moision, & Brown, 1981; Sailors, Sprague & Rix, 1986; Roy & Sailors, 1987). The same reaction was not true for QLOF because the LUF boundary is a fuzzy, vague function that is signal-to-noise dependent. No one could come up with a better idea. Last, FTZ was developed to support the long range shortwave broadcasting service of Deutsche Bundespost. The data that it used in its empirical development all had one common feature: one end point was in Germany. This immediately opens the question as to its global applicability. Even with its detractors, PROPHET continues to be one of the favored tools by certain military users, some commercial broadcasters, and the amateur shortwave radio community.

Subsequent sections will discuss the evolution of FTZ; its use in PROPHET,which will be referred to as FS; the expansion to HFTDA as a successor model in PROPHET and Medusa; and the new improved FTZ4 field strength models. In addition, the more traditional programs, IONCAP, ASAPS, and the raytrace program AMBCOM will be discussed.

THE FTZ MODEL

The basic field strength calculation developed in the original version of FTZ in 1976 remains the same today. It was first derived by Beckmann in 1965 (Beckmann, 1965, 1967) and described the variation in field strength within a transmission range as

$$E = E_o\left[1 - \frac{f_m^2}{f_m^2 + f_1^2}\left(\frac{f_1^2}{f^2} + \frac{f^2}{f_m^2}\right)\right] - 30 + G_t + 10 \log p \qquad (1)$$

where

E	=	Sky-wave rms field strength in dB above 1 μV/m
E_o	=	free space field strength
G_t	=	Gain of the transmitting antenna
p	=	Effective radiated power (erp)
f_m	=	Operational MUF, or the upper frequency limit for a transmitter power of 1 Mw erp, and a receiving field strength of 1 μV/m (or 1 Kw erp and 30 dB below 1 μV/m)
f_1	=	frequency where the field strength of a 1-Mw transmitter is 1 μV/m.

FTZ's approach to field strength calculation is a traditional approach by using CCIR formulation with some "tweaking" in the f_1 and f_m calculations by using locally acquired empirical data. The mistake most people make by using FTZ and FTZ4 is to assume that f_1 is the classical LUF, and that f_m is the classical MUF. In fact, they are not and are quite different.

Damboldt (1976) stressed that the Beckmann formula empirically comprises all different factors influencing propagation. It yields only an estimated field strength. The modes, solar zenith angle, angle of incidence, blanketing and other phenomena, are not dealt with separately, as is the case in the more analytical field-strength prediction methods. These phenomena are contained partly in the characterization of the circuit frequency boundaries with f_1 and f_g, the classical MUF used in the determination of f_m . The empirically determined K-factor of the MUF computation implicitly comprises all other influences on the field-strength calculation.

One of the major strengths of empirically derived models is that the data, used for the modeling, inherently contain the subtle variations that are so difficult to model explicitly. In many cases, empirical models will out-perform a model that uses more traditional analytical approaches.

Damboldt (1976) observed that as the operating frequency increased away from the frequency where the signal is no longer useful, the field strength increased to a point under the MUF, and then started decreasing past the classical MUF to a frequency called the operational MUF (OMUF). The causes of this controversial higher boundary included scatter, transequatorial propagation, field-aligned irregularities, sporadic-E, off-great-circle propagation, and ducting; all phenomena that are not easily modeled, but known to exist. The OMUF is derived by

$$f_m = K * f_g \tag{2}$$

with

$$K = 1 + W\frac{f_g}{f_{g,noon}} + X\left(\sqrt[3]{\frac{f_{g,noon}}{f_g}} - 1\right) + Y\left(\frac{f_{g,min}}{f_{g,noon}}\right)^2 \tag{3}$$

where

f_g = Classical MUF
f_H = gyrofrequency
$f_{g,noon}$ = f_g for local noon of the respective control point.
$f_{g,min}$ = minimum hourly value of the classical MUF.

The constants W,X,Y are chosen empirically; they are dependent on the geographical position of the HF path. To a certain degree, they take into account propagation through the auroral zones and the geomagnetic equator. Values are shown in table I in the original Damboldt paper (Damboldt, 1976) and are given here in table 1.

Table 1. Empirical values of W, X, and Y constants used for the determination of the correction factor K.

Orientation	Constants		
	W	X	Y
East-West	0.1	1.2	0.6
North-South	0.2	0.2	0.4

The theory behind by using the K-factor is briefly presented. The dynamics of the ionosphere are characterized by diurnal and seasonal variations of the classical MUF. On the other hand, ionospheric irregularities become more apparent as the F-layer height increases and its critical frequency decreases; consequently, the highest value for K is obtained in winter nights when the classical MUF values are at their lowest.

The variability of the first two terms in the formula of the *K*-factor is due to the ratio of the hourly values of the standard MUF to the noon value of MUF and its reciprocal value, respectively. The term with the coefficient *X* describes the increase of the *K*-factor from day to night; however, since during the day, the *K*-factor has to reach a certain value, the term with the coefficient *W* is added, counteracting the term described first. That last term, with the coefficient *Y*, varies with the ratio of the minimum standard MUF $f_g, \min$ to the noon value f_g, noon, and it expresses the increase of the *K*-factor from winter to summer.

The classical MUF is based on the CCIR atlas of ionospheric characteristics (CCIR, 1970b). The *Control Point Method* is applied. In the case of the E- and F-layers, the two control points are respectively 1000- and 2000-km away from the terminals. After the great-circle path and the great-circle distances to the control points have been determined, the 24-hourly values of f_g are calculated according to the CCIR atlas.

The calculation of f_1 is derived from the formula for non-deviative absorption, which is the basis of the CCIR LUF calculation. The parameter f_1 is found by setting the free-space field strength for 1000 kW erp, normalized to 1 kW, minus the non-deviative absorption for the minimum hop mode loss equal to 30 dB below 1 μV/m and is given by

$$f_1 = 5.3\ I \left[\frac{\sum_{2N} \sqrt{\cos \chi}\,(1 + 0.009 * R_{12})}{\cos \phi_D \ln \frac{9.5 \times 10^6}{D_P}} \right]^{1/2} - f_H \qquad (4)$$

where

I = a seasonal factor that is also dependent on the geographical positions of both terminals and can be determined from $I = \sqrt{J}$ (National Bureau of Standards, 1948)
χ = solar zenith angle
R_{12} = the 12-month running mean of sunspot number
ϕ_D = the angle of incidence at the D-layer
D_P = the oblique path length
N = the number of penetration points
f_H = the gyrofrequency.

With the above formula for f_1, the LUF is determined for the daylight hours. During the night, the LUF is assumed to be dependent only on the distance between transmitter and receiver so that

$$f_{1n} = \sqrt{\frac{D}{3000}} \qquad (5)$$

In addition, as there is a certain lag between the time of sunset and the decrease of D-region ionization, the decay from day-LUF to night-LUF is accounted for the three hours after sunset by

$$f_1 = 2 f_{1n}\, e^{-0.795\, t} \qquad (6)$$

With the determination of f_m and f_1, the field strength can be calculated by calculating the free-space field strength using

$$E_o = 20 \log \frac{3x10^5\sqrt{P}}{D} \tag{7}$$

where P is the erp, and D is the distance between transmitter and receiver. This is the field strength produced by 1-kW input to a short dipole over perfect ground. The gain of the transmit antenna is 4.8 dB, relative to an isotropic. To determine the field strength relative to an isotropic, it is necessary to subtract 4.8 dB from the field strength given by equation (1).

THE FTZ4 MODEL

In 1989, a revision to FTZ, called FTZ4 (Damboldt & Suessmann, 1989) was introduced. It follows the same approach as FTZ, in that it uses the formula in equation (1), requiring the definition of f_1 and f_m. There were some modifications in how these functions were derived. The parameter K in equation (3) now has a lead constant of 1.2 instead of 1. The value of f_1 for the three hours after sunset is now given by

$$f_1 = 2 f_{1n} e^{-0.23t} \tag{8}$$

The major changes in FTZ4 include an improved MUF derivation model, consideration of E-Region intervention, and some correction factors to consider different ranges.

FTZ4 introduces the FTZMUF2 MUF prediction model. It derives $f_oF2, M(3000)$, for a given location from updated CCIR data bases, and calculates a MUF(4000), as a function of time, by the expression

$$MUF = 1.1 * f_oF2 * M(3000) \tag{9}$$

The f_oF2 and $M(3000)$ values are interpolated as a function of season, local-time, geomagnetic latitude for f_oF2, and geographic latitude for $M(3000)$ from tables developed from CCIR Report 430-4 *Atlas of Ionospheric Characteristics* (CCIR, 1983). The accuracy of this approach is a direct function on the size and accuracy of the tables of coefficients. As is the case in the presentation of any of these mini-HF prediction programs, there is the comparison to MINIMUF to demonstrate its superiority—and this paper is no exception. It is not clear whether or not they used the MINIMUF or MINIMUF 3.5 for the comparison; however, they claim an improvement by reducing the standard deviation in FTZMUF2 by a factor of two. It is a moot point, as MINIMUF 3.5 has been replaced by MUF85, which has demonstrated an even larger improvement.

A second improvement in FTZ4 is the introduction of the E-Region MUF. By using a function determined by Rawer (1952, 1956), the E(D)MUF is calculated. The critical frequencies f_c (E) for the E-layer (in MHz) are determined as follows:

$$\begin{aligned} f_c &= K_E * \cos^n \chi \\ K_E &= 2.25 + 1.5\cos\phi + (0.01 - 0.007\cos\phi)\, R_{12} \\ n &= 0.21 + 0.12\cos\phi + 0.0002 R_{12} \end{aligned} \tag{10}$$

where

R_{12} = 12-month running mean of the sunspot number
χ = sun's zenith angle
ϕ = geographical latitude.

The 24-hourly values of the E-layer E(D)MUF are determined from

$$E(D)MUF = 5 * f_c * E_D \tag{11}$$

with the distance factor

$$\begin{aligned} E_D = & (((((((-4.368*10^{-9}*Earc+1.335*10^{-7})*Earc-5.977*10^{-6}) \\ & *Earc+0.0002625)*Earc-0.005039)*Earc+0.03761) \\ & *Earc-0.01332)*Earc+0.2085 \end{aligned} \tag{12}$$

where Earc = E-layer hop length in radians.

The basic MUF for the whole circuit is chosen by taking the higher value of the E- or F2-MUF for each control point, and then taking the lowest value of all three control points.

The last change in FTZ4 is the addition of a correction factor to the operational MUF (f_m) that is dependent on path length. It has been known for a long time that the Damboldt database is predominantly long paths. In the new model:

$$f_m = K * f_g * C_r \tag{13}$$

where C_r equals 2-(D/4000)^2, for circuits <4000 km, or 1, for circuits >4000 km. This has the effect of reducing the operational MUF for short paths.

A careful check of all the other constants used throughout the FTZ4 indicated that it uses the same constants as were used in the original FTZ, except that the lead constant in equation (3) is now 1.2 instead of 1.0.

FTZ4 comes on a stand-alone 3.5-inch floppy and is suitable for use on a standard desktop mini-computer. In the program comparisons for Project PENEX, the FTZ4 model will be used.

THE MEDUSA PROPHET HF FIELD STRENGTH PREDICTION MODELS

The calculation of field strength in the PROPHET HF Signal Assessment Systems has been under continual change since 1976 as new and improved approaches were developed.

The original PROPHET system was developed to operate in a computer system that contained a very limited amount of memory, either 32 KB or 64 KB of RAM; therefore, when FTZ first appeared, the differential between the classical MUF and the operation MUF was viewed with some skepticism. The first versions of PROPHET took a simple approach, they used the MUF calculated with MINIMUF as the f_m and the LUF value calculated by the original QLOF model as f_l. Over time, it was learned that when compared with small amounts of field strength data, the peak in the calculated FS was occurring too low in the usable bandwidth and the adoption of an operational was necessary.

A simplified method of estimating the operational MUF was implemented (Sailors, 1990). It was assumed that the MUF value, at a given time, season, geographic position, and sunspot number, is a statistical parameter and has a Gaussian distribution. Given this assumption, the operational MUF in PROPHET was determined by the product of the MUF and the 99.1 percentile value of the MUF distribution as expressed by

$$f_m = 1.85 * HPF * MUF \tag{14}$$

where HPF is the 90th-percentile value factor for an assumed Gaussian MUF distribution (Barghausen et al., 1969). The reason that this equation was used, instead of the approach used in FTZ, is that the K-factor was based mainly on data measured on paths terminating at one site (Germany), and might contain aspects specific to that site. Table 2 lists the HPF (F_0) and the FOT (F_1) as a function of time of day.

As revised versions of MINIMUF were introduced, they were adopted into the PROPHET FS calculation. Between 1976 and the present, the models used were MINIMUF, MINIMUF-3.5 and MUF85 (Sailors et al., 1986), the latter being the model presently in the Medusa project PROPHET. MUF85 represented a significant improvement over MINIMUF-3.5, especially at high latitudes (Sailors et al., 1986).

The value of the LUF, f_l, was derived from the empirical QLOF series of models (Sailors & Moision, 1987), the latest of these being QLOF 2.0, which is used in Medusa PROPHET. Except for these revisions, the basic equation (1), as shown in the FTZ discussion, is the equation that is presently being used in Medusa PROPHET. For frequencies above the MUF, the field strength is reduced by a loss of 12 dB per MHz until a maximum increase in loss of 60 dB is obtained.

HFTDA—A HYBRID APPROACH TO FIELD STRENGTH PREDICTION

The empirical approaches of the 1970s and the mid-1980s were driven by the need for simplicity to accommodate limited computer memory. Since 1987, desktop computers have become faster and have more memory, so the original requirement for simplicity has been overcome by events. A new approach was adopted at the Naval Command, Control and Ocean Surveillance Center (NCCOSC), Research, Development and Test Division (NRaD), formerly

Table 2. Factors for calculating FOT and HPF from the MUF and the local time.

Winter (N. Hemisphere (Nov., Dec., Jan., Feb.) / S. Hemisphere (May, June, July, Aug.))

GEO. LAT.	Low (0-30) Sunspot Number												Medium (30-100) Sunspot Number												High (>100) Sunspot Number												GEO. LAT.
	22-02		02-06		06-10		10-14		14-18		18-22		22-02		02-06		06-10		10-14		14-18		18-22		22-02		02-06		06-10		10-14		14-18		18-22		
	F_M	F_L	F_M	F_L	F_M	F_L	F_M	F_L	F_M	F_L	F_M	F_L	F_M	F_L	F_M	F_L	F_M	F_L	F_M	F_L	F_M	F_L	F_M	F_L	F_M	F_L	F_M	F_L	F_M	F_L	F_M	F_L	F_M	F_L	F_M	F_L	
≥ 75°	1.44	.60	1.36	.65	1.43	.69	1.32	.72	1.33	.66	1.40	.67	1.45	.76	1.39	.78	1.44	.68	1.40	.67	1.33	.62	1.45	.78	1.36	.68	1.27	.78	1.41	.74	1.46	.67	1.40	.64	1.43	.73	≥ 75°
65-75°	1.37	.68	1.29	.71	1.38	.75	1.23	.76	1.24	.73	1.35	.70	1.39	.78	1.31	.81	1.37	.74	1.32	.70	1.29	.73	1.41	.73	1.31	.80	1.25	.74	1.34	.77	1.30	.72	1.30	.72	1.36	.78	65-75°
55-65°	1.30	.74	1.24	.78	1.27	.80	1.15	.80	1.17	.82	1.30	.73	1.33	.82	1.24	.83	1.25	.79	1.21	.75	1.22	.80	1.33	.76	1.26	.77	1.23	.78	1.26	.81	1.18	.80	1.21	.79	1.26	.82	55-65°
45-55°	1.25	.79	1.21	.78	1.16	.83	1.12	.85	1.18	.84	1.25	.76	1.30	.84	1.19	.82	1.14	.83	1.15	.81	1.16	.84	1.30	.78	1.19	.83	1.19	.80	1.16	.84	1.11	.87	1.09	.84	1.20	.85	45-55°
35-45°	1.23	.81	1.20	.79	1.13	.85	1.11	.87	1.11	.89	1.23	.77	1.27	.83	1.17	.81	1.12	.85	1.14	.86	1.14	.86	1.28	.79	1.15	.86	1.14	.81	1.13	.87	1.09	.90	1.09	.87	1.14	.87	35-45°
25-35°	1.20	.81	1.20	.74	1.15	.86	1.17	.82	1.15	.85	1.20	.78	1.30	.78	1.21	.76	1.16	.85	1.18	.85	1.18	.85	1.25	.78	1.22	.83	1.24	.76	1.12	.89	1.09	.90	1.11	.88	1.15	.85	25-35°
15-25°	1.24	.78	1.27	.67	1.19	.87	1.20	.75	1.24	.77	1.32	.79	1.33	.76	1.38	.71	1.17	.85	1.22	.84	1.26	.82	1.40	.76	1.32	.78	1.35	.78	1.12	.89	1.12	.90	1.14	.89	1.20	.83	15-25°
< 15°	1.27	.71	1.30	.78	1.18	.88	1.15	.86	1.14	.87	1.20	.79	1.31	.77	1.26	.69	1.14	.87	1.13	.86	1.15	.85	1.23	.78	1.18	.83	1.25	.78	1.14	.89	1.13	.90	1.15	.89	1.20	.84	< 15°

Equinox (Mar., Apr., Sept., Oct.)

GEO. LAT.	Low (0-30) Sunspot Number												Medium (30-100) Sunspot Number												High (>100) Sunspot Number												GEO. LAT.
	22-02		02-06		06-10		10-14		14-18		18-22		22-02		02-06		06-10		10-14		14-18		18-22		22-02		02-06		06-10		10-14		14-18		18-22		
	F_M	F_L	F_M	F_L	F_M	F_L	F_M	F_L	F_M	F_L	F_M	F_L	F_M	F_L	F_M	F_L	F_M	F_L	F_M	F_L	F_M	F_L	F_M	F_L	F_M	F_L	F_M	F_L	F_M	F_L	F_M	F_L	F_M	F_L	F_M	F_L	
≥ 75°	1.42	.67	1.32	.72	1.29	.74	1.26	.73	1.33	.68	1.40	.69	1.45	.64	1.31	.61	1.27	.73	1.28	.74	1.30	.74	1.47	.67	1.44	.66	1.37	.67	1.35	.75	1.40	.66	1.36	.70	1.46	.72	≥ 75°
65-75°	1.36	.70	1.28	.75	1.25	.76	1.23	.74	1.26	.82	1.40	.69	1.41	.66	1.32	.71	1.23	.77	1.26	.74	1.26	.78	1.36	.70	1.42	.67	1.31	.71	1.30	.73	1.31	.70	1.33	.70	1.39	.72	65-75°
55-65°	1.33	.73	1.31	.78	1.32	.80	1.20	.75	1.20	.81	1.31	.73	1.35	.70	1.17	.75	1.20	.80	1.23	.72	1.18	.78	1.29	.73	1.30	.69	1.25	.75	1.27	.72	1.24	.73	1.25	.71	1.30	.72	55-65°
45-55°	1.26	.75	1.19	.80	1.20	.81	1.10	.76	1.16	.81	1.26	.76	1.20	.73	1.15	.77	1.17	.81	1.21	.74	1.13	.76	1.20	.75	1.18	.73	1.20	.78	1.25	.78	1.20	.72	1.16	.74	1.17	.75	45-55°
35-45°	1.22	.77	1.20	.81	1.19	.81	1.16	.77	1.16	.80	1.25	.78	1.22	.77	1.16	.78	1.16	.82	1.18	.78	1.14	.76	1.17	.76	1.15	.78	1.16	.82	1.17	.75	1.15	.78	1.12	.80	1.14	.84	35-45°
25-35°	1.23	.78	1.24	.80	1.18	.82	1.15	.78	1.16	.81	1.28	.74	1.22	.77	1.22	.76	1.15	.82	1.17	.83	1.14	.78	1.23	.74	1.25	.81	1.18	.84	1.16	.87	1.10	.87	1.11	.87	1.15	.86	25-35°
15-25°	1.26	.77	1.23	.75	1.16	.83	1.14	.81	1.18	.83	1.23	.69	1.22	.75	1.26	.73	1.13	.84	1.15	.87	1.17	.81	1.23	.69	1.21	.80	1.23	.79	1.09	.86	1.08	.90	1.14	.90	1.23	.82	15-25°
< 15°	1.23	.76	1.40	.66	1.23	.86	1.13	.89	1.19	.86	1.26	.75	1.18	.79	1.39	.68	1.11	.86	1.13	.89	1.20	.84	1.23	.80	1.21	.86	1.23	.79	1.09	.86	1.08	.90	1.14	.90	1.23	.82	< 15°

Summer (N. Hemisphere (May, June, July, Aug.) / S. Hemisphere (Nov., Dec., Jan., Feb.))

GEO. LAT.	Low (0-30) Sunspot Number												Medium (30-100) Sunspot Number												High (>100) Sunspot Number												GEO. LAT.
	22-02		02-06		06-10		10-14		14-18		18-22		22-02		02-06		06-10		10-14		14-18		18-22		22-02		02-06		06-10		10-14		14-18		18-22		
	F_M	F_L	F_M	F_L	F_M	F_L	F_M	F_L	F_M	F_L	F_M	F_L	F_M	F_L	F_M	F_L	F_M	F_L	F_M	F_L	F_M	F_L	F_M	F_L	F_M	F_L	F_M	F_L	F_M	F_L	F_M	F_L	F_M	F_L	F_M	F_L	
≥ 75°	1.26	.68	1.24	.79	1.15	.84	1.17	.87	1.21	.85	1.32	.76	1.27	.82	1.23	.80	1.20	.82	1.18	.83	1.24	.86	1.23	.79	1.20	.73	1.27	.74	1.17	.82	1.15	.83	1.23	.75	1.24	.75	≥ 75°
65-75°	1.22	.70	1.18	.81	1.14	.83	1.15	.86	1.16	.86	1.18	.77	1.23	.83	1.19	.82	1.19	.79	1.19	.82	1.17	.82	1.19	.82	1.23	.75	1.22	.75	1.20	.77	1.18	.80	1.21	.80	1.22	.79	65-75°
55-65°	1.18	.72	1.17	.84	1.14	.83	1.13	.84	1.14	.86	1.15	.81	1.20	.83	1.16	.82	1.19	.77	1.17	.79	1.16	.82	1.17	.83	1.16	.77	1.18	.76	1.16	.74	1.21	.77	1.19	.80	1.21	.80	55-65°
45-55°	1.17	.75	1.20	.85	1.15	.82	1.16	.83	1.14	.85	1.15	.84	1.17	.81	1.19	.81	1.21	.76	1.17	.77	1.15	.81	1.16	.82	1.14	.79	1.15	.76	1.20	.73	1.22	.75	1.19	.80	1.18	.84	45-55°
35-45°	1.17	.79	1.25	.85	1.17	.80	1.27	.82	1.19	.83	1.16	.85	1.17	.78	1.22	.78	1.23	.75	1.18	.78	1.17	.78	1.19	.78	1.16	.80	1.14	.78	1.20	.75	1.17	.75	1.19	.79	1.16	.84	35-45°
25-35°	1.20	.79	1.30	.82	1.17	.78	1.20	.80	1.19	.82	1.20	.80	1.20	.77	1.30	.83	1.22	.75	1.19	.79	1.18	.77	1.18	.74	1.16	.81	1.15	.76	1.25	.82	1.20	.81	1.17	.79	1.15	.83	25-35°
15-25°	1.20	.77	1.34	.78	1.14	.77	1.24	.79	1.22	.79	1.23	.73	1.26	.77	1.38	.69	1.17	.78	1.23	.81	1.23	.78	1.28	.73	1.23	.81	1.22	.77	1.18	.85	1.15	.86	1.18	.81	1.19	.80	15-25°
< 15°	1.20	.74	1.37	.75	1.13	.88	1.30	.83	1.27	.83	1.20	.69	1.26	.79	1.44	.63	1.11	.84	1.20	.85	1.20	.81	1.22	.77	1.25	.80	1.21	.79	1.13	.86	1.17	.89	1.22	.85	1.23	.78	< 15°

the Naval Ocean Systems Center (NOSC), to develop a new field strength model to replace the versions of FTZ, which had been in use for about 15 years, for one that would more accurately characterize conditions at path lengths of less than 7000 km (Sailors, 1990; Systems Exploration, Inc., 1990). The new model, called HFTDA, reverted to more classical methods by using system loss equations to calculate the predicted path loss between transmitter and receiver. The E-layer, F-layer, and mixed mode hops are calculated. For path lengths greater than 7,000 km, the FTZ model used in PROPHET/Medusa was retained. At these longer ranges, QLOF Version 2.0 is used for obtaining f_l, and f_m is found by using MUFs produced by MINIMUF-85 in equation (14).

HFTDA contains a model relying on propagation, via the regular E-layer, as was first described in ESSA-ITSA1 (Lucas & Haydon, 1966) and the F2 layer that was developed in the semi-empirical modeling for MINIMUF-85 (Sailors et al.,1986). The program finds the lowest order mode for the E-layer, the F-layer, and a mixed E-layer and F2-layer mode. Only one E-layer hop is considered in the mixed mode. The remaining hops are via the F2-layer.

The E-layer MUF is calculated as follows: first, the ionospheric absorption index is determined at each E-layer control point from

$$I = (1 + 0.0037\,R_{12})\cos(0.881\,\chi)^{1.3} \tag{15}$$

where

R_{12} = 12-month running mean of the sunspot number
χ = sun's zenith angle - degrees.

The value of the absorption index at night has a value that is a function of solar activity (Wakai, 1971) and is given by

$$I_{min} = 0.025\,(1 + 0.031\,R_{12}) \tag{16}$$

The value of I used is the maximum of the values given by equations (15) and (16). The above value of I is related to the E(2000)MUF by;

$$E(2000)MUF = 3.41 + 38.43*I - 68.07*I^2 + 89.97*I^3 - 70.97*I^4 + 29.51*I^5 - 4.99*I^6 \quad \text{(MHz)} \tag{17}$$

The f_oE is determined from E(2000)MUF by multiplying it by the E-layer distance factor for zero distance (0.2085). The minimum of the values at the E-layer control points (f_oE_{min}) is used to determine the E-layer MUF; finally, the E-layer MUF (EMUF) is found from

$$EMUF = f_oE_{min} * \sec\phi_E \tag{18}$$

where $\sec\phi_E$ is the secant of the angle of incidence of a ray path with E-region ionization height (110 km) for E-modes.

The minimum hop predicted for the E-Layer is calculated for a peak layer height of 110 km and the path length. The radiation angle associated with this mode must have an angle greater than some predetermined minimum. If not dictated by the user, the angle is assumed to be at the horizon (i.e., zero degrees). Transmission losses are calculated for E-modes for frequencies up to (1.4*EMUF).

The minimum F2-layer hop must be above some preset value for the take-off angle as for the E-layer and must also penetrate the E-layer at the F2-layer angle calculated by using the F2 peak layer height as calculated in HFTDA. The F2-layer hops are increased until the mode take-off angle satisfies the above restrictions. The E-layer penetration frequency is ($f_o E_{\min}$ *$\sec \phi_E$ * 1.05), where $\sec \phi_E$ is the secant of the angle of incidence of a ray path with D-region ionization height (100 km) for F-modes.

The mixed mode is calculated by using the E-layer height (110 km) as the peak layer height to determine a take-off angle. The frequency must be supported by the E-layer at one end of the path and penetrate at the other end for this mode to be possible. One E-layer hop is permitted, and then the path is completed with F2-layer hops. The number of F2-layer hops depends on the path length.

Only one minimum hop is chosen for each mode of propagation for each layer, since the antenna patterns are only chosen by operating frequency and path length, thereby making discrimination, between a 1-hop and 2-hop path, impractical until more realistic antenna patterns are used.

The basic transmission loss for each mode is given by

$$L_b = L_{bf} + L_i + L_c + L_m + L_g + L_h \qquad (dB) \tag{19}$$

where the basic free-space loss is given by

$$L_{bf} = 32.45 + 20 \log f + 20 \log P' \qquad (dB) \tag{20}$$

and

f	=	operating frequency (MHz)
P'	=	virtual slant range (km)
L_i	=	non-deviative ionospheric absorption below the MUF (dB)
L_c	=	loss correction factor for E-modes (dB)
L_m	=	over-the-MUF loss (dB)
L_g	=	ground-reflection losses at intermediate reflection points (dB) (taken as 2 dB per ground reflection)
L_h	=	excess system loss to allow for auroral, sporadic-E obscuration, and other losses not explicitly included in the predictions (dB). In HFTDA, it has a fixed value of 7 dB.

The non-deviative ionospheric absorption equation is the one used in IONCAP with the near specular reflection losses calculated for E-layer modes at low frequencies (Headrick et al., 1971; Teters et al., 1983). The non-deviative ionospheric absorption is given by

$$L_i = \frac{(677.2)\ n\ I \sec \phi_D}{(f + f_H)^{1.98} + 10.2} \qquad (dB) \tag{21}$$

where

I = the average absorption index taken over all the control points
f_H = gryofrequency at 100 km
n = number of hops.

The non-deviative absorption given by equation (21) is an average value for F2-layer modes. The effects of E-region electron density non-deviative absorption, collision frequency were averaged in the curve fitting process; therefore, a loss correction factor for E-layer modes, at low frequencies with near specular reflection valid for frequencies above 2.0 MHz, is calculated by

$$L_c = 1.359 + 8.686 \cdot \log\left(\frac{f}{EMUF}\right) \qquad (dB) \tag{22}$$

The equations for E-mode and F-mode losses assume that the mode goes through the absorbing region (true height of reflection above 95 to 100 km).

The over-the-MUF losses are calculated by using the Phillips (Phillips, 1958; Wheeler, 1966) method for values of the frequency/MUF ratio up to approximately 1.4 to 1.5, depending on the ground distance. For values of this ratio, greater is considered in the *scatter* region (Joint Technical Advisory Committee, 1960). The developer, Don Lucas, of this model was an original developer of IONCAP in the mid-1980s and made significant improvements in the over-the-MUF loss model when he developed the code for HFTDA in 1990. While HFTDA uses several models from IONCAP, the over-the-MUF losses are a significant departure. The over-the-MUF losses are a function of season, sunspot, geomagnetic latitude, local time, and path length. The losses are calculated as follows: first, an initial value of L_m is found from equation [23]; where f_m is the mode MUF; σ is $(0.0391\ f_m)$ for E-layer modes, and $(0.1172\ f_m)$ is for F-layer modes and mixed modes, then

$$\begin{aligned} L_m &= 10 \log P \qquad (dB) \\ P &= \frac{1}{\sqrt{2\pi}} \int_Z^{\infty} \exp\left(-\frac{1}{2}x^2\right) dx \\ Z &= \frac{f - f_m}{\sigma} \end{aligned} \tag{23}$$

If the frequency is above f_{end}, the frequencies at which scatter effects apply, then the losses are calculated from

$$L_m = 10 \log P + 7.5 \log\left(\frac{f}{f_{end}}\right) \qquad (dB)$$

$$P = \frac{1}{\sqrt{2\pi}} \int_z^\infty \exp\left(-\frac{1}{2}x^2\right) dx \qquad (24)$$

$$Z = \frac{f_{end} - f_m}{\sigma}$$

The parameter f_{end} is found from

$$f_{end} = 1.4 * f_m \qquad for\ d \le 1000\ km$$
$$f_{end} = \left(1.4 + 0.0175\left(\frac{d-1000}{1000}\right)\right) * f_m \qquad for\ d > 1000\ km \qquad (25)$$

The parameters f_m and σ are defined as above.

The resulting field strength for each mode in terms of the system loss equation is

$$E_f = 107.2 + P_t + 20 \log f - G_r - L_s \qquad (dB\ above\ 1\ \mu v/m)$$
$$E_f = 107.2 + P_t + G_t + 20 \log f - L_b \qquad (26)$$

with the system loss given by

$$L_s = L_b - (G_t + G_r) \qquad (dB) \qquad (27)$$

where

P_t = effective radiated power in same units as received power (Watts)
L_s = system loss (dB)
G_t = antenna power gain relative to isotropic in free space (dB) for the transmitter antenna
G_r = antenna power gain relative to isotropic in free space (dB) for the receive antenna

The system loss of a radio circuit is defined as the signal power in decibels that is available at the receiving antenna terminals. This excludes any transmitting or receiving antenna transmission line losses, since such losses are considered readily measurable. The system loss does include all the losses in the transmitting and receiving antenna circuits—not only the transmission loss caused by radiation from the transmitting antenna and re-radiation from the receiving antenna, but also any ground losses, dielectric losses, antenna loading coil losses, and terminating resistor losses. Antenna gain is taken as antenna power gain that is the product of antenna directive gain, in the direction aligned with the propagation path in both elevation and azimuth, and of antenna efficiency.

Antenna gains, G_r and G_t, are in the direction of the propagation path and include all antenna losses, such, that G_t+G_r is an approximation of the gain G_p. The values of G_t and G_r are required for any elevation angle, azimuth direction, and frequency. In HFTDA, the antenna

gains are determined from a table of antenna gains for each type antenna represented, which is a function of frequency and elevation angle (21 frequencies and 6 elevation angles). After the take-off angle is determined for the mode, the nearest three elevation angles in the table are used to select table antenna gains for the nearest integer frequency, above, and below, the desired frequency. Then three-point Lagrangian interpolation is used to interpolate the gain for the two integer frequencies. The results of the two Lagrangian interpolations are then interpolated by using a linear interpolation based on the given frequency at the two closest integer table frequencies.

After the field strength is determined for each of the three modes, the predicted field strength is determined from the sum of the fields in microvolts per meter. The resulting field strength is converted back to dB relative to 1-microvolt per meter.

HFTDA program is highly modular, allowing changes in the predicted parameter with some ease.

HFTDA, called LTLFLD in NOSC Technical Document 1848 (Systems Exploration Inc., 1990), has been developed around analytical methods and empirical data for the HF spectrum between 3 to 30 Mhz. Any calculations or predictions outside of this range should be suspect.

Sunspot numbers (SSNs) over 150, a very unlikely event for the next 20 years, should be used with caution since the critical frequencies of the F2-layer (f_oF2) are more related to where you are within a given cycle, rather than the absolute sunspot number. Some scientists believe a saturation effect occurs at SSNs of greater than 150 because the f_oF2 ceases to increase. The impact of f_oF2 saturation with SSN on the determination of transmission loss and field strength itself is not clear.

HFTDA predictions are hourly medians of the monthly medians correlated with monthly medians correlated with a monthly median running average sunspot number. Much care should be taken when predicting for a given day, or a few days ahead. Field strength predictions are weakly associated with daily values of solar activity.

Solar flux data, that are used as an indicator of ionization in the F2-layer may, or may not, effect in the same manner the E-layer and D-layer, which controls most non-deviative absorption calculated by this method. Correlation coefficients are not available for the D-, E-, and F2-layers to warrant daily predictions of field strength. The accuracy of the prediction routine, therefore, depends entirely upon its intended use, which includes frequency assignment in the long term, siting, antenna selection, day-to-day frequency use, and absolute signal determination. The method for predicting field strength at a receiving location, using HFTDA, is the solution of Norton's transmission loss equation (Norton, 1959). It is this equation that is the genesis of most analytical approaches to HF field strength predictions.

The simplest calculations were used to increase speed of the calculation, as accuracy was assumed not to suffer for median values and field strength calculations alone. Fourier series expansions representing the predicted ionospheric coefficients (e.g., f_oF2) are not included in any of the variables.

THE IONCAP MODEL

The IONCAP HF prediction model has had a checkered and controversial history over its first decade. When first delivered to the U.S. Army in 1978, it was, to a large extent,

undocumented. Over the ensuing years *bugs* became obvious, with several analysts working independently toward their elimination. Toward the late 1980s, there were several versions of IONCAP, each with different modifications and improvements. Attempts were made to get all of the changes into one version. A version, called VOACAP, was developed by the Voice of America (VOA) and was released in April, 1993 (Lane, Rhoads, & DeBlasio, 1993; Sweeney et al., 1993). VOACAP will be the object of the PENEX field strength testing, as well as the latest version of IONCAP from the Institute for Telecommunications Science. The following description of the field strength calculation is taken from a 1983 IONCAP Users Manual (Teters et al., 1983).

In IONCAP, the basic parameter models that form the basis for the ionospheric predictions are numerical map representations of the parameters that describe the parameter, their temporal and global variations, in terms of Fourier harmonics. The critical frequency of the E-layer, f_oE, is due to Leftin (1976). The representation of the critical frequency of the sporadic-E layer, f_bEs, is due to Leftin et al. (1968). The D-region ionization is included as an exponential decrease below the E-layer; a height of maximum, h_mE, of 110 km and h_mE/Y_mE ratio of 5.5 are assumed (i.e., $Y_mE = 20$ km). IONCAP uses the numerical map of f_oF1 produced by Rosich and Jones (1973) to predict f_oF1. For the F1-layer, the height of maximum is linearly related to the sun's zenith angle, and the ratio of the height of maximum h_mF1 to the semi-thickness of the F1-layer is assumed to be 4. Models of the critical frequency of the F2-layer, f_oF2, and the monthly median M(3000)F2 factor are due to Jones et al. (1969). The height of the maximum ionization in the F2-region, h_mF2, is determined from the M(3000)F2 factor (Shimazaki, 1955). Having obtained h_mF2, the semi-thickness of the F2-layer, Y_mF2, is obtained from h_mF2 in units of Y_mF2 mapped as a function of geomagnetic latitude and solar activity for solar activity (Lucas & Haydon, 1966). Numerical maps represent the continents for use in ground-loss calculations (Zacharisen, 1972).

The ionospheric profile is divided into four regions: D-E region, F2-region, E-F2 valley, and an F1 ledge. The nose of the E-layer is parabolic. The ionization is assumed to decrease exponentially, starting at the lower part of the E-region (i.e., $h_mE - 0.85\ y_mE$), with constants chosen, such that the slope of the profile is continuous at this point. The F2-region is assumed parabolic. In the E-F2 region, only the total density is modeled, and it is represented by a line from a frequency f_u (0.98 f_oE) to a frequency f_v (0.8516 f_oE) at the E-layer. The F1-layer is considered to be a ledge from the F2-layer to the E-F valley. The F1 ledge may be either a linear layer or a parabolic layer. If the height of maximum ionization of the F1 ledge is less than the height of the F2-layer at the frequency of f_oF1, the parabolic shape is used. If the height of maximum of the F1 ledge is greater than the height of the F2-layer, then the height of maximum of the F1 ledge is reduced to the F2-layer height.

IONCAP uses a simple closed form method to find ray paths from one electron density profile. These ray paths are described by the operating frequency f, the take-off angle, the vertical height of reflection h', the true height of reflection h, and the ground range.

For IONCAP, the basic transmission loss for each mode is given by

$$L_b = L_{bf} + L_i + L_c + L_m + L_g + L_p + L_o + L_R \qquad (dB) \qquad (28)$$

where

L_{bf} = the basic free-space transmission loss expected between ideal, loss-free, isotropic, transmitting and receiving antennae in free space (dB)
L_i = non-deviative ionospheric absorption below the MUF (dB)
L_c = loss correction factor for E-modes (dB)
L_m = over-the-MUF loss (dB)
L_g = ground reflection losses at intermediate reflection points (dB)
L_h = excess system loss to allow for auroral obscuration and other losses not explicitly included in the predictions (dB)
L_p = deviative absorption (dB)
L_o = sporadic-E obscuration loss (dB)
L_R = sporadic-E reflection loss (dB)

The basic free-transmission loss L_{bf} is as given in equation (20). The non-deviative ionospheric absorption L_i is given by equation (21) with the absorption index at each control point given by

$$I = -0.04 + \exp(-2.937 + 0.8445\, f_oE) \tag{29}$$

and the gyrofrequency f_H replaced by the longitudinal component of the gyrofrequency f_l. The formula for absorption index I is in terms of the critical frequency of the E-layer f_oE, which includes the variation in zenith angle and solar activity. This formula is an inversion of that formerly used for obtaining f_oE from I. The correction term to the absorption loss for E-layer modes that do not penetrate the whole of the absorbing layer allows for frequencies below 2 MHz. It is similar to equation [22] and is given by

$$L_c = A + B \log X_e \qquad (dB) \tag{30}$$

with

$$\begin{aligned}
A &= 1.359 \text{ for } f_oE > 2 \text{ MHz},\\
&= 1.359\left(\frac{f_oE - 0.5}{1.5}\right) \text{ for } 0.5 \le f_oE \le 2 \text{ MHz},\\
&= 0.0 \text{ for } f_oE < 0.5 \text{ MHz},\\
B &= 8.617 \text{ for } F_oE > 2 \text{ MHz},\\
&= 8.617\left(\frac{f_oE - 0.5}{1.5}\right) \text{ for } 0.5 \le f_oE \le 2 \text{ MHz},\\
&= 0.0 \text{ for } f_oE < 0.5 \text{ MHz},\\
X_E &= f_v / f_oE \text{ for } h > 90 \text{ km},\\
&= f_v\,(90) / f_oE \text{ for } h \le 90 \text{ km},\\
h &= \text{true height of reflection},\\
f_v &= \text{equivalent vertical sounding frequency}.
\end{aligned} \tag{31}$$

The equations for the E- and F-layer mode losses given by equations (29) and (30) assume that the mode goes through the absorbing region (true height of reflection above 95 to 100 km). When the true height of reflection is below 90 km, these equations give losses much higher than those observed. In IONCAP, the constant term, 10.2, in equation (21), is replaced by $(\overline{\nu}/2\pi)$ for values of the true height h less than 88 km and is given by

$$\left(\frac{\overline{\nu}(h_v)}{2\pi}\right)^2 = 63.07 \exp\left(-2\frac{h_v-60}{4.39}\right)$$
$$h_v = 61 + 3\left(\frac{h-70}{18}\right) \qquad (32)$$

Because a complete electron density is used in IONCAP, any high-or low-angle mode will be considered. Deviative losses are considered to be averaged into the above equations for reflection heights less than that at the layer MUF. For modes with reflection heights greater than that at the layer MUF and for modes just past the E-F cusp, a deviative loss term is added. The equation for this term L_p is based on the relationship that the loss is proportional to the product of collision frequency with the difference between group path and phase path. The deviative absorption loss in dB L_p is given by

$$L_p = \frac{B(f_v)\,(h' - h)_N \sec(\phi_o)\,[(f_v + f_l)^{1.98} + 10.2]}{(f + f_l)^{1.98} + 10.2} \quad (dB) \qquad (33)$$

where

f_v = vertical sounding frequency
h' = virtual height of reflection
h = true height of reflection
f = oblique sounding frequency
f_l = longitudinal component of the gyrofrequency
N = electron density profile
ϕ_o = angle of earth's normal-to-ray path at 100 km

The calculation of the function $B(f_v)$ depends on the presence of the F1-layer. In the case when the F1-layer is not present, f_v is taken as f_oE for the determination of L_p for the F2-layer, to preserve continuity at the E- to F2-layer transition. In the case when the F1-layer is present, f_v is taken as f_oE for the F1-layer deviative absorption calculation, and f_v is taken as f_oF1 for the F2-layer deviative absorption calculation. This assures a smooth calculation of loss for all electron density profiles. The deviative absorption is taken as the maximum value of all the possible layer hops possible.

IONCAP does not assume that propagation ceases at the MUF, but that it is allowed to decrease according to the probability that the critical frequencies of the E-, F1-, or F2-layers are above the predicted values of the MUFs (Phillips, 1958; Wheeler, 1966). The equation for this loss term is

$$L_m = 10 \log P \qquad (dB)$$

$$P = \frac{1}{\sqrt{2\pi}} \int_z^{\infty} \exp\left(-\frac{1}{2}x^2\right) dx \tag{34}$$

$$Z = \frac{f - f_m}{\sigma}$$

where f is the oblique sounding frequency, f_m is the MUF for the circuit elevation angle and distance, and σ is the standard deviation of the distribution of the MUFs for mode being calculated. For the E- and F1-layers, σ is given by the maximum of 0.01 or 0.1 times the layer MUF. For the F2-layer, σ is given by

$$\sigma = \frac{|(F_{u,l} - 1)\ F2MUF|}{1.28} \tag{35}$$

where $F_{u,l}$ is either F_l for $f \leq$ F2MUF or F_u for $f >$ F2MUF from table 2. Table 2 shows the distribution of daily values of the F2 MUF about their monthly median, F2MUF, as the ratios of upper and lower decile MUFs to median F2MUF (F_u and F_l, respectively) for a given season, a given solar activity, 4-hour local time blocks at the path midpoint, and for each 10 degrees of geographic latitude from 15 to 75 degrees, north or south. For the sporadic-E layer, σ is given below.

The ground reflection loss calculation for randomly polarized sky waves assumes equal amounts of energy in the horizontally and vertically polarized fields. The losses are represented by the following equation

$$L_g = 10 \log\left(\frac{K_V^2 + K_H^2}{2}\right) \qquad (dB) \tag{36}$$

where K_V is the magnitude of the vertical reflection coefficient at the take-off angle Δ, and K_H is the magnitude of the horizontal reflection coefficient at Δ. These reflection coefficients are a function of the relative dielectric constant of earth, the conductivity of earth (mhos/meter), the dielectric constant of free space (farad/meter), the frequency transmitted, and the take-off angle. This equation is inadequate for take-off angles of less than 2 degrees.

There are two transmission-loss terms associated with modes of propagation with the sporadic-E layer. The layer is modeled as a thin layer occurring at the height $h'Es$ (usually 100 to 110 km). Its effect on modes of propagation passing through it is given by the Es obscuration loss. It is calculated by a method proposed by Phillips (1963) and modified to use the now available maps of f_oE s, the median value of the highest ordinary wave frequency reflected from the sporadic-E layer at vertical incidence:

$$
\begin{aligned}
L_o &= 10 \log(1 - P) \qquad (dB) \\
P &= \frac{1}{\sqrt{2\pi}} \int_z^{\infty} \exp\left(-\frac{1}{2}x^2\right) dx \\
Z &= \frac{f - f_m Es}{\sigma} \\
f_m &= f_o Es \sec \phi
\end{aligned}
\tag{37}
$$

The variance σ is obtained from the 50% and 10% (or 90%) values of $f_o Es$ according to

$$
\sigma = \frac{f_m Es}{1.28155} \left| \frac{f_o Es - SC}{f_o Es} \right| \tag{38}
$$

where SC is the upper decile of $f_o E$ s, if f $\geq f_m$ Es, or SC is the lower decile of $f_o E$s if f $< f_m$ Es. For modes that have reflected from the sporadic-E layer, the basic transmission loss is the absorption losses supplemented by a reflection loss (corresponding to the over-the-MUF loss) defined by

$$
L_R = 8.91 \; P^{-0.7} \qquad (dB) \tag{39}
$$

Note that this is effectively the same as $L_R = 8.91 - 10 \log P$. The probability P is obtained as in the above equation.

The excess system loss L_h allows for auroral, sporadic-E obscuration, over-the-MUF losses, and other losses not explicitly included in the predictions. In IONCAP, this loss is determined from table 3 for path lengths less than 2500 km, and table 4 for path lengths equal, or greater, than 2500 km. The value obtained from the respective table is the median value for a given geomagnetic latitude, local time, and season. Over-the-MUF losses are subtracted from the table value. When the sporadic-E layer is calculated, the sporadic-E obscuration loss is subtracted from that value.

The sky-wave field strength for each mode is directly related to the basic transmission L_b. This is the loss as contrasted to *system loss* that would be observed if the actual antennas were replaced by ideal, loss-free isotropic transmitting and receiving antennas. The field strength is

$$
E = 107.2 + 20 \log f_{ob} + G_t + P - L_b \qquad (isotropic) \tag{40}
$$

where

E	=	rms field strength in dB above 1 μV/m;
G_t	=	transmitting antenna gain (dB) in the direction of the ray path used to determine L_s (decibels referred to an isotropic antenna);
P	=	transmitter power delivered to the transmitter antenna in decibels referred to one watt;
f_{ob}	=	operating frequency in MHz.

Table 3. Expected excess system loss (dB) for paths less than 2500 km.

WINTER (NOV., DEC., JAN., FEB.)

G. M. LAT.	01-04 LMT			04-07 LMT			07-10 LMT			10-13 LMT			13-16 LMT			16-19 LMT			19-22 LMT			22-01 LMT			G.M. LAT.
	Med.	S_ℓ	S_u	Med.	S_ℓ	S_u	Med.	S_ℓ	S_u	Med.	S_ℓ	S_u	Med.	S_ℓ	S_u	Med.	S_ℓ	S_u	Med.	S_ℓ	S_u	Med.	S_ℓ	S_u	
00-40	9.0	4.0	9.0	9.0	4.0	7.6	9.0	4.0	7.6	9.0	4.0	6.4	9.0	4.0	6.4	9.0	4.0	7.6	9.0	4.0	7.6	9.0	4.0	9.0	00-40
40-45	9.0	4.3	9.0	9.1	4.3	8.3	9.1	4.6	8.6	9.0	4.5	7.1	9.0	4.2	6.2	9.0	4.6	8.1	9.0	4.6	7.9	9.0	4.2	9.1	40-45
45-50	9.1	4.7	9.1	9.3	4.6	9.0	9.6	5.2	9.6	9.0	5.1	7.8	9.1	4.4	6.5	9.1	5.2	8.6	9.3	5.2	8.3	9.1	4.5	9.2	45-50
50-55	9.6	5.1	9.2	9.8	5.0	9.7	10.6	5.9	10.7	9.1	5.7	8.7	9.3	4.6	6.9	9.6	5.8	9.1	10.0	5.8	8.7	9.3	4.8	9.3	50-55
55-60	10.5	5.3	10.0	11.1	6.7	9.6	13.4	8.2	14.6	9.7	5.0	10.6	9.8	4.8	7.2	11.2	6.5	9.0	11.5	5.4	10.6	10.3	5.1	9.5	55-60
60-65	13.8	8.0	13.5	17.2	12.7	13.0	19.5	12.3	23.7	11.7	6.8	20.5	10.6	5.8	8.7	14.7	8.3	14.1	16.3	8.9	17.2	14.2	7.2	9.9	60-65
65-70	15.7	7.7	14.6	20.0	13.5	13.2	22.5	11.8	22.5	12.0	6.0	22.0	10.7	5.4	8.2	14.8	7.8	11.3	17.6	7.8	18.6	15.0	6.8	11.5	65-70
70-75	14.7	6.3	9.4	16.9	8.9	15.2	19.7	9.9	14.3	10.7	5.4	13.9	9.9	4.8	7.5	12.6	6.5	10.5	13.1	5.8	14.8	13.0	6.0	9.0	70-75
75-80	11.5	5.6	9.4	14.0	7.7	8.8	16.1	8.4	10.2	9.9	6.3	10.7	9.3	4.7	6.7	10.9	5.4	8.6	11.3	4.9	11.5	11.0	5.4	8.5	75-80

EQUINOX (MAR., APR., SEPT., OCT.)

G.M. LAT	01-04 LMT			04-07 LMT			07-10 LMT			10-13 LMT			13-16 LMT			16-19 LMT			19-22 LMT			22-01 LMT			G.M. LAT.
	Med.	S_ℓ	S_u	Med.	S_ℓ	S_u	Med.	S_ℓ	S_u	Med.	S_ℓ	S_u	Med.	S_ℓ	S_u	Med.	S_ℓ	S_u	Med.	S_ℓ	S_u	Med.	S_ℓ	S_u	
00-40	9.0	4.0	9.0	9.0	4.0	9.0	9.0	4.0	7.6	9.0	4.0	6.4	9.0	4.0	6.4	9.0	4.0	7.6	9.0	4.0	7.6	9.0	4.0	9.0	00-40
40-45	9.0	4.5	10.0	9.1	4.4	11.5	9.2	5.3	9.8	9.1	4.7	9.0	9.1	4.5	8.9	9.3	5.0	11.3	9.2	4.8	10.0	9.1	4.7	10.0	40-45
45-50	9.4	5.0	11.1	9.4	4.8	14.1	9.9	6.6	12.0	9.6	5.4	11.6	9.4	5.0	11.4	10.3	6.0	15.0	9.9	5.6	12.5	9.8	5.4	11.0	45-50
50-55	10.0	5.6	12.2	10.0	5.2	16.6	11.7	8.0	14.3	10.8	6.2	14.2	10.2	5.6	13.9	11.7	7.0	18.7	11.1	6.4	15.0	11.1	6.2	12.0	50-55
55-60	11.0	5.7	17.6	12.0	6.4	22.0	15.2	8.3	15.3	12.7	7.6	18.3	11.6	5.6	15.5	13.5	7.5	20.2	13.0	7.7	19.5	14.0	7.4	13.3	55-60
60-65	13.7	7.7	30.3	17.0	9.3	29.3	21.0	14.0	23.4	16.5	10.6	33.0	14.6	8.3	19.2	16.8	10.3	27.0	18.0	11.3	29.0	20.8	13.0	26.7	60-65
65-70	15.8	8.1	28.0	20.6	11.1	31.0	28.6	18.2	26.9	17.8	10.0	27.9	15.3	7.0	18.0	16.8	8.4	24.0	19.3	11.3	28.8	23.6	11.2	17.5	65-70
70-75	13.9	7.0	21.7	20.7	13.8	20.8	29.0	12.8	20.2	15.2	8.8	18.9	12.3	6.2	14.2	13.9	7.2	18.0	16.7	8.6	22.0	18.5	8.0	16.5	70-75
75-80	11.0	6.1	15.5	16.5	7.5	18.7	18.2	9.7	14.4	12.9	7.5	13.6	10.6	5.4	12.0	12.0	6.2	14.1	13.2	6.4	20.6	13.1	6.3	15.7	75-80

SUMER (MAY, JUNE, JULY, AUG.)

G.M. LAT.	01-04 LMT			04-07 LMT			07-10 LMT			10-13 LMT			13-16 LMT			16-19 LMT			19-22 LMT			22-01 LMT			G.M. LAT.
	Med.	S_ℓ	S_u	Med.	S_ℓ	S_u	Med.	S_ℓ	S_u	Med.	S_ℓ	S_u	Med.	S_ℓ	S_u	Med.	S_ℓ	S_u	Med.	S_ℓ	S_u	Med.	S_ℓ	S_u	
00-40	9.0	4.0	9.0	9.0	4.0	7.6	9.0	4.0	7.6	9.0	4.0	6.4	9.0	4.0	6.4	9.0	4.0	7.6	9.0	4.0	7.6	9.0	4.0	9.0	00-40
40-45	9.1	4.4	9.8	9.1	4.3	9.9	9.0	4.7	9.1	9.1	4.5	7.2	9.1	4.5	8.1	9.2	5.1	8.6	9.1	4.9	9.5	9.0	4.7	10.0	40-45
45-50	9.5	4.8	10.6	9.4	4.7	12.2	9.5	5.5	10.7	9.4	5.0	8.1	9.5	5.0	9.8	10.1	6.2	9.7	10.0	5.9	11.4	9.3	5.4	11.0	45-50
50-55	10.3	5.3	11.4	10.1	5.1	14.6	10.4	6.3	12.3	10.0	5.5	9.0	10.1	5.5	11.6	12.0	7.3	10.8	11.9	6.9	13.4	9.7	6.1	12.0	50-55
55-60	11.9	5.5	17.8	11.4	5.5	16.1	12.0	7.2	15.6	11.6	6.0	10.6	11.9	5.8	13.5	14.8	8.5	11.0	14.8	7.8	14.1	10.8	6.4	18.0	55-60
60-65	15.0	7.5	24.5	13.1	5.8	22.7	15.0	10.7	26.0	14.3	7.8	18.8	13.3	6.2	19.9	17.4	9.1	14.2	17.6	10.1	20.5	13.4	8.9	21.1	60-65
65-70	15.0	6.5	22.1	13.6	6.2	21.8	16.3	9.2	26.7	14.0	6.7	19.5	13.2	5.7	16.6	16.2	7.2	13.8	17.8	7.9	21.9	14.0	7.8	19.0	65-70
70-75	12.7	5.4	15.6	12.8	5.8	15.0	14.0	6.8	18.2	12.5	6.2	12.0	12.2	5.5	13.3	13.8	6.9	11.1	15.0	7.6	17.8	12.4	6.8	16.0	70-75
75-80	11.4	5.7	12.8	11.8	6.0	11.3	12.1	5.3	16.8	11.7	5.7	9.5	11.3	5.3	12.1	12.8	7.0	10.2	13.3	7.2	11.8	11.1	6.8	12.7	75-80

Table 4. Expected excess system loss (dB) for paths greater than 2500 km.

WINTER (NOV., DEC., JAN., FEB.)

G.M. LAT.	01-04 LMT			04-07 LMT			07-10 LMT			10-13 LMT			13-16 LMT			16-19 LMT			19-22 LMT			22-01 LMT			G.M. LAT.
	Med.	S_L	S_u	Med.	S_L	S_u	Med.	S_L	S_u	Med.	S_L	S_u	Med.	S_L	S_u	Med.	S_L	S_u	Med.	S_L	S_u	Med.	S_L	S_u	
00-40	9.0	4.0	9.0	9.0	4.0	7.6	9.0	4.0	7.6	9.0	4.0	6.4	9.0	4.0	6.4	9.0	4.0	7.6	9.0	4.0	7.6	9.0	4.0	9.0	00-40
40-45	9.0	4.2	9.1	9.0	4.3	7.8	9.0	4.2	9.0	9.0	4.2	7.3	9.0	4.0	6.5	9.0	4.3	7.7	9.0	4.3	7.6	9.0	4.3	9.2	40-45
45-50	9.1	4.4	9.3	9.1	4.6	8.0	9.1	4.5	10.4	9.0	4.4	8.2	9.1	4.1	6.7	9.1	4.7	7.8	9.2	4.6	7.6	9.2	4.6	9.4	45-50
50-55	9.4	4.6	9.5	9.4	5.0	8.2	9.2	4.8	11.9	9.0	4.6	9.2	9.4	4.1	6.9	9.4	5.1	7.9	9.9	4.9	7.6	9.8	4.9	9.6	50-55
55-60	10.1	4.7	9.6	10.8	5.5	8.3	9.9	5.6	12.4	9.2	5.2	10.4	10.2	4.6	7.4	10.4	5.5	7.6	11.0	5.0	7.9	11.3	5.3	9.8	55-60
60-65	12.3	5.7	11.4	15.2	6.8	9.5	11.6	7.3	14.1	10.3	5.2	15.2	11.6	4.1	8.3	12.4	6.7	8.0	12.6	5.6	8.9	16.6	7.8	13.8	60-65
65-70	14.5	6.5	10.2	15.4	6.3	10.9	13.1	8.3	14.2	11.0	4.4	15.8	13.1	5.1	7.7	12.6	6.2	7.3	13.4	6.1	8.5	18.9	8.6	11.1	65-70
70-75	12.9	3.4	9.7	13.6	6.5	7.8	12.3	6.8	11.2	10.3	4.8	11.2	13.0	4.7	7.1	11.2	5.4	7.4	12.1	5.1	8.6	17.0	6.5	9.2	70-75
75-80	11.2	5.1	9.2	12.2	5.9	8.1	10.9	5.7	10.2	9.7	4.8	9.2	11.7	4.4	7.0	10.2	5.0	7.5	10.3	4.8	8.2	11.9	5.0	9.7	75-80

EQUINOX (MAR., APR., SEPT., OCT.)

G.M. LAT.	01-04 LMT			04-07 LMT			07-10 LMT			10-13 LMT			13-16 LMT			16-19 LMT			19-22 LMT			22-01 LMT			G.M. LAT.
	Med.	S_L	S_u	Med.	S_L	S_u	Med.	S_L	S_u	Med.	S_L	S_u	Med.	S_L	S_u	Med.	S_L	S_u	Med.	S_L	S_u	Med.	S_L	S_u	
00-40	9.0	4.0	9.0	9.0	4.0	7.6	9.0	4.0	7.6	9.0	4.0	6.4	9.0	4.0	6.4	9.0	4.0	7.6	9.0	4.0	7.6	9.0	4.0	9.0	00-40
40-45	9.0	4.1	10.0	9.0	4.1	8.5	9.0	4.2	8.3	9.1	4.4	7.9	9.0	4.3	8.8	9.1	4.5	9.0	9.0	4.3	8.9	9.0	4.2	10.6	40-45
45-50	9.2	4.2	11.0	9.2	4.2	9.4	9.2	4.5	9.0	9.2	4.9	9.4	9.1	4.6	10.7	9.5	4.9	10.4	9.6	4.6	10.2	9.4	4.4	11.5	45-50
50-55	9.5	4.4	12.1	9.6	4.3	10.3	9.5	4.8	9.7	9.6	5.4	11.0	9.5	5.0	12.1	10.6	6.1	11.9	10.8	5.5	10.9	10.1	5.6	12.2	50-55
55-60	10.0	4.5	13.2	10.3	4.6	10.6	10.3	5.7	9.8	10.7	6.0	11.2	10.3	5.6	13.2	12.4	7.8	12.5	12.8	7.2	11.6	11.4	7.5	13.8	55-60
60-65	11.9	5.7	15.5	12.8	5.9	10.8	13.2	7.9	11.4	13.1	8.5	13.1	11.9	8.6	14.7	15.3	9.5	15.2	17.4	9.8	14.7	16.3	9.7	16.6	60-65
65-70	13.3	5.7	14.3	14.6	6.6	10.6	15.4	7.7	13.8	14.1	8.1	12.4	13.4	7.5	16.1	15.3	8.6	13.2	18.2	8.5	14.3	18.3	8.4	16.2	65-70
70-75	12.0	4.9	13.1	13.7	5.3	9.8	14.0	6.1	10.9	12.0	7.1	10.5	11.4	6.7	11.7	12.4	6.9	12.2	14.4	6.0	13.8	13.8	7.8	15.8	70-75
75-80	10.3	4.8	11.0	10.9	4.6	9.0	11.2	5.7	10.6	9.8	6.3	10.2	9.8	5.7	11.2	9.8	6.1	11.0	10.2	5.4	13.7	10.1	6.9	15.4	75-80

SUMER (MAY, JUNE, JULY, AUG.)

G.M. LAT.	01-04 LMT			04-07 LMT			07-10 LMT			10-13 LMT			13-16 LMT			16-19 LMT			19-22 LMT			22-01 LMT			G.M. LAT.
	Med.	S_L	S_u	Med.	S_L	S_u	Med.	S_L	S_u	Med.	S_L	S_u	Med.	S_L	S_u	Med.	S_L	S_u	Med.	S_L	S_u	Med.	S_L	S_u	
00-40	9.0	4.0	9.0	9.0	4.0	7.6	9.0	4.0	7.6	9.0	4.0	6.4	9.0	4.0	6.4	9.0	4.0	7.6	9.0	4.0	7.6	9.0	4.0	9.0	00-40
40-45	9.1	4.4	9.1	9.0	4.4	9.1	9.0	4.5	8.1	9.0	4.2	6.9	9.0	4.5	7.6	9.0	4.2	8.1	9.0	4.9	8.2	9.1	4.4	9.6	40-45
45-50	9.5	4.8	9.2	9.3	4.9	10.6	9.4	5.0	8.6	9.2	4.4	7.5	9.4	5.0	8.8	9.1	4.5	8.6	9.6	5.8	8.9	9.5	4.9	10.3	45-50
50-55	10.1	5.2	9.4	10.1	5.4	12.2	10.1	5.6	9.3	9.6	4.7	8.1	10.2	5.6	10.1	9.4	4.8	9.1	10.9	6.7	9.6	10.3	5.4	11.0	50-55
55-60	11.5	5.4	9.6	11.9	6.2	13.0	11.6	6.5	9.7	10.1	4.9	9.3	11.5	5.9	12.3	10.2	5.1	10.7	12.8	6.8	11.8	11.9	5.7	13.4	55-60
60-65	13.9	6.7	9.8	16.5	8.8	16.8	15.2	9.3	13.8	11.2	6.4	13.1	12.8	6.8	16.4	11.6	6.1	14.3	14.2	7.1	17.2	14.0	7.2	18.4	60-65
65-70	14.0	6.1	10.0	16.8	7.4	16.7	15.1	8.2	16.5	11.3	6.2	13.1	12.8	6.3	12.0	11.7	5.4	12.4	13.8	6.4	15.2	14.0	6.4	15.1	65-70
70-75	12.2	4.8	8.9	14.4	6.5	11.9	12.4	5.9	14.1	10.5	5.8	10.1	11.2	5.5	9.2	9.9	5.1	11.0	11.6	5.8	12.3	12.2	5.3	12.1	70-75
75-80	11.0	5.3	8.2	13.1	6.0	10.0	10.5	5.5	13.1	10.1	5.6	8.6	9.8	5.4	8.4	9.1	5.0	10.2	9.9	5.6	9.9	10.4	5.5	10.3	75-80

The antenna gains in IONCAP are determined by a two-dimensional linear interpolation on a table of antenna gains for each type of antenna represented. The table gives antenna gains, 46 elevation angles from 0 to 90 degrees, for every integer frequency from 2 to 30 MHz. The resulting array is 46 by 29. The gain determined for the transmitting antenna includes a factor to account for its transmission efficiency.

The predicted field strength is determined from the sum of the field strengths of the individual modes in microvolt per meter. This result is then converted back to dB, relative to 1 microvolt per meter.

THE ASAPS MODEL

The ASAPS model (Caruana, 1993) is used by the Australian Government Ionospheric Prediction Service (IPS) Radio and Space Services to predict HF sky-wave system performance and to analyze ionospheric parameters. ASAPS stands for Advanced Stand-Alone Prediction System. ASAPS makes good use of graphical displays that make life easier for the user. The model predicts the maximum usable frequency (MUF), absorption limiting frequency (ALF), elevation angles, mode probability, path loss, field strength, radio noise, noise-path loss(NP), and signal-to-noise power ratio for a range of possible propagation modes. ASAPS assumes great-circle propagation, with mirror reflections from the regular E- and F-layers.

In ASAPS, the MUF and ALF of a mode are used to determine the availability of a mode. The MUF is evaluated by using the IPS world maps of ionospheric characteristics (Fox, 1988; Fox & McNamara, 1986, 1988). The mode's ALF is determined, from an empirical formula in terms of the solar zenith angle.

The computation of path loss is based on path range. For circuit ranges less than 9000 km, the basic transmission loss is essentially the method described in the Supplement to CCIR Report 252-2 (CCIR, 1980). For paths greater than 11,000 km, the path loss is given by the FTZ method. For path lengths between 9000 and 11,000 km, a separate path loss is computed by using both the CCIR method and the FTZ method. The resultant path loss is the weighted average of these two. For the CCIR separate-loss-term procedure, the steps in the computation include (1) determination of the ray paths of the mostly normal propagation modes between transmitter and receiver on purely geometrical terms, (2) prediction of the state of the ionosphere at each sky reflection point to determine which of these modes are open—the operating frequency must fall between the ALF and the upper decile of the MUFs for the path—and (3) computation of the path loss for each open mode. The FTZ method makes circuit predictions for only a composite mode (i.e., no specific modes are considered).

The separate transmission loss and gain factors that are specifically taken into account in ASAPS for paths lengths $< 11{,}000$ km are as follows:

- spatial attenuation, including focusing of rays with low elevation angles and rays propagated to very long distances (L_{bf} and G_f)
- non-deviative and deviative absorption (L_a)
- polarization coupling loss (L_p)
- ground-reflection loss (L_g)
- sporadic-E obscuration loss (L_q)
- transmitting and receiving antenna gains (G_t and G_r, respectively)

The basic transmission loss for path lengths < 11,000 km is given by

$$L_b = L_{bf} + L_a + L_p + L_g + L_q - G_f \qquad (dB) \tag{41}$$

The basic free space attenuation L_{bf} is the same as given in equation (20) for HFTDA. The ground reflection loss L_g for multiple-hop modes is the same as given in equation (36) for IONCAP. Depending on circuit path length, the horizon focus gain G_f is calculated using one of the following two methods:

For circuit paths that are less than one-quarter of the Earth's circumference in length (about 10,000 km), the horizon focus gain for E- and F-modes is calculated by the Bradley (1970) method. This method gives G_f as a function of the mean elevation angle of the upgoing rays over all hops. It is independent of the number of hops, and it reaches a maximum of 9 dB at grazing incidence. G_f has been approximated by four 6-degree Chebychev polynomials:

- For mean elevation angles ≤ 10 degrees

$$\begin{aligned} G_f(E\text{-}modes) &= 4.14 - 4.00x + 3.007x^2 + 0.069x^3 \\ &\quad - 1.06x^4 + 0.681x^5 - 0.347x^6 \\ G_f(F\text{-}modes) &= 6.03 - 3.161x + 1.4x^2 + 0.624x^3 \\ &\quad - 1.413x^4 + 0.088x^5 + 0.533x^6 \end{aligned} \tag{42}$$

where

$$x = \frac{mean\ elevation\ angle - 5}{5} \tag{43}$$

- For mean elevation angles > 10 degrees

$$\begin{aligned} G_f(E\text{-}modes) &= 0.81 - 0.876x + 0.353x^2 - 0.028x^3 \\ &\quad - 0.227x^4 - 0.274x^5 + 0.387x^6 \\ G_f(F\text{-}modes) &= 1.50 - 1.244x + 0.173x^2 + 0.540x^3 \\ &\quad - 0.267x^4 - 1.136x^5 + 0.853x^6 \end{aligned} \tag{44}$$

where

$$x = \frac{mean\ elevation\ angle - 50}{40} \tag{45}$$

For circuit path lengths that are greater than one-quarter of the earth's circumference, the horizon focus gain G_f is given by the following formula (Hortenbach & Rogler, 1979):

$$G_f = -20 \log\left(\left|1 - \frac{n\pi R}{D}\right|\right) \tag{46}$$

where

D = great-circle path length between transmitter and receiver in kilometers

n = 1 for D < three-quarters of the Earth's circumference ($3\pi R/2$) and 2 for longer distances

R = Earth's radius (6370 km).

The horizon focus gain is limited to a maximum value of 30 dB.

The types of absorption taken into account in ASAPS are the normal non-deviative and deviative absorption (including the median winter-anomaly absorption). The auroral absorption, the extra attenuation of radio waves that traverse the auroral zones, is not calculated in ASAPS. The estimation of the non-deviative and deviative absorption in ASAPS is based on the analysis of vertical-incidence absorption measurements (George, 1971). The absorption estimation uses a relationship between the absorption at vertical and oblique incidence obtained by George and Bradley (1973) from the results of ray-tracing calculations through model ionospheres. The procedure is described in detail by George and Bradley (1974). This takes no account of absorption in the F-region arising from collisions between electrons and ions.

The absorption L_a, experienced by the ordinary wave frequency f_{ob} reflected obliquely from the ionosphere, is given in terms of the absorption $L_a(f_v)$ of the ordinary wave at vertical incidence on a related frequency f_v

$$L_a(f_{ob}) = \frac{L_a(f_v)\,(f_v + f_l)^2 \sec i_{100}}{(f_{ob} + f_l)^2} \tag{47}$$

where f_l, the electron gyrofrequency about the vertical component of the geomagnetic field, is taken as positive. This is approximately 1.5 MHz for the E-modes and 1.0 MHz for the F-modes. The parameter f_v is given in terms of f_{ob} by

$$f_v = f_{ob} \cos i_{100} \tag{48}$$

i_{100} is the incidence angle of the unrefracted ray at a layer height of 100 km, such that

$$\sin i_{100} = 0.9845 \cos \Delta \tag{49}$$

where Δ is the ray's elevation angle at the ground.

George (1971) showed that at noon the term $A(f_v) = L_a(f_v)(f_v + f_l)^2$ was related to A_T, the limiting value of $A(f_v)$ for a sufficiently high frequency that signals traverse the whole of the absorbing region without deviation, and ϕ_n is a function of the ratio of f_v to f_oE as given by

$$\phi_n\left(\frac{f_v}{f_oE}\right) \equiv \frac{A(f_v)}{A_T} \tag{50}$$

The function ϕ_n is approximately independent of location, season or solar epoch and is given in figure 1. (The figure given here and used by ASAPS is the same as figure 7 in the Supplement to CCIR Report 252-2 (CCIR, 1980), except that the maximum value of ϕ_n is limited to 1.56.) Equation (50) holds under normal absorption conditions and also applies approximately for winter-anomaly absorption. Samuel and Bradley (1975) have shown that equation (50) may also be extended to other times of day than noon. For a given month and location, A_T increases linearly with 12-month running mean sunspot number R_{12} and changes diurnally as a function of the solar zenith angle χ. For a given month and location, A_T in ASAPS is given by

$$A_T(T,\chi) = A_T(0,0)\cos^p(0.881\chi)\,(1 + 0.0067\,T) \qquad (51)$$

where A_T (0,0) is the value of A_T at solar minimum (T =0) and solar noon ($\chi = 0$). The parameter T is the ionospheric index used by IPS, and its relationship to R_{12} is given in table 5 (Turner, 1968).

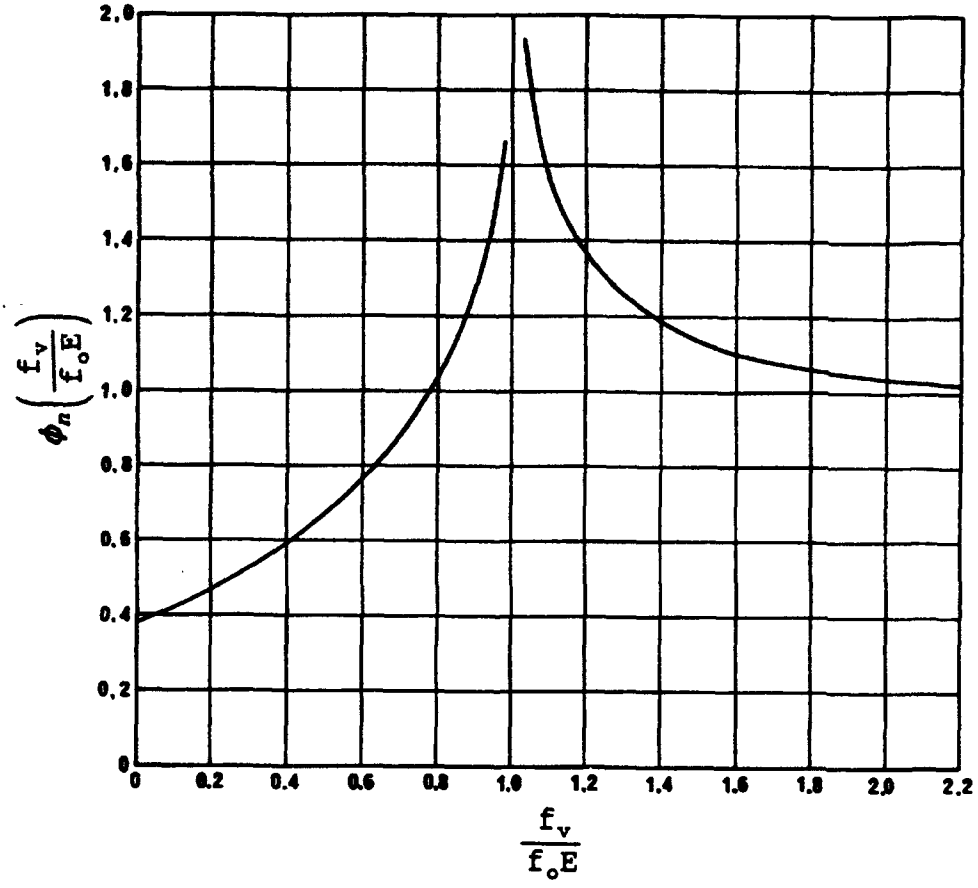

Figure 1. The George absorption function ϕ_n.

Table 5. Relationship between the IPS ionospheric index T and R_{12} (Turner, 1968).

Month	Ordinates at origin (c)	Slope (d)
January	-1.58	0.96
February	0.81	0.94
March	-0.65	0.97
April	-0.54	0.99
May	-0.06	1.00
June	0.34	1.01
July	-0.18	1.00
August	1.19	0.97
September	2.70	0.93
October	1.87	0.93
November	2.45	0.92
December	-0.04	0.96

where

$$T = c + d * R_{12}$$

The parameters $A_T(0,0)$ and p are functions of month and of modified dip latitude $|\chi|$ where

$$\tan X = \frac{I}{\sqrt{\cos \Lambda}} \tag{52}$$

The parameter I is the magnetic dip angle in radians (considered positive if north of the magnetic equator), and Λ is the geographic latitude of the point. Figures 2 and 3 (figures 8 and 9 in the Supplement to CCIR Report 252-2 [CCIR, 1980]) give p and $A_T(0,0)$, respectively, for each month and $|\chi|$ value. At high latitudes with $|\chi| > 70°$, values of $A_T(0,0)$ and p are taken as for $|\chi| = 70°$; hence, combining equations (47), (50), and (51) gives the daytime absorption for ASAPS

$$L_a(f_{ob}) = \frac{A_T(0,0)\cos^p(0.881\chi)\,(1 + 0.0067\,T)\,\phi_n\left(\frac{f_v}{f_o E}\right)\sec i_{100}}{(f_{ob} + f_l)^2} \tag{53}$$

For a multiple-hop mode, the absorption on each hop is evaluated separately by using mid-hop position ionospheric characteristics and a mean elevation angle for the upward and downward legs of the hop.

After sunset, the absorption falls to a small non-zero value. The total nighttime absorption (Wakai, 1975) is given by

$$L_a(f_{ob}) = \frac{(7 + 0.019\,D)\,(1 + 0.015\,T)}{f^2_{ob} + 10} \quad (dB) \tag{54}$$

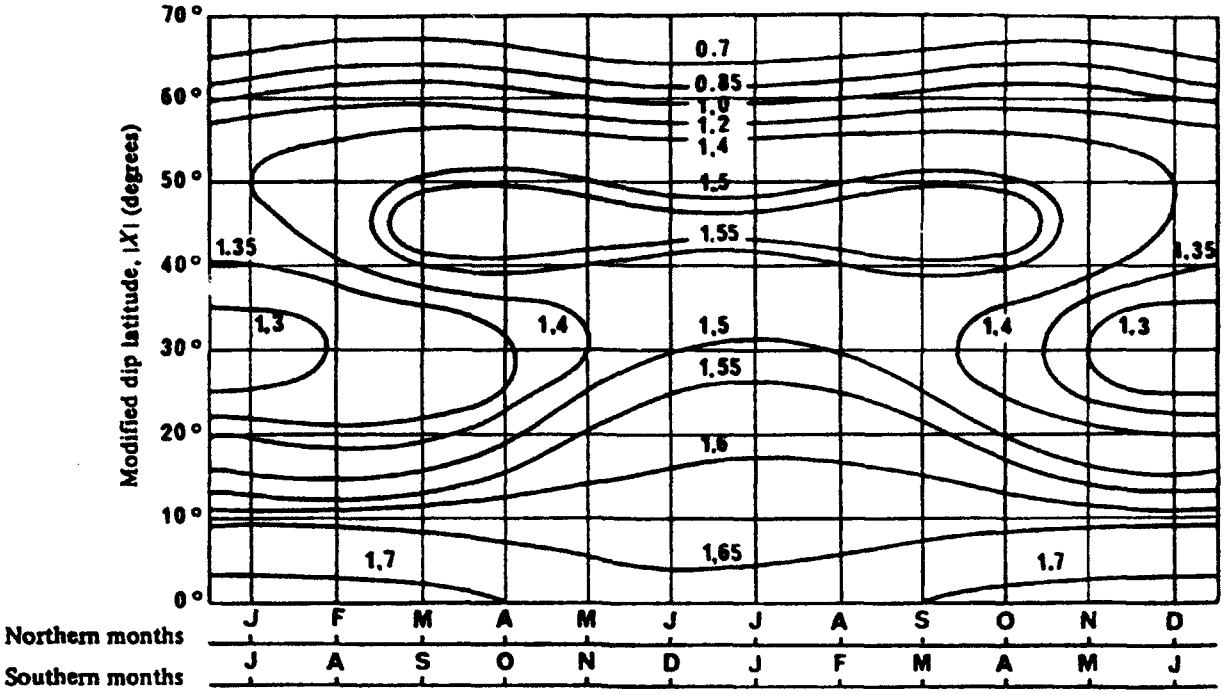

Figure 2. The diurnal absorption exponent p.

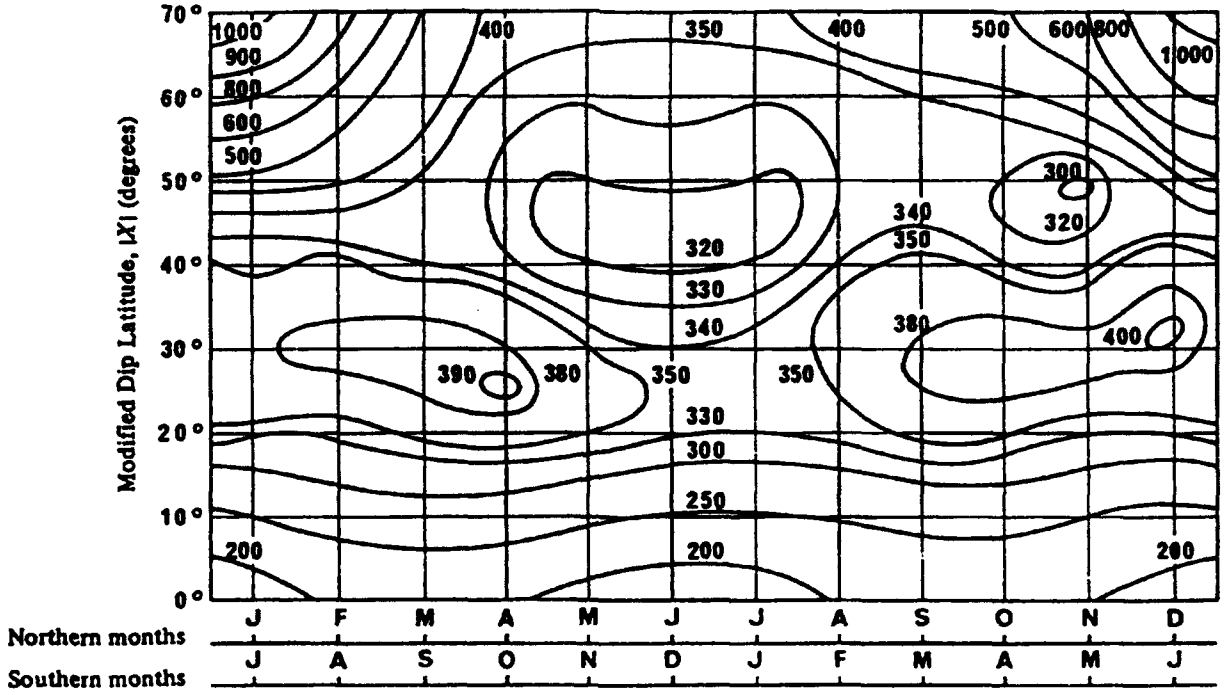

Figure 3. The daytime absorption factor A_T (0,0).

where f_{ob} is the operating frequency in MHz, and D is the total ground range between transmitter and receiver in km. The values determined are regarded as applying separately to each of the propagation modes that can exist. The value for L_a, determined from equation (54), is taken for the mode when it gives a value larger than that obtained from equation (53).

When an upgoing wave is incident on the ionosphere, it leads to the excitation of an ordinary (O) and an extraordinary (X) wave. These waves, having different polarizations, may be regarded as propagating independently within the ionosphere and being subject to different amounts of absorption. This polarization coupling loss L_p is given in ASAPS by the empirical formula

$$L_p = A + B * (hop\ length) + (number\ of\ hops) \qquad (dB) \qquad (55)$$

where the constants A and B depend on the mode, as defined in table 6, and the hop length is expressed in radians, with a maximum value equivalent to a hop length of 15,000 km.

Table 6. Polarization loss constants.

Constants	E-modes	F-modes
A	2.400	2.060
B	2.548	1.019

Sporadic-E obscuration losses are taken into account in ASAPS by using an empirical formula developed by Sinno et al. (1976). For a wave frequency f in MHz and an incidence angle i_{100} of the oblique ray at a height of 110 km, the obscuration loss for one traverse of the Es-layer by an F-mode is given by

$$L_q = -\log (1 - S^2) \qquad (dB) \qquad (56)$$

where

$$S = \frac{1}{1 + 10\left(\frac{f}{f_oEs \sec i_{110}}\right)^8} \qquad (57)$$

The sporadic-E critical frequency f_oE s is approximated by 1.2 * f_oE, with a lower limit of 1.2 MHz. Equation (56) gives L_q = 0.04 dB for $f = f_oE$ s * sec i_{100}, and $L_q \rightarrow \infty$ as $f \rightarrow 0$. Because sporadic-E obscuration loss can become quite large for small frequencies, sporadic-E obscuration loss in ASAPS is limited to a maximum value of 54 dB per hop. L_q is evaluated separately for each hop, then summed.

Finally, for circuit lengths < 9000 km, ASAPS determines the rms field strength from

$$E_{rms} = 107.2 + 20 \log f + P_t + G_t - L_b \qquad (dB\ above\ 1\ \mu V/m) \qquad (58)$$

where

P_t = signal power (in dBW) at the input to the transmitting antenna
f = transmitting frequency in MHz
G_t = transmitting antenna gain in dB relative to an isotropic antenna in the direction of the propagation mode
L_b = basic transmission loss for the mode in dB

The antenna gains that are in ASAPS are determined by a two-dimensional linear interpolation from tables of antenna gain given at 6 take-off angles and 21 frequencies.

For circuit lengths >11,000 km, ASAPS uses a variance of the FTZ method adopted by the CCIR for use at circuit ranges greater than 9000 km (CCIR, 1990a). The median field strength is given by

$$E_{median} = E_o X - 66.4 + P_t + G_t + G_{ap} - L_y \qquad (dB\ above\ 1\ \mu V/m) \qquad (59)$$

where

$$E_o = 139.4 - 20 \log D'$$

$$X = 1 - \frac{(f_M+f_H)^2}{(f_M+f_H)^2 + (f_L+f_H)^2} \left[\frac{(f_L+f_H)^2}{(f+f_H)^2} + \frac{(f+f_H)^2}{(f_M+f_H)^2} \right] \qquad (60)$$

and

E_o = free-space field strength for 3,000 kW erp
D' = virtual slant path length in km between transmitter and receiver
f_M = upper limit frequency (operational MUF) given in equations [2] and [3] with 1.2 replacing 1.0 MHz
f_L = lower limit frequency (MHz) (similar to equation [4], but includes winter anomaly effects
f_H = F-layer gyrofrequency (MHz)
f = transmission frequency (MHz)
P_t = transmitter power in dBW
G_t = antenna gain of transmitter antenna in dBi
G_{ap} = focus gain on very long paths in dB
L_y = extra empirical loss (or gain), currently defined as –4.2 dB

The focus gain is given by

$$G_{ap} = 10 \log \left[\frac{D}{R \left| \sin\left(\frac{d}{R}\right) \right|} \right] \qquad (dB) \qquad (61)$$

where R is the Earth's radius, and D is the great-circle distance between transmitter and receiver, in km. G_{ap} is limited to a maximum value of 15 dB, since it tends towards infinity as D approaches a multiple of πR. The rms field strength is taken to be 1.6 dB above the median value

$$E_{rms} = E_{median} + 1.6 \tag{62}$$

By equating the CCIR and FTZ rms field strengths, the equivalent FTZ pathloss (L_{FTZ}) becomes

$$L_{FTZ} \equiv L_b = 167.8 + 20 \log f - E_o X - G_{ap} \qquad (dB) \tag{63}$$

For circuit path lengths between 9,000 and 11,000 km, a separate pathloss is computed in ASAPS by both the CCIR method (L_b) given in equation [41] and the FTZ method (L_{FTZ}) given in equation [63]. The resultant pathloss (L_{av}) is the weighted average of the two

$$L_{av} = (1 - w)\, L_b + w\, L_{FTZ} \qquad (dB) \tag{64}$$

where the weight w is given in terms of the path length (D) by

$$w = \frac{D - 9000}{2000} \tag{65}$$

The rms field strength, for circuit path lengths between 9,000 and 11,000 km, is then given by the CCIR formula in equation [58] with L_b replaced by L_{av}.

THE AMBCOM HF PREDICTION MODEL

The AMBCOM (Hatfield & Smith, 1987) is a fast, versatile, two-dimensional (2D) ray tracing program for simulating high-frequency (HF) ionospheric sky-wave propagation and the resulting performance of various HF systems, for example, communications, broadcast, geolocation, surveillance and over-the horizon radar (OTHR) systems. Its name is an acronym for Ambient Communications, by analogy with the Nuclear Effects on Communications (NUCOM) code, from which it is largely derived.

The basic premise, underlying the design of AMBCOM, is that the accuracy of the propagation model should be compatible with the accuracy available in the ionospheric model. Since only enough ionospheric profile information is normally available to portray three-parameter layers, little purpose is served by employing a ray path calculation that presumes more detailed knowledge of the profile. On the other hand, strong horizontal gradients in critical frequency and height are apparent even in maps of monthly median parameters. Neglect of these systematic variations can be equally misleading: gross errors in range estimation or in the computed elevation angle at the receiver, or both, can occur under certain conditions. AMBCOM is designed to account for such variations to the first order.

The distinguishing feature of AMBCOM is the propagation model, which combines the advantages of open-ended ray tracing with the speed of analytic integration through parabolic

layers. By "open-ended" it is meant that the path of the ray through the ionosphere—and the range at which it returns to earth—are determined by the refractive effects of the ionosphere. This is in contrast to virtual-geometry codes, where the point at which the ray returns to earth is specified in advance and each hop is symmetric about its predetermined reflection point. Examples of widely used virtual-geometry codes are HFMUFES, IONCAP, and RADARC. Such codes cannot predict "unconventional" modes of propagation, such as, topside reflections (M-modes) and chordal modes. Because AMBCOM uses ray tracing, it will handle large ionospheric gradients and will predict asymmetric hops and unconventional modes when they are indicated by the ionospheric model. Significant differences in the ionosphere and propagation models used by AMBCOM, RADARC, and IONCAP are summarized in tables 7 and 8.

Another AMBCOM feature is that it is one of the most thoroughly documented propagation codes. Although originally developed for mainframe computers, a PC-based version has been developed recently.

AMBCOM is based on the NUCOM code developed by the Stanford Research Institute (SRI) during the 1960s and 1970s under sponsorship of the Defense Atomic Support Agency (DASA) and its successor, the Defense Nuclear Agency (DNA), to predict the performance of HF communication systems under normal (i.e., ambient) and nuclear ionospheric conditions (Nielson et al., 1967). AMBCOM employs the ray tracing and communication system concepts of NUCOM, but it is intended primarily for use under ambient conditions. The current version of AMBCOM incorporates additional models of the ambient ionosphere that were developed in the late 1970s (Hatfield, 1980).

Table 7. Summary of significant model differences.

Models	Program Names		
	RADARC	AMBCOM	IONCAP
Ionosphere Generation			
Median models	Yes	Yes—including Auroral Ionosphere	Yes
Spatial representation	4 samples	41 samples	4 samples
Real-data input	ionograms at 4 locations	9 parabolic parameters at up to 41 locations	ionograms at 4 locations
Propagation Model			
Raytracing method	Martyn's Theorem	Semi-analytic raytrace	Martyn's Theorem
Tilts, gradients	No	Yes	No
Topside reflections	No	Yes	No
Radar propagation	Yes	Yes	No
Point-to-point propagation	No	Yes	Yes
Radio System Simulation			
Circuit reliability	No	No	Yes

Table 8. Differences in the input ionospheric and noise data.

Variables	Program Name		
	RADARC	AMBCOM	IONCAP
f_oF2			
– Coefficients reference	Oslo (CCIR, 1967)	New Delhi (Jones & Obitts, 1970)	Oslo (CCIR, 1967)
– SSN variation	Linear	Second order	Linear
– Centered on	15th of month	15th of month	15th of month
f_oF1	Analytic (formula)	Filled layer based on E, F2	Coefficients (Rosich, 1973)
f_oEs	Coefficients (Leftin et al., 1968)	Coefficients (Leftin et al., 1968)	Coefficients (Leftin et al., 1968)
f_oE	Coefficients (Leftin, 1967)	Coefficients (Leftin, 1976)	Coefficients (Leftin, 1976)
M(3000)F2			
– Method used	Coefficients	Coefficients	Coefficients
– SSN variation	Linear	Linear	Linear
Land mass	Coefficients	Coefficients	Coefficients
Atmospheric Noise			
– Coefficients	Yes	Yes	Yes
– Time variable	LMT (hours) (Lucas & Harper, 1965)	UT (hours) (Zacharisen & Jones, 1970)	LMT (hours) (Lucas & Harper, 1965)

The ionosphere is modeled with three parabolic layers of electron density. The f_oF2 is represented by a set of coefficients developed by Jones and Obitts (1970). The M(3000)F2 is represented by coefficients due to Jones et al. (1969). The height of the F2-layer is determined from the M(3000)F2 by using a relationship by Shimazaki (1955). This result is corrected for retardation in the E- and F1-regions (Wright and McDuffie (1960). The f_oE is represented by coefficients due to Leftin et al. (1968). The height of the E-layer is modeled at 115 km, with a semi-thickness of 25 km, and with no day/night variation. The height and semi-thickness of the pseudo-F1 layer are computed from the parameters of the E- and F2-parabolic layers. The bottom of this layer is set at 130 km, and this layer is required to overlap with the F2 layer by one-half its own semi-thickness (75 km). The critical frequency f_oF1 is related to f_oE by

$$f_oF1 = (f_oE)\,2^n$$
$$n = \frac{y_mF1}{120} \qquad (66)$$

The maximum value of f_oF1 is limited to being less than 0.695 f_oF2. The f_oEs is represented by coefficients developed by Leftin et al. (1968). The height and semi-thickness of the Es-layer are set to 110 km and 1 km, respectively.

Special features of AMBCOM include the following:

- A model of the electron density profile in the high latitude ionosphere (including the auroral zone).
- A model for computing auroral absorption.
- Models for computing reflection and penetration losses for the Es-layer, as functions of the maximum frequency and blanketing frequency of the layer.
- Consideration of both topside and bottomside reflections from the Es-layer (e.g., M modes).
- An option to search for high rays on one- and two-hop F2 modes (1F1H and 2F2H modes).

The new model of the high-latitude ionosphere is, itself, a modification of the RADC-POLAR model developed by Elkins and Rush (1973a, 1973b). It is based on the incoherent-scatter radar measurements of electron density profiles in the auroral ionosphere (Vondrak et al., 1978) by SRI at Chatanika, Alaska. The auroral absorption model was developed by SRI from previously compiled riometer data. It describes the variation of median auroral absorption as a function of corrected geomagnetic latitude, longitude, season, local time, solar activity, and geomagnetic activity (Vondrak et al., 1978).

The expression for basic transmission loss for AMBCOM is given by

$$L_b = L_{bf} + L_{D2} + L_{A1} + L_{A2} + L_{A3} + L_p + L_{Aur} + L_o + L_R + L_g \qquad (dB) \qquad (67)$$

where

L_{bf} = free-space loss (dB)
L_{D2} = divergence loss for F2 high-ray modes (dB)
L_{A1} = nuclear D-region absorption (dB)
L_{A2} = E-F1 absorption (dB)
L_{A3} = non-deviative D-region absorption (Li) (dB)
L_p = F1-F2 deviative absorption (dB)
L_{Aur} = auroral absorption (dB)
L_o = Sporadic-E obscuration loss (dB)
L_R = Sporadic-E reflection loss (dB)
L_g = summed ground-reflection loss at intermediate ground-reflection points (dB).

The free-space spreading loss term for AMBCOM is the same as that given by equation (20). The defocusing loss term for F2-layer high-ray modes is given by

$$L_{D2} = 10 \log \left[\frac{R \sin \frac{D}{R} \frac{\sin \Delta}{\cos \beta} \left| \frac{dD}{d\beta} \right|}{(P')^2} \right] \qquad (dB) \qquad (68)$$

where

P' = group path (km)
β = take-off angle
Δ = arrival angle
D = ground range (km)
R = earth radius (km).

To improve the accuracy, L_{D2} is calculated for both forward and reverse rays, then, the average of these two values is used. For the reverse calculation, angles Δ and β are interchanged.

AMBCOM provides models for estimating several components of absorption loss, according to the altitude at which the absorption occurs and the source of the ionization responsible for the absorption—solar radiation, nuclear radiation, or auroral precipitation. These are computed individually (if appropriate) in various parts of the program and are combined at the end of each hop. Up going and down going legs of a hop are treated separately to take into account spatial variations in electron density and possible changes in the angle of incidence of the ray.

Solar-controlled absorption is computed in three height regimes: the D-region (below 92 km), where the absorption is non-deviative; the E-F1 region (92 to ~150 km), where both deviative and non-deviative absorption may occur; the F1-F2 region (above 150 km), where the absorption is treated as strictly deviative. (If desired, the nuclear absorption can be computed for the same three height regimes; however, the nuclear routines are bypassed, unless externally generated electron-density profiles are input.) The solar D-region absorption L_{A3} for the ordinary ray is evaluated at each D-region traversal by

$$L_{A3} = \begin{cases} \dfrac{119(1.0 + 0.0037\ SSN)(\cos 0.881\chi)^{1.3}\sec\phi_D}{(f + f_H)^{1.98}} & for\ \chi \le 102^\circ \\ 0 & for\ \chi > 102^\circ \end{cases} \quad (69)$$

where

SSN = sunspot number
χ = solar zenith angle at location of D-region crossing
ϕ_D = ray angle of incidence at 70 km
f = operating frequency (MHz)
f_H = electron gyrofrequency at 100-km altitude (MHz).

The second solar-controlled absorption region extends from 92 km to about 150 km and considers total ionospheric absorption in each parabolic layer (both deviative and non-deviative). The same expression is used for ambient and nuclear cases, but the values of some of the parameters differ. The term L_{A2} is computed by

$$L_{A2} = \sum \Delta A_i \quad dB/layer\ traversed$$

$$\Delta A_i = \frac{5.7x10^2(\nu_{eair} + \nu_{eox})}{4\pi^2(f + f_H)^2} f^2 \frac{\beta y(2y_m - y)}{\sqrt{\cos^2\phi_o - \beta y(2y_m - y)}} \Delta y \quad dB/slab \quad (70)$$

where

Δy	=	slab thickness (km)
y	=	vertical distance of the slab from the layer bottom (km)
y_m	=	layer semi-thickness (km)
ν	=	collision frequency with air molecules and oxygen atoms, appropriate to the slab altitude (millions of collisions/s)
ϕ_o	=	incidence angle at the entrance to the layer
f	=	operating frequency (MHz)
f_H	=	electron gyrofrequency at the slab height
f_c	=	layer critical frequency (MHz)

and

$$\beta = \frac{f_c^2}{f^2 y_m^2}. \tag{71}$$

At altitudes greater than about 150 km, the collision frequency is generally about three orders of magnitude smaller than the wave frequency. This leads to a relatively simple expression for the total deviative absorption incurred as given by

$$L_p = \frac{8.7\nu}{2c} \; (P' - P) \qquad (dB) \tag{72}$$

where P' and P are the group and phase paths for that portion of the ray path above 150 km, and $\nu = 10^3\ s^{-1}$. The deviative absorption is usually small, except at near-vertical incidence.

The auroral absorption model, L_{Aur}, is based on a method proposed by Foppiano (1975) and adopted (after certain modifications) by the CCIR (1980). The Foppiano (1975) model was developed by fitting equations to published riometer data from 27 stations in the northern hemisphere to model the spatial and temporal variations of auroral absorption. The resulting equations can be used to predict the monthly one-way-vertical absorption, A_m, at a frequency of 30 MHz (a typical riometer frequency) as a function of corrected geomagnetic (CGM) latitude (ϕ), corrected geomagnetic longitude (θ), corrected geomagnetic time (T), sunspot number (R), and month (M). This is subsequently converted to a value A_{Kp}, which is a function of magnetic index K_p. Both the CCIR (1980) and Hatfield (1987) describe how this value is, in turn, converted to an operating frequency at oblique incidence on the auroral D-region, L_{Aur}.

Foppiano's model of monthly median absorption combines the effects of auroral substorms occurring over an entire month at a given hour of the day, for a given month of the day, and for a given level of solar activity (specified by the 12-month running-average sunspot number, R). Although the median absorption is implicitly related to magnetic activity, through its dependence on sunspot number, the model does not have an explicit dependence on magnetic activity; consequently, the large increases in auroral activity tend to be obscured in the averaging process. Conversely, a few large substorms may contaminate the quiet-day predictions. This model is not appropriate for use with an HF ray tracing code when the structure of the refracting regions is defined as a function of magnetic activity in a 3-hour time frame.

Accordingly, SRI developed a model (Vondrak et al., 1978) that closely follows Foppiano's formulation, but adds an average magnetic-activity dependence. The auroral absorption on an HF ray path, L_{Aur}, is calculated in three steps as follows:

1. Compute Q1, the percentage probability that one-way-vertical absorption at 30 MHz exceeds 1 dB. This parameter was chosen by Foppiano because much of the available auroral-absorption data is presented in terms of Q_1.
2. Using an empirical relationship between Q_1 and A_m, compute A_m and convert to the related Kp-dependent value, A_{Kp}, by using the input value of Kp.
3. Convert the one-way-vertical absorption at 30 MHz (i.e, A_{kp}) to absorption at the desired operating frequency for the angle of incidence of the ray on the D-region.

Further details about this model can be obtained from Smith and Hatfield (1987).

To assess the effects of sporadic-E on received signal strength, one must take account of the fact that sporadic-E is partially reflecting and partially transparent; thus, some signal attenuation is incurred in reflection from, or penetration through, the layer. The reflection loss is denoted here as L_R, and the transmission (or obscuration) loss by L_o. Two methods of estimating L_R and L_o are provided in AMBCOM: the Phillips model (Phillips, 1963), and the Sinno model (Sinno et al., 1976). The user selects the method to be used by specifying an input.

For the Phillips method, L_R and L_o are given respectively by

$$\begin{aligned} L_R &= 10 \log P_{Eb} \qquad (dB) \\ L_o &= 10 \log (1 - P_{Eb}) \qquad (dB) \\ P_{Eb} &= \frac{f_b Es}{f_o Es} P \end{aligned} \tag{73}$$

where f_bEs is the sporadic-E blanketing frequency, f_oEs is the maximum vertical incidence ordinary-ray frequency for the sporadic-E layer, and the probability P is determined by equation [37], as is done in IONCAP.

For the Sinno model, the empirical formula for the reflection coefficient r is given by

$$\begin{aligned} r &= \frac{1}{1 + 10p^n} \\ n = -\frac{2.077}{\log p_b} &= \frac{2.077}{\log f_o Es - \log f_b Es} \\ p_b &= \frac{f_b Es}{f_o Es} \end{aligned} \tag{74}$$

Then L_R is given by

$$L_R = -20 \log r = 20 \log (1 + 10p^n) \qquad (dB) \tag{75}$$

When $p_b = 0.55$ (a typical value for summer midnight), $n = 8$. When $p_b = 0.9$ (a typical daytime value), $n = 50$, such that L_R increases sharply for $f_v > f_oEs$; this implies a thicker layer with a relatively well-defined critical frequency. At $p = 1$ ($f_bEs = f_oEs$), $L_R = 21$ dB for all n . To estimate the obscuration loss L_o, it is assumed that the transmission coefficient τ is given by

$$\tau = \sqrt{1 - r^2} \tag{76}$$

giving L_o as

$$\begin{aligned} L_o &= -20 \log r \qquad (dB) \\ &= -10 \log \left\{ 1 - \left[\frac{1}{1 + 10p^n} \right]^2 \right\} \end{aligned} \tag{77}$$

When $n = 8$ (summer night), $L_R = L_o$ for $p = 0.67$; that is, the layer is equally reflecting and transparent when the equivalent vertical incidence frequency is about two-thirds of f_oEs . The parameter f_oEs is obtained in these formulas from Leftin et al. (1967). The values of f_bEs are estimated as a function of latitude (lat), day, and night from an expression due to Kolawole (1978)

$$f_bEs = \begin{cases} f_bEs^H = \left[0.5 + 0.2 \left(\frac{SSN}{100} \right) \right] f_oEs & |lat| \geq 70 \\ f_bEs^L = \begin{cases} 0.65\, f_oEs & night \\ 0.9\, f_oEs & day \end{cases} & |lat| \leq 50 \\ f_bEs^H \left(\frac{|lat| - 50}{20} \right) + f_bEs^L \left(\frac{70 - |lat|}{20} \right) & 50 < |lat| < 70 \end{cases} \tag{78}$$

Smith and Hatfield (1987) generally prefer the Sinno model.

The ground losses are calculated as in IONCAP at each reflection point.

The field strength in AMBCOM is calculated differently than in the other analytical programs. The field strength, e_f, for each mode is obtained by

$$e_f = \sqrt{120\pi p_o} * 10^3 \tag{79}$$

where the power density is

$$p_o = \frac{p_t g_t}{l} \tag{80}$$

and

$$l = 4\pi (P')^2 * l_{D2} * l_A * l_p * l_{Aur} * l_o * l_R * l_g. \quad (81)$$

with

P'	=	Group Path (m)
l_{D2}	=	divergence loss for F2 high-ray modes
l_A	=	absorption loss terms
l_p	=	F1-F2 deviative absorption
l_{Aur}	=	auroral absorption
l_o	=	Es obscuration loss
l_R	=	Es reflection loss
l_g	=	ground-reflection loss
p_t	=	power transmitted in watts
g_t	=	transmit gain relative to an isotropic

In AMBCOM, e_f is converted into decibel units by

$$20 \log e_f = E_f = P_o + 85.8 \quad (dB>1\ mv/m) \quad (82)$$

relative to 1-watt radiated; or equivalently

$$\begin{aligned} E_f &= P_o + 115.8 \quad (dB>1\ \mu v/m) \\ E_f &= 115.8 + P_t + G_t - L_b \end{aligned} \quad (83)$$

where P_t is the power transmitted in dB, relative to 1 watt, and G_t is the transmit antenna gain in dB, relative to an isotropic. This is the equation for field strength for a half-wave dipole over ground (Nielson et al., 1967). In AMBCOM, this field strength is converted to that of an isotropic antenna by adding 8.6 dB onto the free-space loss. In AMBCOM, the field strengths for each individual mode are not summed to obtain one value representing a particular frequency as in the other programs considered here. In AMBCOM, the antenna gains are interpolated from tables for each antenna type. These tables are given at 27 take-off angles and 15 frequencies.

STATISTICAL DATA PROCESSING

The CCIR (1990b) describes a preliminary standardized procedure for comparing predicted and observed sky-wave signal intensities at frequencies between 2 and 30 MHz. Such comparisons provide information on the accuracy of prediction methods and desirable improvements to them. To obtain comparable results, the CCIR suggests that the same data set and procedure be used when making comparisons between predicted and observed field strengths. They also suggest that their latest database be used. Although this allows the results to be compared to others by using their database, and even though most of the programs compared here will be like

those that the CCIR might be interested in, the PENEX database will be used instead. They also suggest that the comparisons should include the count, the mean differences, and the standard deviation. The data screening program described below outputs these parameters, as well as other parameters useful in determining the accuracy of a prediction program.

In the comparison of a program against measured data , it is highly desirable to subdivide the database into subsets according to variables influencing the predicted and observed results (e.g., path length, season, month, year, geomagnetic latitude, sunspot number, local time at path midpoint, etc.). The CCIR (1990b) suggest that the data be subdivided according to the frequencies transmitted, path great-circle distance, geomagnetic latitude, sunspot number, local time at path midpoint, origin of data, and ratio of transmitted frequency to predicted monthly median basic MUF. They suggest that the following parameters should be transferred to the comparison program: month, year, sunspot number, circuit identifier, frequency, great-circle distance, 24 predicted hourly values (always monthly median values) of sky-wave field strength in dB relative to μV/m, of path basic MUF, and of the percentage of the days per month when the frequency is below the path basic MUF. Based on the descriptions of the programs above, the following parameters should also be transferred to the comparison program: solar zenith angle, cosine of the solar zenith angle, E-layer critical frequency, E-layer MUF, secant of the angle of incidence on the D-layer, critical frequency of the sporadic-E layer f_oEs, the sporadic-E layer blanketing frequency f_bEs, and the magnetic index K_p. To accomplish this, a computer program called DASCR3 (acronym for Data Screening 3) will be used. This program will be the cornerstone of the PENEX HF prediction program comparison.

DASCR3

DASCR3 is a program designed to perform data screening and statistical comparison of two large matrices of observations—the observed data and the predicted data. For each set of matrices, up to 10 sets of information are read in on screening propositions to be satisfied and limits on a selected variable. In turn, a portion of each matrix is read in and tested for each set of propositions. For each subset satisfying a given set of conditions, the variable to be analyzed is stored temporarily on disc. The next portion of each matrix is then read in and screened, and the good observations are added to those already on disc. When the entire matrix has been screened, data are then read into core, and the difference (or residual) between the two matrices is taken. These arrays are then sorted, to ensure maximum computer efficiency for the statistical evaluation. Finally, a statistical evaluation is performed on the screened data and their residuals.

DASCR3 has been used extensively in past propagation prediction model analysis. The following samples are taken from this past work to show DASCR3 analytical outputs (Sailors, Moision & Brown, 1981). An example of the output from DASCR3 is shown in figure 4. In this sample, the ITSA-1 MUF prediction is compared to observed data. The proposition to be satisfied is the data to be evaluated for the month 1 (January). In the printout, the observed data are represented by column A and the predicted values represented by column B. The residual (the observed data minus the predicted value) is given by column D. The relative residual is given by column D/A, and the absolute relative residual, by column ABS (D)/A. The left-half side of the page shows the statistics calculated for each of these columns and includes the parameters suggested by the CCIR. In addition, the correlation coefficient between the observed and predicted data is given. Included also are the slope, intercept, and mean square error of

DATA SCREENING PROBLEM 1 ESSAITSA1(UNIV) HF PROPAGATION

CONDITIONS TO BE SATISFIED
MONTH EQ 1.000000

SUMMARY STATISTICS FOR VARIABLE 15 OBSERVED MUF PREDICTED MUF

STATISTIC	A	B	D	D/A	ABS(D)/A
TOTAL	4722.10	4929.80	-207.700	-20.0221	74.8681
POPULATION SIZE	288.000	288.000	288.000	288.000	288.000
AVERAGE	16.3962	17.1174	-.721180	-.695212-001	.259969
R.M.S. VALUE	18.0713	18.5028	1.92614	.997201-001	.479291
MEAN ABSOLUTE ERROR	6.48109	6.23854	.788841	.581069-001	.259738
STANDARD DEVIATION	7.59857	7.02492	1.85933	.714906-001	.402668
3RD MOMENT ABOUT MEAN	256.095	114.787	-42.1341	.116453-004	.185098
4TH MOMENT ABOUT MEAN	6728.90	4435.80	972.297	.607845-004	.284619
5TH MOMENT ABOUT MEAN	55936.0	27346.4	-6165.19	-.390453-006	.459818
6TH MOMENT ABOUT MEAN	.104155+J07	564099.	98842.0	.924003-006	.774823
LOWER DECILE	7.78750	9.14708	-5.69917	-.158918	.141667-001
LOWER QUARTILE	9.52083	10.1660	-2.35834	-.124982	.472322-001
MEDIAN QUARTILE	15.2083	16.0792	-1.21669	-.680700-001	.110185
UPPER QUARTILE	21.9791	22.7201	1.36250	-.269668-001	.267593
UPPER DECILE	28.4972	27.1050	5.99083	.628031-001	.725648
.00TH PERCENTILE	.000000	.000000	.000000	.000000	.000000
.00TH PERCENTILE	.000000	.000000	.000000	.000000	.000000
SEMI-INTERQUARTILE RANGE	6.22916	6.27708	1.88042	.490076-001	.115185
COEFFICIENT OF VARIATION	.463436	.410398	-5.35141	-1.02833	1.52897
MINIMUM	0.00000	0.00000	-13.6000	-.238806	.000000
MAXIMUM	32.0000	33.0000	9.20000	.647729-001	.228809
COEFFICIENT OF SKEWNESS	.311340	.331106	-1.73989	-.318717-001	2.75847
COEFFICIENT OF EXCESS	-.981562	-1.17860	1.58279	-.672996	7.78814
INTERVAL SIZE	5.00000	5.00000	2.28000	.305531-001	.226667
GIVEN LOWER BOUND	.000000	.000000	.000000	.000000	.000000
GIVEN UPPER BOUND	50.0000	50.0000	.000000	.000000	.000000
CORRELATION COEFFICIENT	.663568				

A MATRIX = OBSERVED

MEAN SQUARE ERROR	15.414810
LINEAR MEAN SQUARE ERROR	14.67997
SLOPE	.934087
INTERCEPT	.407082

Figure 4. Output example from DASCR3.

linear regression. In this example, 288 data points were selected from 4668 data points by DASCR3. The average absolute relative residual for this case is 25.9%. As this is an early application of the data screening program, this particular example does not include the capability to determine a probability distribution representing the residuals described below.

SCREENING DATA BASE

In the following examples, each computer program was run to produce a database corresponding to the observed database. Auxiliary information outputted by the prediction program for screening in this particular application included the following: universal time of propagation; month; year; sunspot number; path length, in kilometers; geographic latitude and longitude of the path midpoint; the local time at path midpoint; the path orientation with respect to North; the geomagnetic latitude at each of the control points; the predicted MUF; E-Layer MUF; F-layer MUF; FOT; HPF, and path identification.

Before the actual data screening started, data points in both observed and predicted bases corresponding to observed values at the extremes of the particular measurement site were removed. In other words, obviously pathological outlying data were removed.

ANALYSIS OF RESIDUALS

Introduction

An indication of the accuracy of the numerical predictions of a parameter, the MUF in this case, can be obtained from a study of the residuals between observed data and predicted values. The terms, *residual*, *relative residual*, and *absolute relative residual* are used with the following standard meaning:

$$\begin{aligned} Residual &= (Observed\ Datum) - (Predicted\ Value) \\ Relative\ Residual &= \frac{Residual}{Observed\ Datum} \\ Absolute\ Relative\ Residual &= \frac{Absolute\ Residual}{Observed\ Datum} \end{aligned} \tag{84}$$

Certain statistical measures of these terms have proven useful in past ionospheric studies comparing predicted and observed data. These include the following:

1. The average residual (avg. res.)
2. Root-mean-square residual (rms res.)
3. Mean absolute error of the residual (mae res.)
4. Average relative residual (avg. rel. res.)
5. Root-mean-square relative residual (rms rel res.)
6. Mean absolute error of relative residual (mae rel. res.)
7. Average absolute relative residual (avg. abs. rel. res.)

8. Correlation coefficient between observed and predicted values
9. Standard error of the estimate of linear regression
10. The fit of the residual distribution to an empirical probability distribution.

Examples of each of these parameters, as produced by DASCR3 (except the last), are shown in figure 4 (Sailors, Moision & Brown, 1981).

Description of Parameters

The average residual and the average relative residual locate the center of the distributions of error, and they are sometimes referred to as the "bias" in the estimate. Figures 5 and 6 (Sailors, Moision, & Brown, 1981) illustrate the average residual and the average relative residual, respectively, as a function of month for the four programs compared. In this example, MINIMUF-3.5 is shown to have the smallest bias; whereas, HFMUFES4 tends to always predict high by as much as 3.5 MHz, or 17.5%.

The mean absolute errors of the residual and the relative residual are a measure of the range of error. The errors are the first moments about the average residual and average relative residual, respectively. They provide information about the range of variation. Figures 7 and 8 (Sailors, Moision, & Brown, 1981) are examples of these two parameters, respectively, for MINIMUF-3.5. They are displayed as bars about the average residual (bias) as a function of month; however, figure 5 (Sailors, Moision, & Brown, 1981) shows that during the equinox months of March and September, the range of variation in the error is greater than the other months.

The average absolute relative residual is a measure of the average magnitude of the error. Figure 9 shows a plot of the average absolute relative residual as a function of month for the four programs being compared.

The root-mean-square residual and relative residual are measures of the dispersion in the error. In fact, the RMS residual and the RMS relative residual are the standard deviations of the error about the origin (zero bias), and they are related to the standard deviation about the mean according to

$$\sigma^2 = \nu_2 - \nu_1^2 \tag{85}$$

where ν_2 is the mean square error (the square of the RMS error), and ν_1 is the bias. When the bias is small, or nearly zero,then the standard deviation and the RMS error are nearly the same. Otherwise, the rms error is larger than the standard deviation. Figures 10 and 11 (Sailors, Moision, & Brown, 1981) are examples of the RMS residual and RMS relative residual, respectively, for the four programs being compared to as a function of month. MINIMUF-3.5 has the lowest RMS error, reaching its highest value of 4 MHz (plus 12%) during October; whereas, HFMUFES4 has its lowest values during the summer months, but has the highest RMS error during the winter months.

A measure of the degree of association, or the closeness of fit, between variables is given by the correlation coefficient. It indicates the strength of the tendency for high (or low) values of one variable to be associated with high (or low) values of the other variable. Figure 12 (Sailors, Moision, & Brown, 1981) is an example of the correlation coefficients as a function of month

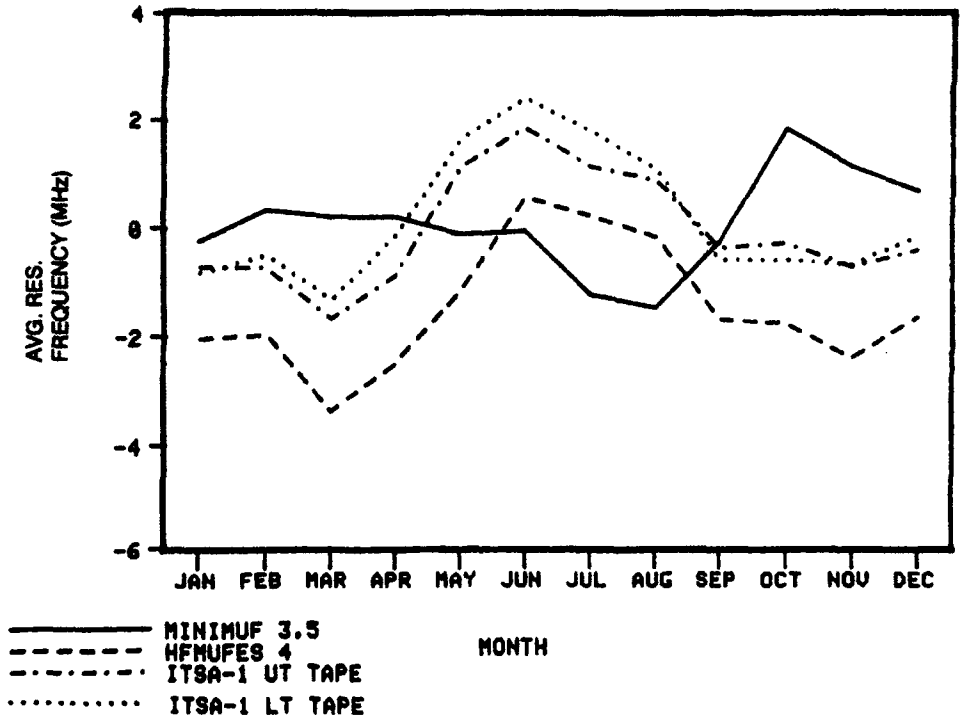

Figure 5. Average residual (bias) as a function of month.

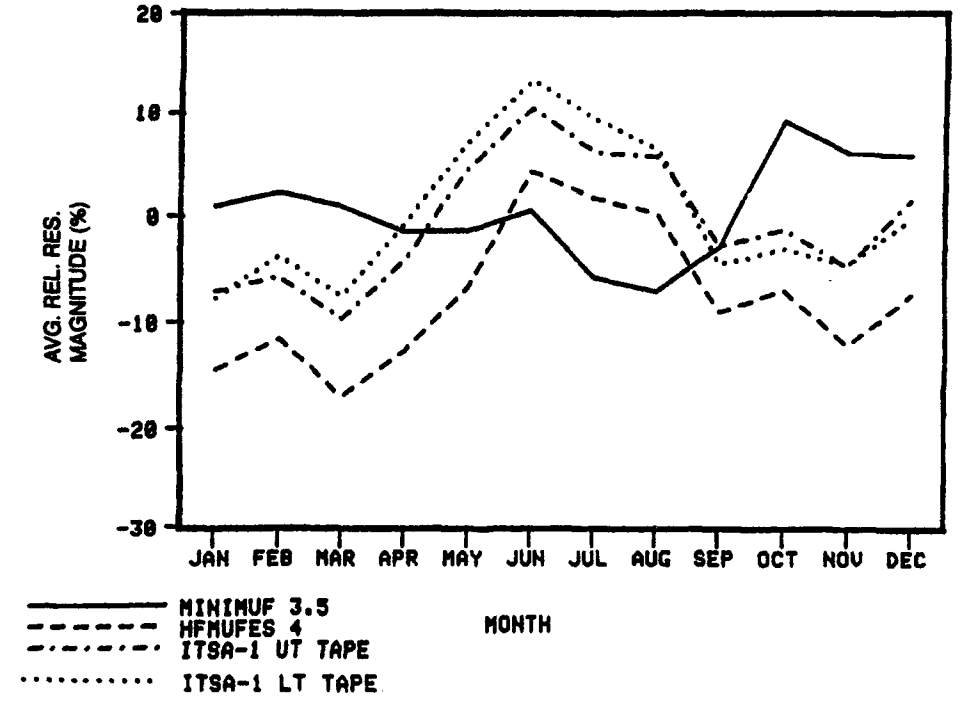

Figure 6. Average relative residual (relative bias) as a function of month.

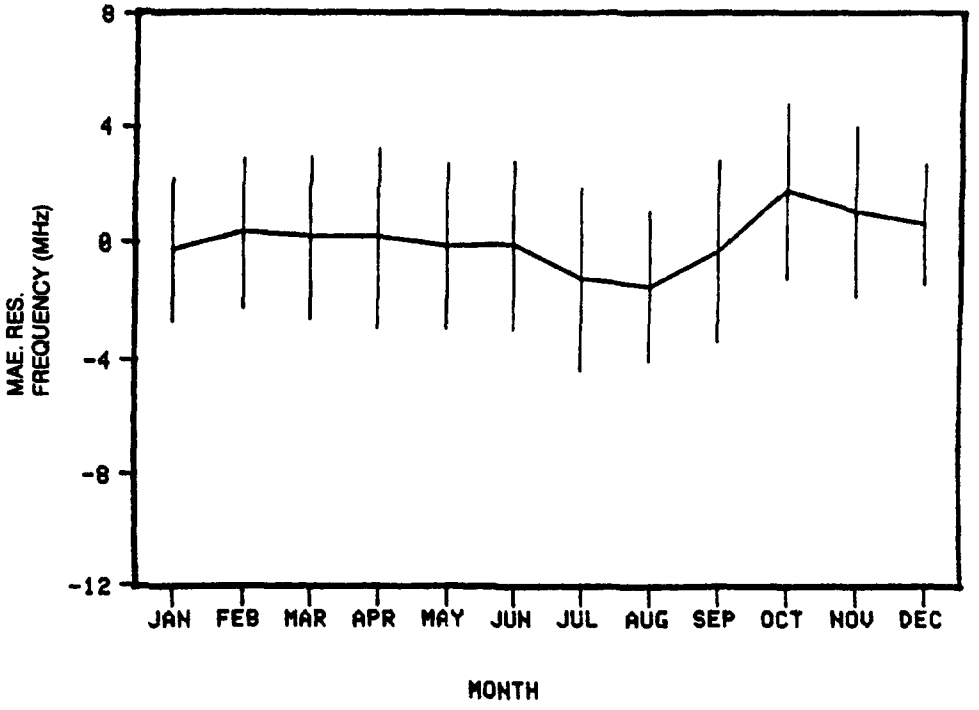

Figure 7. Average residual (bias) for MINIMUF-3.5 with the mean absolute error about the relative residual.

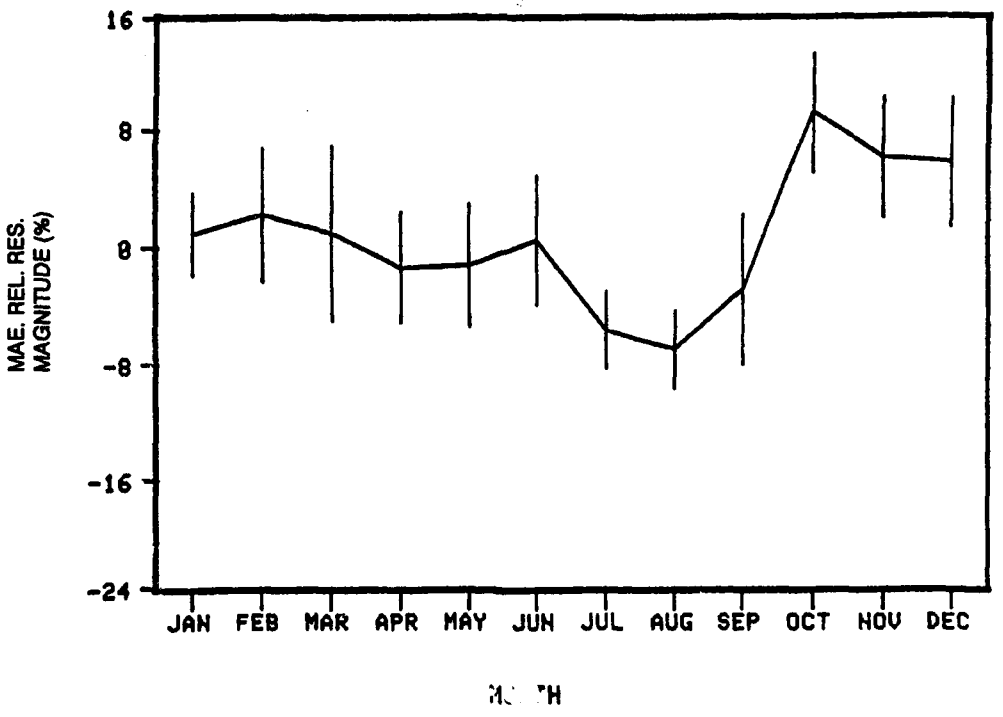

Figure 8. Average relative residual (relative bias) for MINIMUF-3.5 with the mean absolute error about the average relative residual.

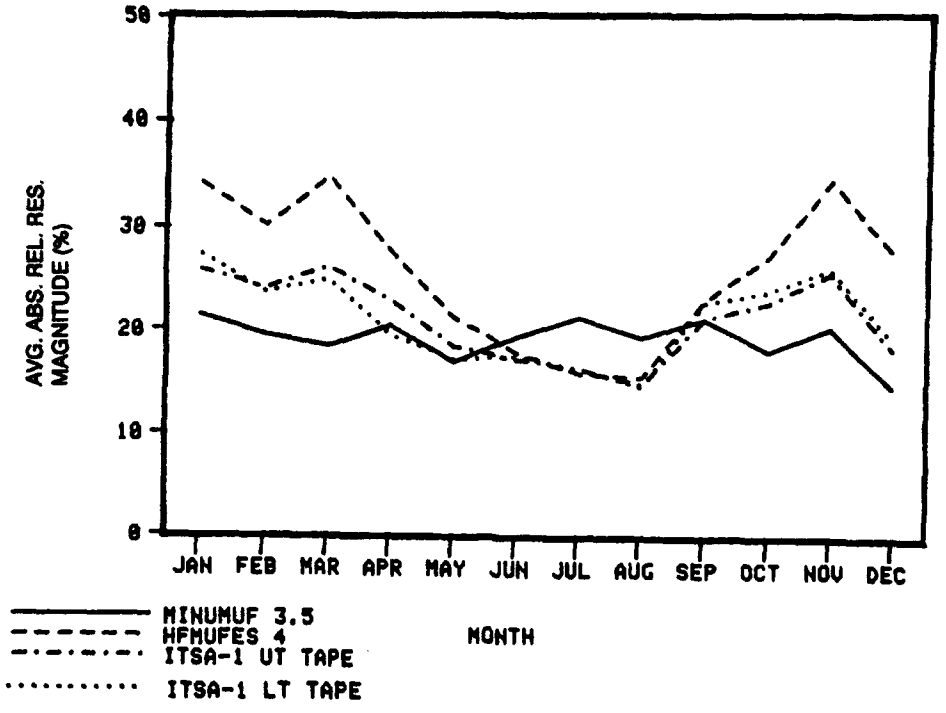

Figure 9. Magnitude of the error (average absolute relative residual) as a function of month.

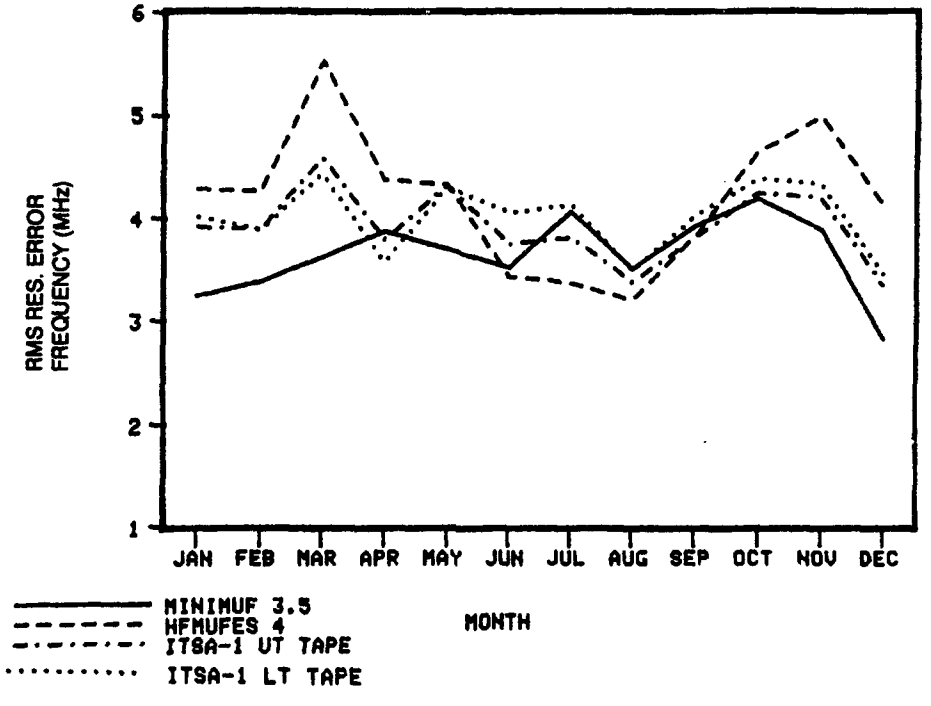

Figure 10. Rms error (in MHz) as a function of month.

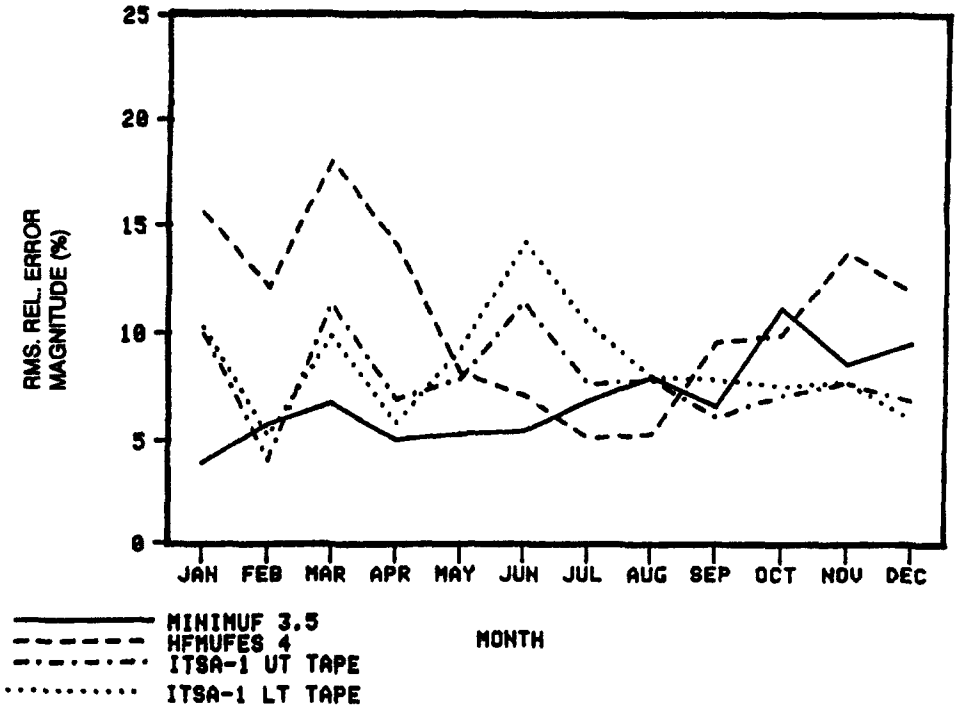

Figure 11. Rms relative error (in percent) as a function of month.

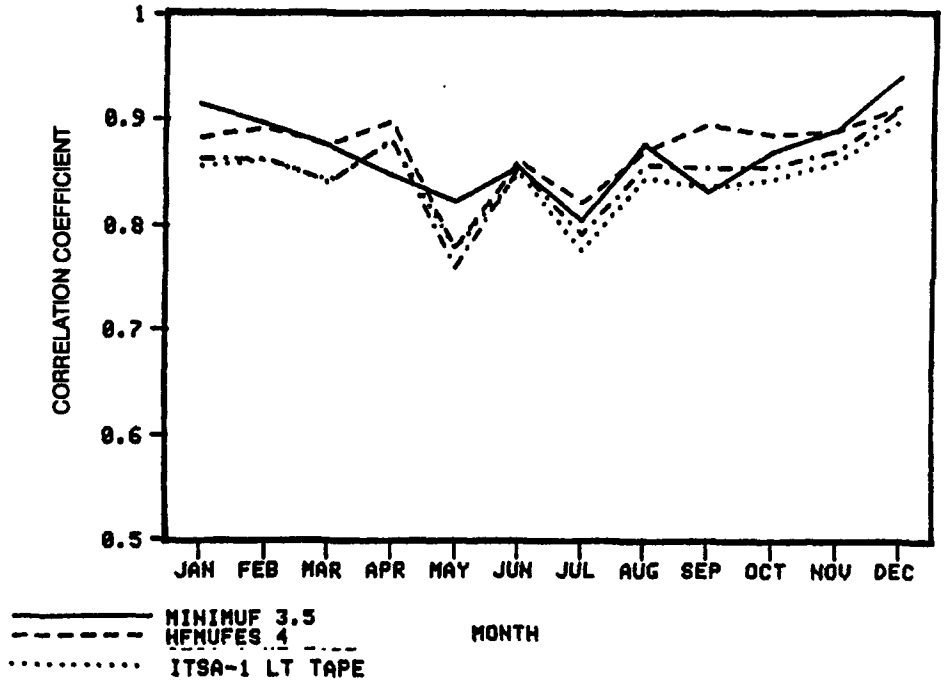

Figure 12. Correlation coefficients as a function of month.

for the four programs being compared. In this example, HFMUFES4 generally has the highest correlation coefficient with MINIMUF-3.5 also showing consistently high values. A low value of the correlation of an auxiliary parameter may mean that the auxiliary parameter is not important in the determination of accuracy. In this example from a previous accuracy study, it was found that the E-MUF was not important in the determination of the MUF; hence, in subsequent accuracy studies of the MUF, the E-MUF was not used as an auxiliary parameter.

A description of the nature of the relationship between variables is called regression analysis. Regression analysis is concerned with the problem of describing, or estimating the value of, one variable, called the dependent variable, on the basis of one or more other variables, called independent variables. In other cases, regression may be used merely to describe the relationship between known values of two, or more, variables.

Regression analysis that involves the determination of a linear relationship between two variables is referred to as simple linear regression. Here, the variable y is given as $y = a + bx$, where x is the independent variable, and y is the dependent variable. The coefficients, a and b, are determined in the regression analysis. A measure of the success of linear regression analysis is the standard error of the estimate give by

$$S_{y.x} = \sqrt{\sigma_y^2 \ (1 - \gamma^2)} \tag{86}$$

where σ_y is the standard deviations in the observed datum, and the γ is the correlation coefficient between the observed data and the predicted values. If the relationship is truly linear, then the bias of the estimate should be removed (or made nearly zero). An estimate of the standard error of the mean is

$$S_{\bar{y}.x} = \frac{S_{y.x}}{\sqrt{n}} \tag{87}$$

A measure of the error in the regression coefficient is given by

$$S_b = \sqrt{\frac{S_{\bar{y}.x}}{\sigma_x}} \tag{88}$$

where σ_x is the standard deviation in the predicted values. The parameter n is the population size. Figures 13 and 14 (Sailors, Moision, & Brown, 1981) show the standard error of the estimate of linear regression, and of standard error of mean in linear regression, respectively, as a function of month. When figure 13 is compared to figure 12 (Sailors, Moision, & Brown, 1981), the largest change occurs for HFMUFES4. Very little change is shown for ITSA-1 with local time tape. MINIMUF-3.5 shows some changes for some months, but not all. Figure 13 shows that linear regression has removed much of the bias in the predicted MUFs.

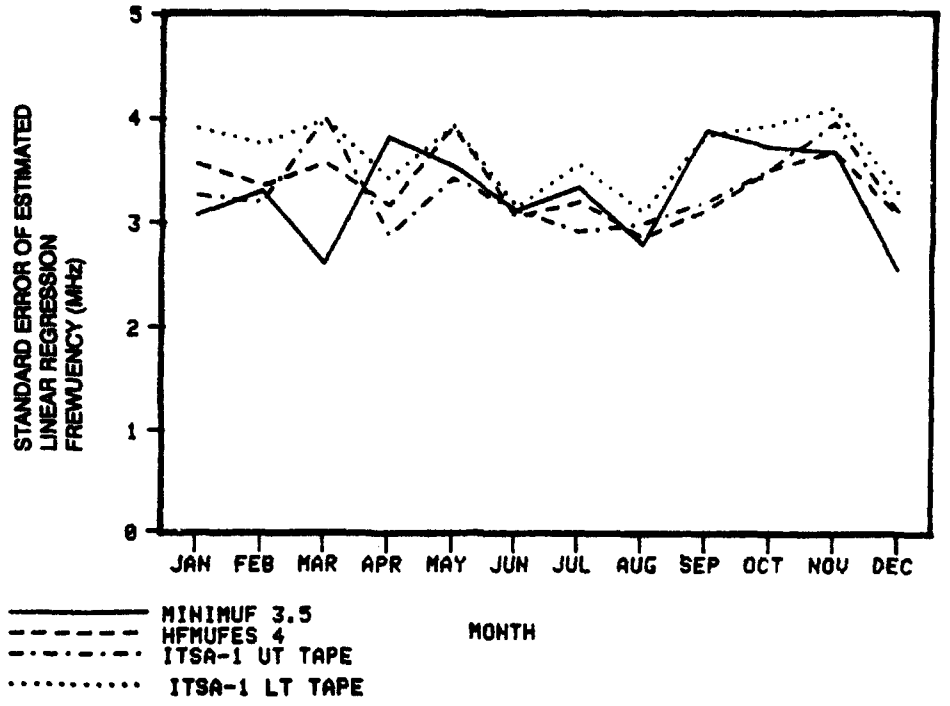

Figure 13. Standard error of estimate of linear regression as a function of month.

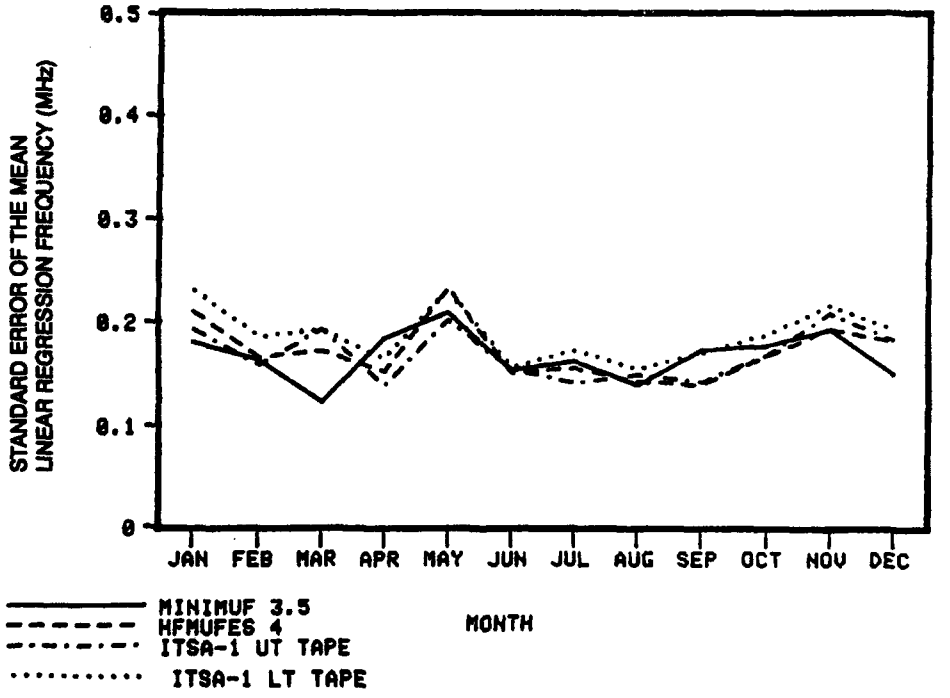

Figure 14. Standard error of the mean of linear regression as a function of month.

In the application used to describe the data screening program, it turned out that HFMUFES4 had the largest bias (7.2%), rms error (8.3%) and magnitude of error (26.09%). An explanation was given for HFMUFES4's poor results. The fact that HFMUFES4 showed a large reduction in the standard error of regression as a function of range, as compared to the rms error, led to the conclusion that the f_oF2 model was in error; that is, the f_oF2 is the linear portion of the MUF model. Had the results not shown a reduction in the standard error of regression, as compared to rms error, then the error in the MUF model would have been due to the non-linear portion—the M-factor model. Possibly as a result of this study, newer prediction programs, such as IONCAP, did not use the set of f_oF2 coefficients that were used in HFMUFES4.

Example of DASCR3 Usage to Improve a Model

Figures 15 through 20 describe the accuracy of QLOF Version 2.0 as a function of local time at the path midpoint by using several of the statistical measures of error discussed above (Sailors and Moision, 1987). The bias is nearly zero, from 6 to about 17 local mean time (LMT). Since QLOF is basically a daytime model, these results are encouraging; however, at night, the model is more than 1.0 MHz (20%) low on the average, and the relative rms error is more than 30%, as compared to 20% for daytime. At night, the average absolute relative residual is as high as 30%, as compared to values around 15% during the day. At night, there are some hours when the correlation coefficient has a significant decrease. The error at night was probably because the LUF in QLOF Version 2.0 is set to 2 MHz at night.

Because of this error at night, QLOF was modified to include nightly D-region absorption by using a model due to Wakai (1961; 1971) and Wakai et al. (1971). This was accomplished by adding Wakai's nighttime sunspot number dependence into the existing absorption model. The nighttime sunspot number dependence is given by

$$I_n = 0.025 * (1 + 0.013 * R_{12}) . \qquad (89)$$

The new sunspot number dependence replaces the existing dependence whenever the solar zenith angle at the control point exceeds approximately 103 degrees. The QLOF Version 2.1 showed considerable improvement over Version 2.0. Table 9 contains a comparison of the accuracy of Version 2.0 and Version 2.1 over the entire database of observed LOFs. It is divided according to the time of day. In each cell in the table, two values are given for the particular statistical parameter: the first value is for Version 2.0; the second, is Version 2.1. This database consisted of 1814 LOF monthly median LOF observations over a range of path lengths, seasons, geographical locations, times and sunspot numbers. It is described in detail by Sailors and Moision (1987).

Table 9. Comparison of the accuracy of QLOF Versions 2.0 and 2.1 for day and night.

Statistical Parameter	Time of Day	
	Daytime	Nighttime
Bias (MHz)	.682/.545	1.16/.063
RMS Error (MHz)	2.02/1.94	1.80/1.26
Correlation Coefficient	.845/.854	.716/.762
Number of Data Points	1,371 (75.6%)	443 (24.4%)

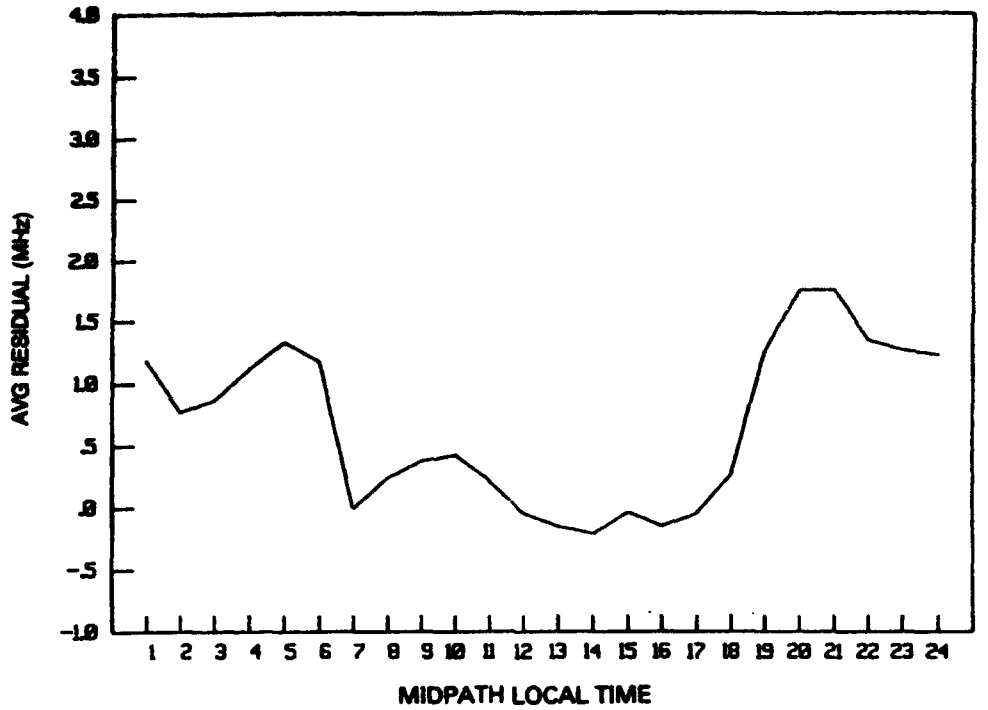

Figure 15. QLOF Version 2.0 average residual as a function of midpath local time.

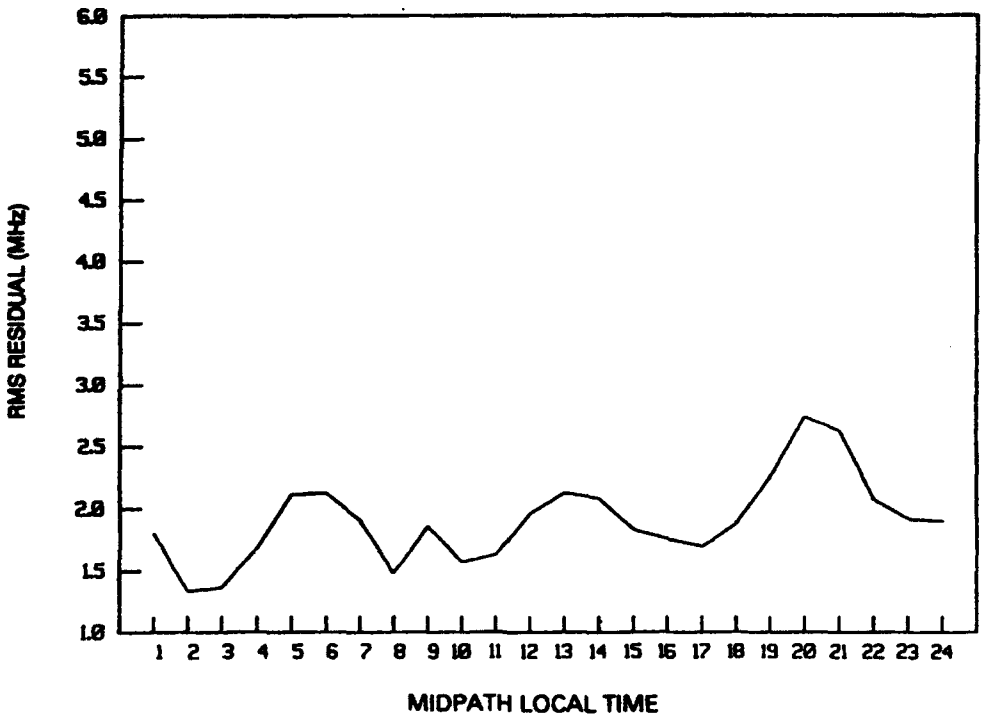

Figure 16. QLOF Version 2.0 root-mean-square residual as a function of midpath local time.

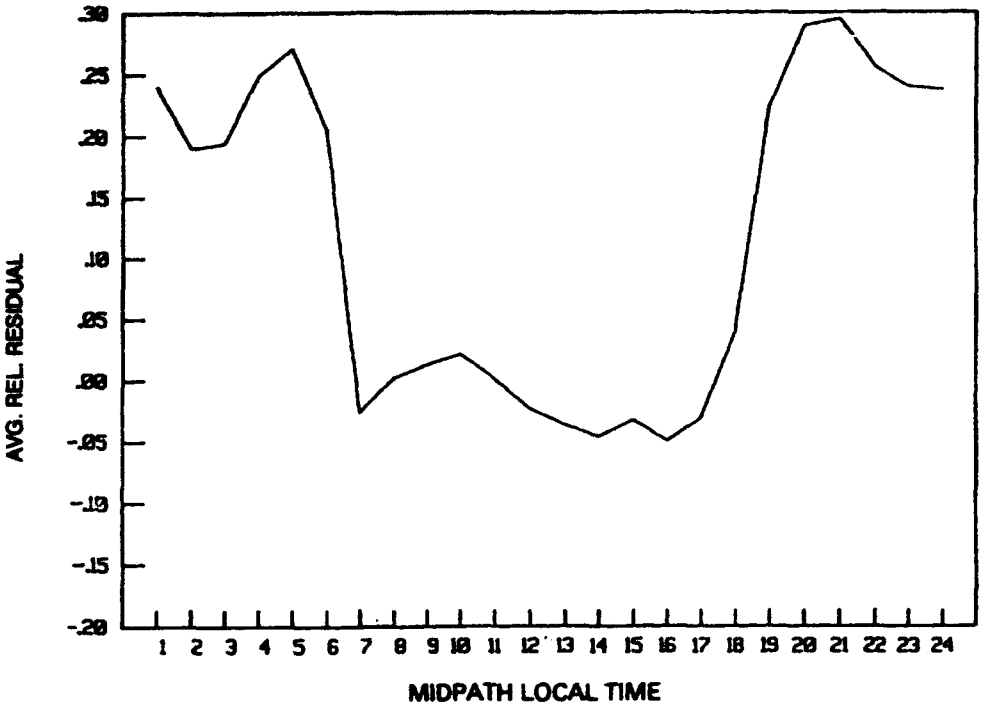

Figure 17. QLOF Version 2.0 average relative residual as a function of midpath local time.

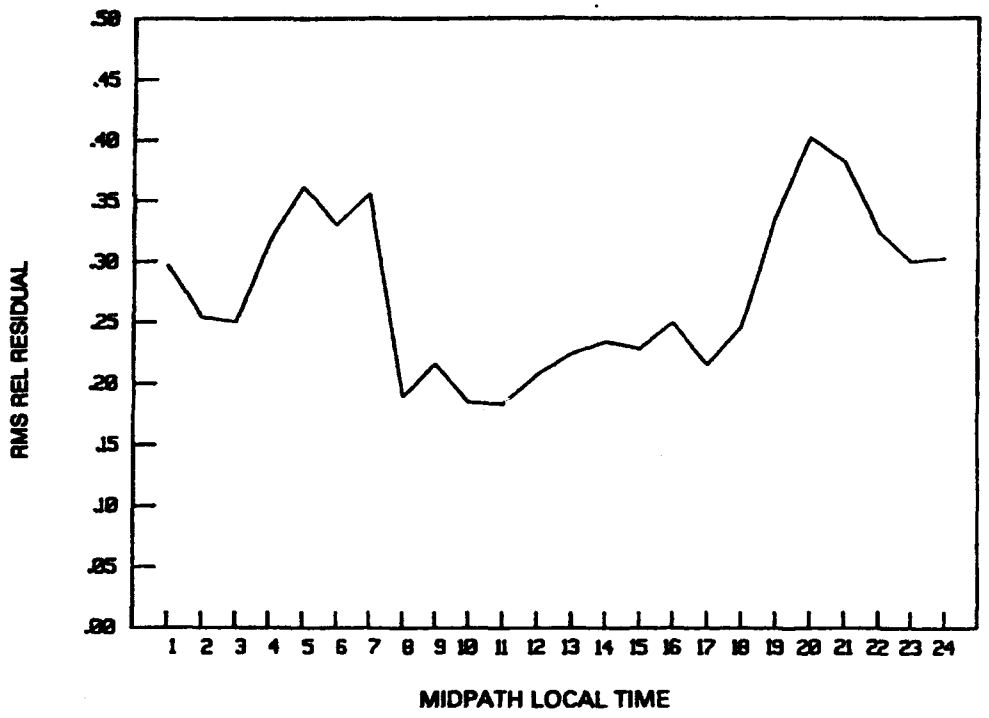

Figure 18. QLOF Version 2.0 root-mean-square relative residual as a function of midpath local time.

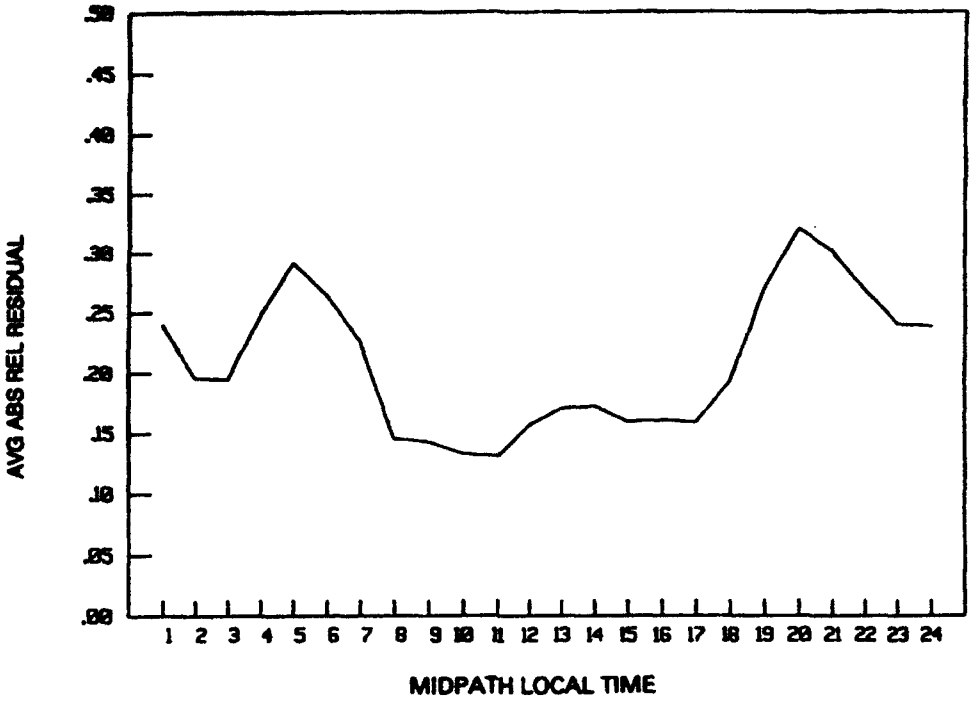

Figure 19. QLOF Version 2.0 average absolute relative residual as a function of midpath local time.

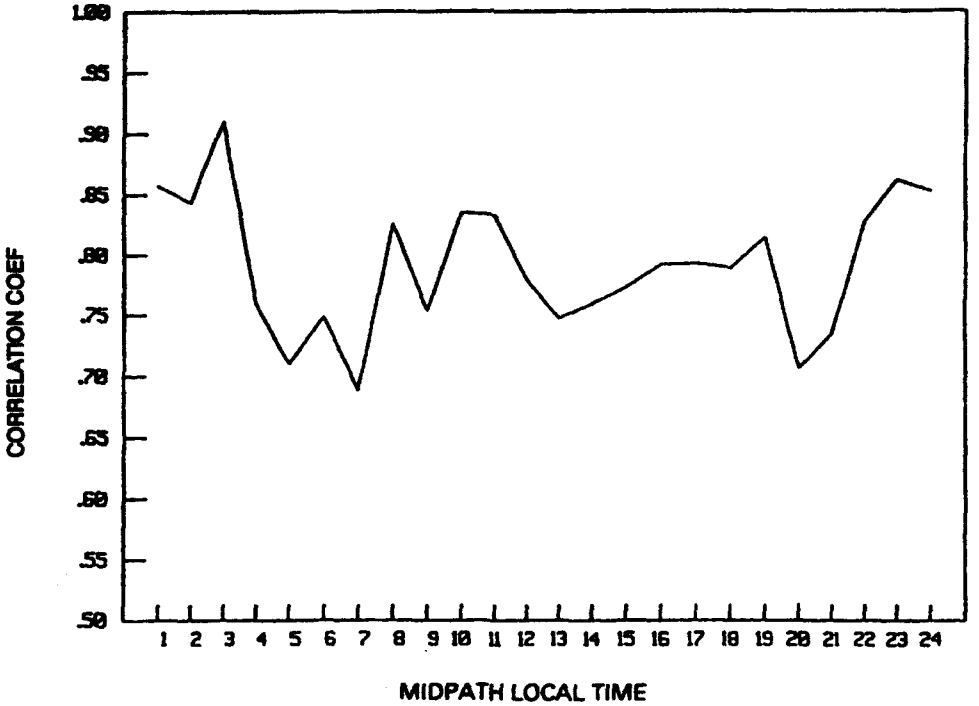

Figure 20. QLOF Version 2.0 correlation coefficient as a function of midpath local time.

The results presented in table 9 show that the bias of Version 2.1 is markedly reduced from that of Version 2.0. This is especially noticeable in the nighttime results. Similarly, there is an improvement in the rms error for Version 2. The Version 2.1 bias, as function of midpath local time, is shown in figure 21. This figure should be compared to figure 22, which shows similar results for Version 2.0. Immediately noticeable is the reduction in the bias in Version 2.1 for midpath local times after 1700 hours and before 0700 hours. Figures 21 and 22 also indicate the standard deviations of the residual distribution at each hour.

Empirical Error Probability Distribution

An additional capability in the data screening program, which may prove useful in the PENEX project, is its ability to fit an empirical distribution function to the probability distribution representing the residuals (the errors) between the observed parameters and the corresponding predicted parameters. The residuals for a particular model are fit to a Johnson system of frequency curves (Johnson, 1949) by using an algorithm, which is credited to Hill et al. (1976), Hill, Hill, & Holder (1976), Hill & Wheeler (1981), Dodgson & Hill (1983), that uses the methods of moments to obtain the required parameters. This distribution represents all univariate distribution systems. Its simplicity of calculation, once the Johnson parameters have been determined, makes it adaptable to minicomputer and microcomputer applications because the transformation of the Johnson variables to the normal system allows the use of normal probability algorithms in its application. The nature of distribution and an example of its application follow. The discussion of the determination of its parameters can be found in Sailors (1987a; 1987b).

The Johnson curves are an empirical family of curves satisfying the following chosen conditions: (1) they should be easy to evaluate once their parameters are determined; (2) they are a monotonic function of y, where $y = x(-\xi)/\lambda$, λ is a scale factor, ξ is a location factor of the distribution, and x is the variable being represented by the distribution; (3) the range of values of f(y), corresponding to the actual range of values of y, should be from $-\infty$ to $+\infty$, and (4) the resulting system of distributions of y (and so of x) should include distributions of most, if not all, of the kinds encountered in collected data. The Johnson system of frequency curves consist of the following three types:

$$\begin{aligned}
&\text{the lognormal system (or } S_L\text{):} && z = \gamma + \delta \ln\left[\frac{x-\xi}{\lambda}\right], && \xi < x, \\
&\text{the unbounded system (or } S_U\text{):} && z = \gamma + \delta \sinh^{-1}\left[\frac{x-\xi}{\lambda}\right], && -\infty \le x \le \infty \\
&\text{the bounded system (or } S_B\text{):} && z = \gamma + \delta \ln\left[\frac{x-\xi}{\xi+\lambda-x}\right], && \xi < x < \xi+\lambda
\end{aligned} \tag{90}$$

where z is the standardized normal variate in each case. The parameters γ and δ determine the shape of the distribution of x.

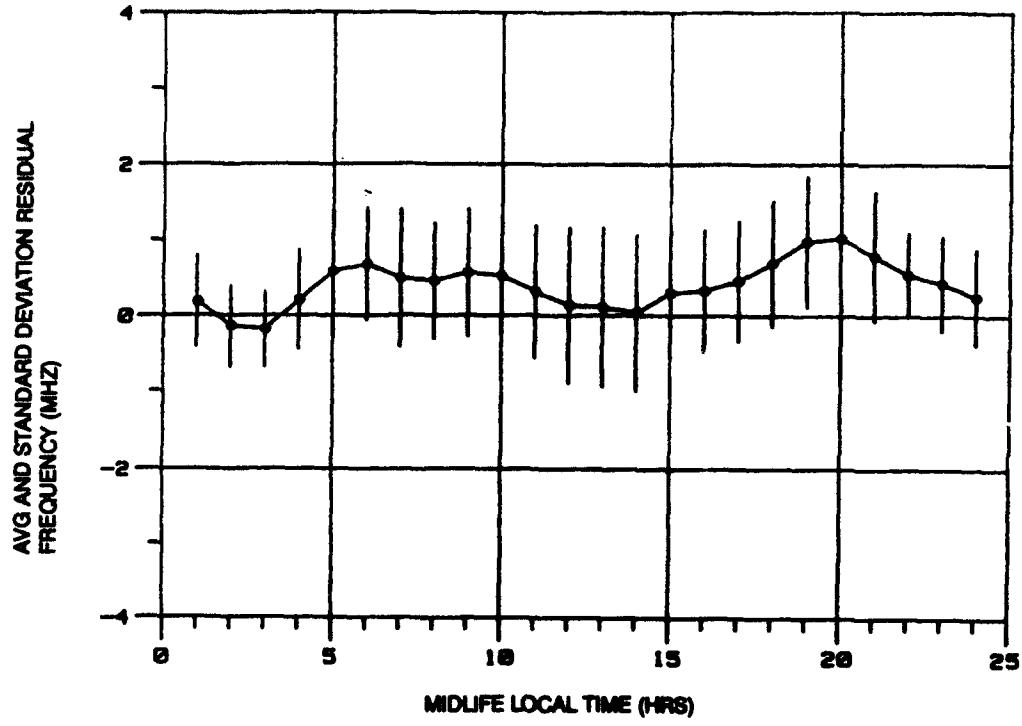

Figure 21. QLOF Version 2.1 average residual and standard deviation of the residuals as a function of midpath local time.

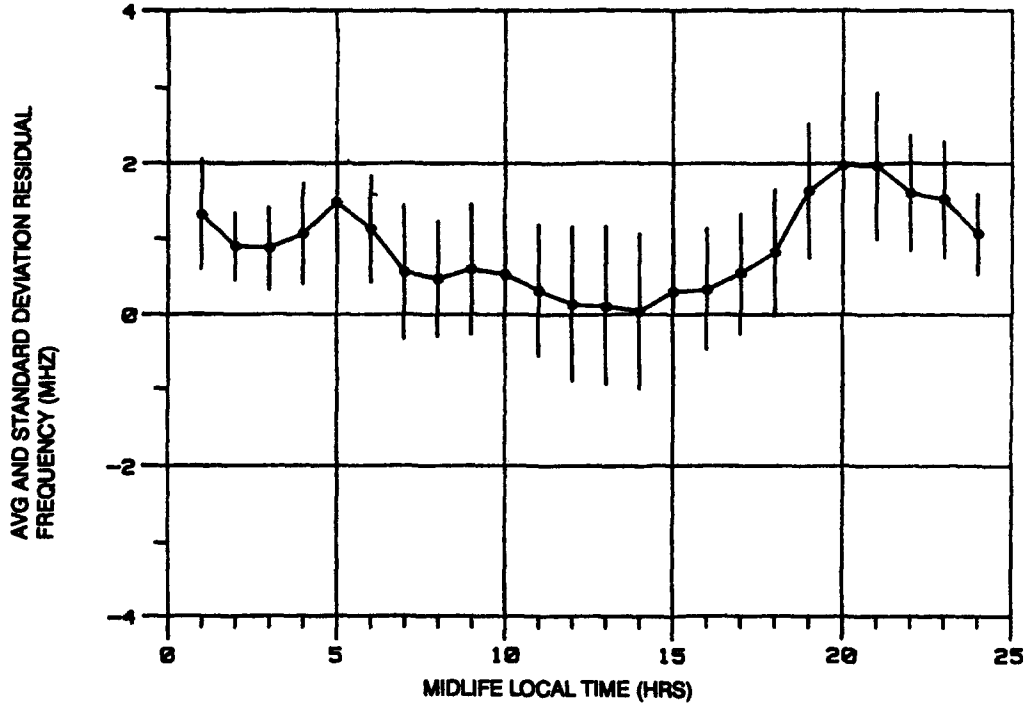

Figure 22. QLOF Version 2.0 average residual and standard deviation of the residuals as a function of midpath local time.

To decide which one of the three Johnson families should be used for a given set of data, the usual procedure is to obtain the data estimates of the third and fourth statistical moments about the mean—the skewness $\sqrt{\beta_1}$ and kurtosis β_2. These are then plotted on a graph such as figure 23. Also shown are other common sampling distributions: normal (N), Student's t, Rayleigh (R), and gamma (or χ^2). Figure 24 shows data plotted in the (β_1, β_2) plane by Sailors (1981) that show the propagation properties of the lowest observable frequency (LOF) measured on the France-to-Iceland path during 1975. In the case of the LOF data, the distribution was shown to be the S_B type of the Johnson curve.

The data screening program automatically determines which one of the three Johnson families should be used by a given set of data. It then determines the parameters for that particular curve. An algorithm called JNSN, known by the Royal Statistical Society as algorithm AS 99, is used (Hill et al., 1976; Hill & Wheeler, 1981; Dodgson & Hill, 1983: Griffiths & Hill, 1985). This algorithm uses the first four sample moments to determine the type of Johnson curve and its parameters. When the moments are large, the method of moments are not always statistically efficient; consequently, alternate methods are used to obtain a second set of parameters. These methods include (1) maximum likelihood (Hahn & Shapiro, 1967; Johnson, 1949), (2) the use of quantiles or percentiles (Hahn & Shapiro, 1967; Johnson, 1949), and (3) the use of frequency moments (Ord, 1972). The particular method used depends on the Johnson curve being evaluated. A chi-square test of fit is used to choose between the sets of parameters so chosen (Hahn & Shapiro, 1967; Williams, 1950). A 5% level of significance is used.

After determining the Johnson distribution parameters by using the data screening program, it might be applied in one of two ways. The first way is, that for a given probability, it might be desired to know the error in the model. The second is, that given a certain error in the model, what is the corresponding probability? The algorithms necessary for these two applications are contained in Sailors (1987a) and discussed below.

In the first application, the given probability is converted to the corresponding normal standard deviate by using the algorithm function PPND (Beasley & Springer, 1977; Griffith & Hill, 1985). Then, the corresponding Johnson deviates are found by using the algorithm AJV (Dodgson & Hill, 1983; Griffiths & Hill, 1985; Hill, 1976; Hill & Wheeler, 1981). The parameters necessary as input are outputted by the data screening program. The Johnson deviates are the error for the model being employed.

In the second application, the given error is converted to normal standard deviates by using the second algorithm SNV due to Hill (1976), Dodgson & Hill (1983), Griffiths & Hill (1985), Hill & Wheeler (1981). Then the corresponding probability level can be found by using a normal integral algorithm (Hill, 1973) called ALNORM. This particular algorithm has the capability to calculate either the upper or lower tail area of the standardized normal curve corresponding to any given argument.

A sample of the Johnson distribution application is given in figure 25. This figure of the MUF model in HFBC84, shows the residual variation as a function of path range. The predicted residual is given for seven different standard normal deviates (snv) and their corresponding probability levels. The residuals range from values that might occur from 0.1% to 99.9% of the time.

These same tools will be used in the analysis and presentation of the PENEX field strength data.

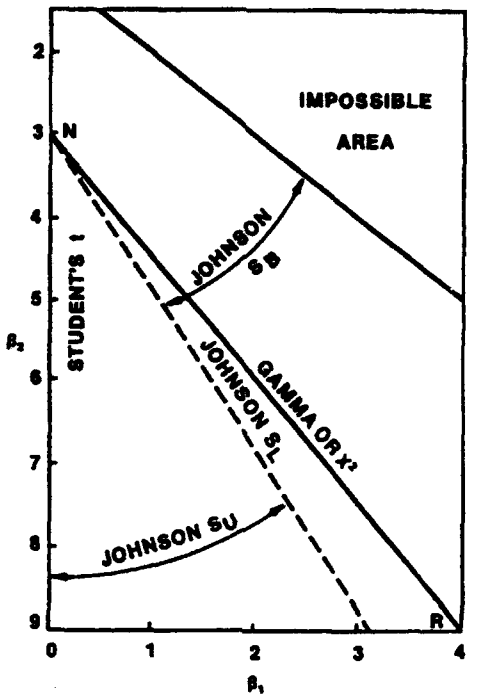

Figure 23. Region in (β_1, β_2) plane for the Johnson system of curves.

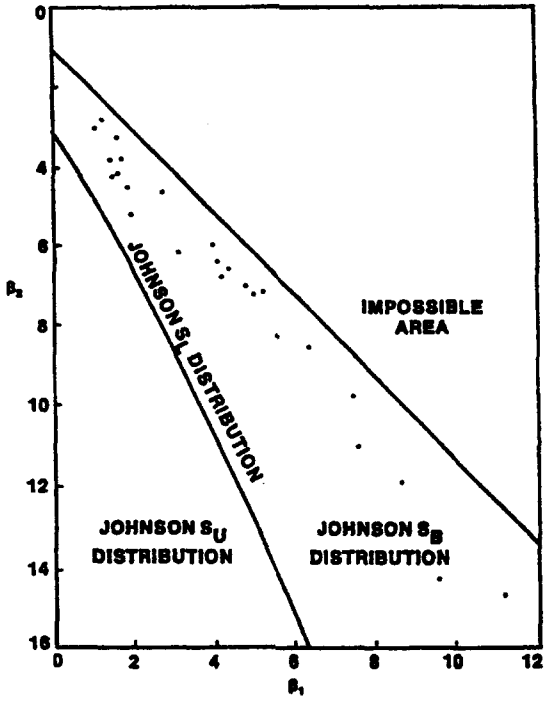

Figure 24. LOF propagation properties for the France to Iceland path, October 1975.

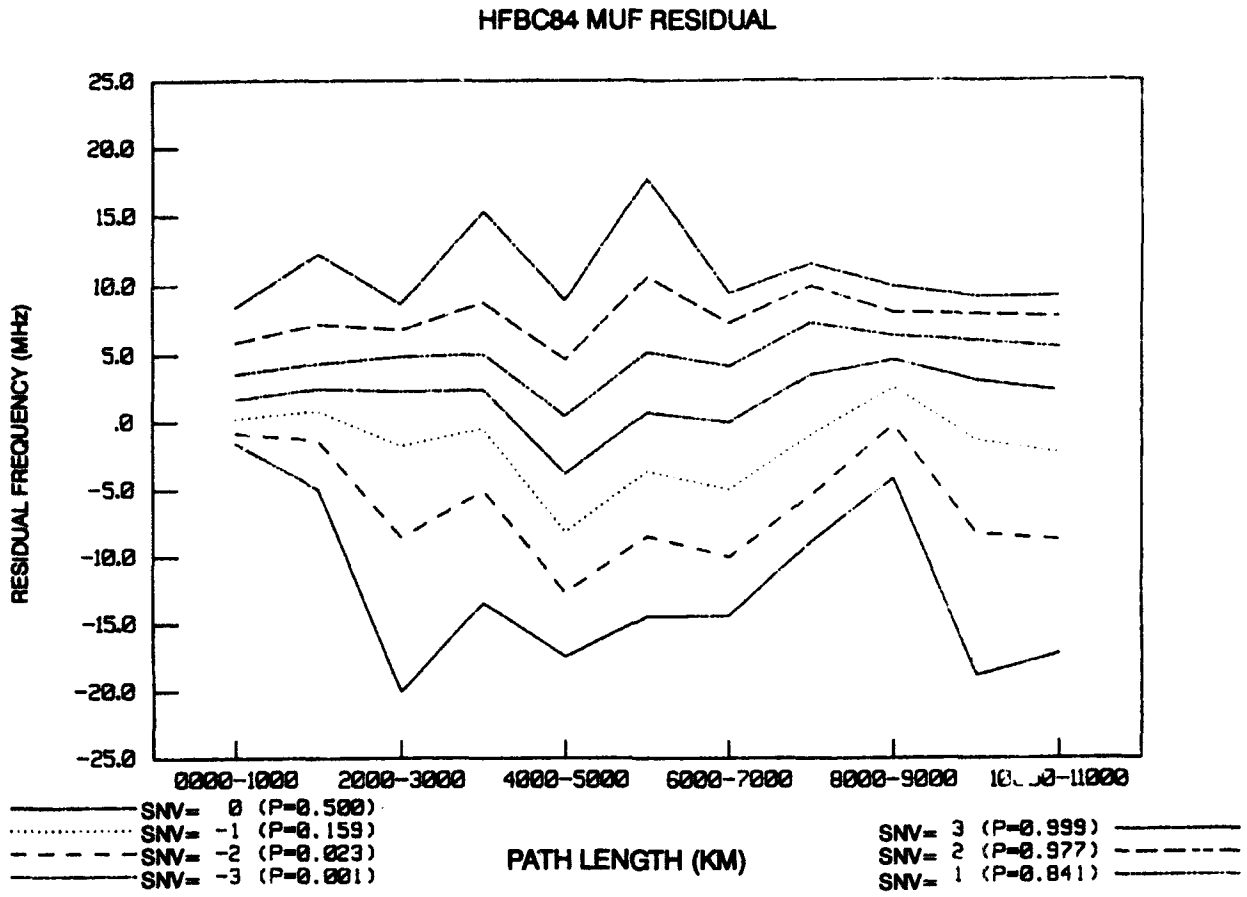

Figure 25. Predicted residual for the HFBC84 MUF for the given standard normal deviates and their corresponding probability levels with path range.

CONCLUSIONS

This report has reviewed how seven HF propagation prediction programs derive field strength. This review included three empirical programs (Medusa PROPHET, FTZ, and FTZ4), and four analytical programs (HFTDA, IONCAP, ASAPS and AMBCOM). Although Medusa PROPHET uses the FTZ approach, the derivation of f_m and f_l is quite different.

All of these analytical approaches contain similar structures. The first term is a constant that has been derived from summing a number of constants along with several conversion factors. A second term accounts for the frequency that is in use, and the third term is a loss term. There are two basic analytical approaches in propagation prediction, the Lucas approach, which spawned versions from ESSA-ITSA1 through IONCAP, and the ray tracing approach used in AMBCOM.

The prediction schemes produce median predictions of the rms field strength. When FTZ produces a value (e.g., 65 dB above 1 microvolt per meter), it is a median value for a given hour in a given month. The median value is bounded by the description of the distribution of the error about that median. The primary value in the PENEX comparisons is in determining the size of the standard deviations and variances, such that the median value is bounded.

The implementation of the data screening program DASCR3 will allow the development and generation of a powerful statistical description of the measured field strength characteristics and of how accurately the seven candidate programs predict observations. It offers all the statistical requirements suggested by the CCIR (1990b) for the determination of the accuracy of a field strength prediction program. Its ability to allow and store up to 40 different auxiliary variables allows the comparison to be sub-divided into the required categories. In fact, 17 auxiliary variables for this effort were identified as desirable parameters to be added to the data screening database. These variables include: the month; year; sunspot number; circuit identifier (name and path transmitter and receiver coordinates); frequency; great-circle distance; 24 predicted hourly values (always monthly median values) of sky-wave field strength in dB relative to 1 μV/m, of path basic MUF, of the percentage of the days per month when the frequency is below the path basic MUF, of solar zenith angle and cosine of the solar zenith angle at path midpoint, of E-layer MUF; 24 predicted hourly values at each reflection point (control point) of E-layer critical frequency, secant of the angle of incidence on the D-layer, critical frequency of the sporadic-E layer f_oEs, and the sporadic-E layer blanketing frequency f_bEs; and the eight 3-hour magnetic index K_p values. Useful statistical parameters produced by DASCR3 that can describe the accuracy of the predicted field strength include the following: average residual (bias); root-mean-square residual (standard deviation); average relative residual (relative bias); root-mean-square relative residual; average absolute relative residual (magnitude of the error in the model); correlation coefficient between observed and predicted values; standard error of the estimate of linear regression; the constants necessary to represent the residual distribution by a Johnson probability distribution, and its corresponding test of fit information. DASCR3 usage will also allow the determination of possible improvements that might be made to these field strength prediction programs.

REFERENCES

AGARDograph No. 326, "Radio Wave Propagation Modeling, Prediction and Assessment," pp. 69–72, 1990

Barghausen, A. F., J. W. Finney, L. L. Proctor, and L. D. Schultz, "Predicting long-term operational parameters of high frequency sky-wave telecommunication systems," Environmental Science Administration Technical Report ERL 110–ITS 78, 1969

Beasley, J. D., and S. G. Springer, "Algorithm AS 111. The percentage points of the normal distribution," *Appl. Statist.*, vol. 26, pp. 118–121, 1977

Beckmann, B., "Bemerkungen zur abhängigkeit der empfangsfeldstärke von den grenzen des übertragungsfrequenzbereiches (MUF, LUF)," *Nachrichtentechnische Zeitschrift*, vol. 19, pp. 643–653, 1965

Beckmann, B., "Notes on the relationship between the receiving-end field strength and the limits of the transmission frequency range MUF, LUF," *NTZ-Commun. J.*, vol. 6, pp. 37–47, 1967

Bradley, P.A., "Focusing of radio waves reflected from the ionosphere at low angles of elevation," *Electron. Lett.*, vol. 6, pp. 457–458, 1970

Caruana, J., "IPS ionospheric propagation model," IPS Radio and Space Services, Sidney, Australia, Internal Report, Doc. No: IPS JC–92–01, 10 May 1993

CCIR XIth Plenary Assembly, Oslo, *CCIR Atlas of Ionospheric Characteristics; Report 340*, Geneva, ITU, 1967

CCIR XIIth Plenary Assembly, New Delhi, *CCIR interim method for estimating sky-wave field strength and transmission loss at frequencies between the approximate limits of 2 and 30 MHz; Report 252-2*, Geneva, ITU, 1970a

CCIR XIIth Plenary Assembly, New Delhi, *Supplement no. 1 to Report 340; CCIR. Atlas of Ionospheric Characteristics*, Geneva, ITU, 1970b

CCIR XIVth Plenary Assembly, Kyoto, *Second CCIR Computer-Based Interim Method for Estimating Sky-wave Field Strength and Transmission Loss at Frequencies Between 2 and 30 MHz; Supplement to Report 252-2, Geneva*, ITU, 1980

CCIR XVth Plenary Assembly, Geneva, "Propagation prediction methods for high frequency broadcasting; Report 894," *Propagation in Ionized Media, Recommendations and Reports of the CCIR*, 1982, vol. VI, Geneva, ITU, 1982

CCIR XVth Plenary Assembly, Geneva, *CCIR Atlas of Ionospheric Characteristics; Report 430-4*, Geneva, ITU, 1983

CCIR XVIth Plenary Assembly, Dubrovnik, "Simple HF propagation method for MUF and field strength; Report 894-1," *Propagation in Ionized Media, Recommendations and Reports of the CCIR*, 1986, vol. VI, Geneva, ITU, 1986

CCIR XVIIth Plenary Assembly, Düsseldorf, "CCIR HF propagation prediction method; Report 894-2," *Propagation in Ionized Media; Reports of the CCIR*, 1990, Annex to vol. VI, Geneva, ITU, 1990a

CCIR XVIIth Plenary Assembly, Düsseldorf, "Standardized procedure for comparing predicted and observed HF sky-wave signal intensities at frequencies above 1.6 MHz; Report 1150," *Propagation in Ionized Media; Reports of the CCIR*, 1990, Annex to vol. VI, Geneva,ITU, 1990b

CCIR, Geneva, *Improvements in the Propagation Prediction Method To Be Used for the HF Bands Allocated Exclusively to the Broadcasting Service; CCIR Report from Study Group 6 in Response to Recommendation no. 514 (HFBC-87)*, Geneva, ITU, 1991

Damboldt, T., "A comparison between the Deutsche Bundespost Ionospheric HF radio propagation predictions and measured field strength," AGARD Conf. Proc. no. 173 on Radio Systems and the Ionosphere, Athens, Greece 26–30 May 1976

Damboldt, T., and P. Suessmann, "The FTZ HF Propagation Model for use on small computers and its accuracy," AGARD Conf. Proc. no. 453 on Operational Decision Aids for Exploiting or Mitigating Electromagnetic Propagation Effects," 1989

Dodgson, J. M., and I. D. Hill, "A remark on algorithm 100: Normal-Johnson and Johnson-Normal transformations," *Appl. Statist.*, vol. 32, p. 345, 1983

Elkins, T. J., and C. M. Rush, "A statistical predictive model of the polar ionosphere," *Air Force Surveys in Geophys.*, no. 267, Air Force Geophysics Laboratory, pp. 1–100, 1973a

Elkins, T. J., and C. M. Rush, "A statistical predictive model of the polar ionosphere," An Empirical Model of the Polar Ionosphere, T. Elkins, Ed., Air Force Cambridge Research Laboratories Technical Report AFCRL-TR-73-0331, 1973b

Foppiano, A. J., "A new method for predicting the auroral absorption of HF sky waves," CCIR IWP 6/1 Docs. 3 and 10, 1975

Fox, M. W., "Improved empirical world maps of foF2 II. Validation and further refinements," IPS Radio and Space Services, Sidney, Australia, IPS-TR-88-07, 1988

Fox, M. W,. and L. F. McNamara, "Improved world maps of foF2 1. The method," IPS Radio and Space Services, Sidney, Australia, Technical Report IPS-TR-86-03, 1986

Fox, M. W., and L. F. McNamara, "Improved world-wide maps of monthly median foF2," *J. Atmos. Terr. Phys.*, vol. 50, pp. 1077–1086, 1988

George, P. L., "The global morphology of the quantity $\int N\nu.dh$ in the D- and E-regions of the ionosphere," *J. Atmos. Terr. Phys.*, vol. 33, pp. 1893–1906, 1971

George, P. L., and P. A. Bradley, "A new method of predicting the ionospheric absorption of high frequency waves at oblique incidence," *Telecommun. J.*, vol. 41, pp. 307–312, 1974

George, P. L., and P. A. Bradley, "Relationship between h.f. absorption at vertical and oblique incidence," *Proc. IEE*, vol. 120, pp. 1355–1361, 1973

Griffiths, P., and I. D. Hill, *Applied Statistics Algorithms*, Ellis Horwood Limited, London, 1st ed., 1985

Hahn, G. J., and S. S. Shapiro, *Statistical Models in Engineering*, John Wiley and Sons, New York, pp. 302–308, 1967

Hatfield, V. E., "HF communications predictions 1978 (an economical up-to-date computer code, AMBCOM)," Solar-Terrestrial Predictions Proceedings, vol. 4, 1980

Hatfield, V. E., and G. Smith, "AMBCOM USERS GUIDE FOR ENGINEERS," AF Contract F08606–85–C–0018, SRI International, January 1987

Hatfield, V. E., B. T. Bumbace, K. K. Bailey, and G. Smith, "AMBCOM user's guide for programmers," SRI International, 1987

Haydon, G. W., M. Leftin, and R. Rosich," Predicting the performance of high frequency skywave telecommunications systems (the use of the HFMUFES4 program)," Office of Telecommunications Sciences Report 76–102, 1976

Headrick, J., J. F. Thomason, D. L. Lucas, S. R. McCammon, R. A. Hanson, and J. L. Lloyd, "Virtual path tracing for HF radar including an ionospheric model", Naval Research Laboratory Report 2226, Mar 1971

Hill, I. D., "The normal integral," *Appl. Statist.*, vol. 22, pp. 424–427, 1973

Hill, I. D., "Algorithm AS 100: Normal-Johnson and Johnson-Normal transformations," *Appl. Statist.*, vol. 25, pp. 190–192, 1976

Hill, I. D., R. Hill, and R. L. Holder, "Fitting Johnson curves by moments," *Appl. Statist.*, vol. 25, pp. 180–189, 1976

Hill, I. D., and R. E. Wheeler, "A remark on algorithm AS 99: fitting Johnson curves by moments and AS 100: Normal-Johnson and Johnson-Normal transformations," *Appl. Statist.*, vol. 30, p 106, 1981

Hortenbach, K. J., and F. Rogler, "On the propagation of short waves over very long distances: predictions and observations," *Telecommun. J.*, vol. 46, pp. 320–327, 1979

International Communications Union (ITU), "World Administrative Radio Conference for the planning of the HF bands allocated to the broadcasting service," *Report to the Second Session of the Conf.*, General Secretariat of the ITU, 1984

Johnson, N. L., "Systems of frequency curves generated by methods of translation," *Biometrika*, vol. 36, pp. 149–176, 1949

Joint Technical Advisory Committee, "Radio transmission by ionospheric and tropospheric scatter, Pt. 1, Ionospheric scatter transmission," *IRE Proc.*, vol. 48, pp. 4–29, 1960

Jones, W. B., R. P. Graham, and M. Leftin, "Advances in ionospheric mapping by numerical methods," Environmental Science Services Administration Report ERL 107-ITS 75, 1969

Jones, W. B., and D. L. Obitts, "Global representation of annual and solar cycle variation of foF2 monthly median 1954-1958," Office of Telecommunications/Institute of for Telecommunication Sciences Research Report 3, 1970

Kolawole, L. B., "The transparency characteristics for Es types," *Radio Sci.*, vol. 13, pp. 159–165, 1978

Lane, G., F. J. Rhoads, and L. De Blasio, "Voice of American Coverage Analysis Program (VOACAP) A Guide to VOACAP," United States Information Agency, Bureau of Broadcasting/ Planning and Technology Assessment Division (B/ESA) Report 01–93, April 1933

Leftin, M., "Numerical representation of monthly median critical frequencies of the regular E-region (foE)," Office of Telecommunications Report 76-88, 1976

Leftin, M., S. M. Ostrow, and C. Preston, "Numerical maps of monthly median h'F, F2 for solar cycle minimum and maximum," Environmental Science Services Administration IERTM-ITSA 69, 1967

Leftin, M., S. M. Ostrow, and C. Preston, "Numerical maps of foEs for solar cycle minimum an maximum," Environmental Science Services Administration Report IERTM-ITSA 69, 1968

Levine, P. H., "MINIMUF: A semi-empirical model of Maximum Usable Frequencies in HF propagation," Megatek Report No. R2005–078–IF–1, 18 November 1976

Lloyd, J. L., and D. L. Lucas, "Estimating the Performance of telecommunication systems by using the Ionospheric Transmission Channel (IONACP)", U.S. Army Electromagnetic Office, Propagation Engineering Division, Technical Report, EMEO-PED-79-7, September 1978.

Lucas, D. L., and J. D. Harper, Jr., "A numerical representation of CCIR Report 322 high frequency [3-30 MC/S] atmospheric radio noise data," National Bureau of Standards Technical Note 318, 1965

Lucas, D. L., and G. W. Haydon, "Predicting the statistical performance indexes for high frequency ionospheric telecommunication systems," Environmental Science Services Administration Technical Report IER 1-ITSA-1, August 1966.

National Bureau of Standards, "Ionospheric Radio Propagation," Circular 462, 1948

Nielson, D. L., J. B. Lomax, and H. A. Turner, "The prediction of nuclear effects on HF communications," Stanford Research Institute Project 5481, Contract DA-49-146-XZ-436, Final Report, 1967

Norton, K. A. 1959. "System loss in radio wave propagation," *J. Res. National Bureau of Standards-D, Radio Propagation*, vol. 63D (July – August), no. 1, pp. 53–73.

Ord, J. K., *Families of Frequency Distributions*, Hafner Publishing Co., 1st ed., 1972

Phillips, M. L., "F-layer radio transmission on frequencies above the conventionally calculated MUF," Project EARMUFF (Engineering and Research Maximum Usable Frequencies), RCA Service Company Final Report, Data Analysis Contract DA-36-029-SC-72802, Appendix B, pp. 137–161, 1958

Phillips, M. L., "Auxiliary procedures used in theoretical evaluation of H-F backscatter observations and other communication problems," Electro-Physics Laboratories External Technical Memorandum No. E14, 1963

Rawer, K., *Die Ionosphäre*, P. Noordhoff, LTD., Groningen, Holland, 1982

Rawer, K., *The Ionosphere*, Frederick Ungar Publishing Co., New York, 1956

Rosich, R. K., and W. B. Jones, "The numerical representation of the critical frequency of the F1 region of the ionosphere," Office of Telecommunications Report 73-22, 1973

Roy, T. N., and D. B. Sailors, "HF maximum usable frequency (MUF) model uncertainty assessment," Naval Ocean Systems Center Technical Report 1184, 1987

Sailors, D. B., "An empirical model for the probability distribution of the lowest observed frequency," paper presented at the Ionospheric Effects Symposium on Radiowave Systems, Alexandria, VA, 14–16 April, 1981

Sailors, D. B., "Empirical models for the probability distribution of the residuals of the Advanced PROPHET models: MINIMUF-3.5, MINIMUF-85, QLOF Version 2.0, and FLDSTR," Naval Ocean Systems Center Technical Report 1190, 1987a

Sailors, D. B., "Empirical models representing the error in the predicted MUF and field strength from HFBC84," paper presented at the Ionospheric Effects Symposium on the Effect of the Ionosphere on Communication, Navigation, and Surveillance Systems, Springfield, VA, 5–7 May 1987b

Sailors, D. B., and W. K. Moision, "Quiet time lowest observable frequency model," Naval Ocean Systems Center Technical Report 1189, 1987

Sailors, D. B., W. K. Moision, and R. P. Brown, "Accuracy of high frequency maximum usable frequenies (MUF) prediction," Naval Ocean Systems Center Technical Report 695, 1981

Sailors, D. B., R. A. Sprague, and W. H. Rix, "MINIMUF-85: an improved HF MUF prediction algorithm," Naval Ocean Systems Center Technical Report 1121, 1986

Sailors, D. B., "A review of the history of field strength models in PROPHET," paper presented at the Ionospheric Effects Symposium on the Effect of the Ionosphere on Radiowave Signals and System Performance, Springfield, VA, 1–3 May 1990

Samuel, J. C., and P. A. Bradley, "A new form of representation of the diurnal and solar-cycle variations of ionospheric absorption," *J. Atmos. Terr. Phys.*, vol. 37, pp. 131–141, 1975

Schultz, L. D., and R. M. Gallet," A survey and analysis of normal ionospheric absorption measurements", Environmental Science Services Administration Professional Paper 4, 1970

Shimazaki, T., "World-wide variations in the height of the maximum electron density of the ionospheric F2 layer," *J. Radio Res. Labs., Japan*, vol. 2, pp. 85–97, 1955

Sinno, K., M. Kam, and Y. Kirukawa, "On the reflection and transmission losses for ionospheric radio-wave propagation via the sporadic E," *J. Radio Res. Labs., Japan*, vol. 23, pp. 65–84, 1976

Smith, G., and V. E. Hatfield, "AMBCOM User's Guide for Engineers," SRI International, 1987

Spaulding, A. D., and J. S. Washburn, "Atmospheric radio noise: worldwide levels and other characteristics," National Telecommunications and Information Administration Report 85-173, 1985

Sweeney, N., F. J. Rhoads, L. De Blasio, and G. Lane, "Voice of America Coverage Analysis Program A users guide for VOACAP," United States Information Agency, Bureau of Broadcasting/Planning and Technology Assessment Division (B/ESA) Report 02-93, April 1993

Systems Exploration, Inc., "Sounder update and field strength software modifications for special Operations Radio Frequency Management System (SORFMS)," Naval Ocean Systems Center Technical Document 1848, 1990

Teters, L. R., J. L. Lloyd, G. W. Haydon, and D. L. Lucas," Estimating the performance of telecommunications systems by using the ionospheric transmission channel - Ionospheric Communications Analysis and Predictions (IONCAP) program user's manual, " National Telecommunication and Information Administration Report 83-127, 1983.

Turner, J. F., "The development of the ionospheric index T," Ionospheric Prediction Service, Sydney, Australia, Report IPS-R11, 1968

Vondrak, R. R., G. Smith, V. E. Hatfield, R. T. Tsunoda, V. R. Frank, and P. O. Perreault, "Chatanika model of the high-latitude ionosphere for application to HF propagation prediction," SRI International Final Report RADC-TR-768-7, Contract F19628-77-C-0102, 1978

Wakai, N., "Non-deviative absorption at night," *J. Radio Res. Labs., Japan*, vol. 8, pp. 213–218, 1961

Wakai, N, "Nomogram for easy readout of the night-time absorption," CCIR IWP 6/1 Doc. 12, 1975

Wakai, N., "Ray paths and absorption of MF and HF radio waves incident on the nighttime ionosphere," *J. Radio Res. Labs., Japan*, vol. 18, pp. 191–206, 1971

Wakai, N., M. Ose, and K. Tanohata, "Solar control of HF radio wave absorption in the nighttime," *J. Radio Res. Labs., Japan*, vol. 18, pp. 1–17, 1971

Westover, D. E., and L. A. Roben, "Adaption of the Kift–Fooks ionospheric ray-tracing technique to a high-speed digital computer," Stanford University SEL Report No. 63-103, 1963

Wheeler, J. L., "Transmission loss for ionospheric propagation above the standard MUF," *Radio Sci.*, vol. 1, pp. 1303–1308, 1966

Williams, C.A., Jr., "On the choice of the number and width of classes for the chi-square test of goodness of fit," *J. Am. Sta. Assn.*, vol. 45, pp. 77–86, 1950

Wright, J. W., and R. E. McDuffie, "The relation of h_{max} F2 to M(3000)F2 and h_tF2," *J. Radio Res. Labs., Japan*, vol. 7, pp. 409–420, 1960

Zacharisen, D. H., " Numerical mapping of the continents for use in high frequency skywave radio predictions," Office of Telecommunications Research, Engineering Report 31, 1972

Zacharisen, D. H., and E. L.Crow," Fitting distributions of telecommunication variables with chi-squared distribution," *Radio Sci.*, vol. 5, pp. 1307–1315, 1970

Zacharisen, D. H., and W. B. Jones," World maps of atmospheric radio noise in universal time," Institute for Telecommunication Sciences Research Report 2, 1970

REPORT DOCUMENTATION PAGE

Form Approved
OMB No. 0704-0188

1. AGENCY USE ONLY (Leave blank)	2. REPORT DATE	3. REPORT TYPE AND DATES COVERED
	September 1993	Final: Mar – Jun 1993

4. TITLE AND SUBTITLE
HF SKY-WAVE FIELD STRENGTH PREDICTIONS

5. FUNDING NUMBERS
ACN: DN302027
PE: 0603013N
PN: R1947

6. AUTHOR(S)
D. B. Sailors, R. B. Rose

7. PERFORMING ORGANIZATION NAME(S) AND ADDRESS(ES)
Naval Command, Control and Ocean Surveillance Center (NCCOSC),
RDT&E Division
San Diego, CA 92152–5001

8. PERFORMING ORGANIZATION REPORT NUMBER
TR 1624

9. SPONSORING/MONITORING AGENCY NAME(S) AND ADDRESS(ES)
Naval Security Group Command
Code 391006
3801 Nebraska Ave., N.W.
Washington, DC 20390

10. SPONSORING/MONITORING AGENCY REPORT NUMBER

11. SUPPLEMENTARY NOTES

12a. DISTRIBUTION/AVAILABILITY STATEMENT
Authorized for public release; distribution is unlimited.

12b. DISTRIBUTION CODE

13. ABSTRACT (Maximum 200 words)

A description is given on how the field strength of an HF signal, expressed in decibels (dB) above or below 1 microvolt per meter reference, is calculated by seven different HF propagation prediction programs, and on how the accuracy of the predicted field strength values from these programs can be determined and presented. These seven programs include three empirical based programs (Medusa PROPHET, FTZ, and FTZ4), and four analytical programs (HFTDA, IONCAP, ASAPS, and AMBCOM). AMBCOM is the only ray tracing program included. All of these prediction programs produce median predictions of the rms field strength.

The accuracy of these seven programs will be determined for the Polar, Equatorial Near vertical incidence Experiment (PENEX) Project. A data screening program, DASCR3, will be used to assess the accuracy of these programs. DASCR3 allows the development and generation of powerful statistical descriptions of the characteristics of the measured field strength and of how well the candidate programs predict the observations. Useful statistical parameters for describing the accuracy of the programs are given. DASCR3's ability to allow and store up to 40 different auxiliary variables permits comparisons to be subdivided into many subcategories. Recommendations for these subcategories for the field strength accuracy study are given. DASCR3 also allows the determination of improvements that might possibly be made to these field strength prediction programs.

14. SUBJECT TERMS
Propagation
Expert Systems
High Frequency
Propagation Forecast
PROPHET

15. NUMBER OF PAGES
80

16. PRICE CODE

17. SECURITY CLASSIFICATION OF REPORT	18. SECURITY CLASSIFICATION OF THIS PAGE	19. SECURITY CLASSIFICATION OF ABSTRACT	20. LIMITATION OF ABSTRACT
UNCLASSIFIED	UNCLASSIFIED	UNCLASSIFIED	SAME AS REPORT

21a. NAME OF RESPONSIBLE INDIVIDUAL	21b. TELEPHONE (Include Area Code)	21c. OFFICE SYMBOL
D. B. Sailors	(619) 553-3063	Code 542

INITIAL DISTRIBUTION

Code 0012	Patent Counsel	(1)
Code 02712	Archive/Stock	(6)
Code 0274B	Library	(2)
Code 54	J. H. Richter	(1)
Code 542	J. A. Ferguson	(10)
Code 542	D. B. Sailors	(20)
Code 542	W. K. Moision	(1)
Code 542	R. Rose	(1)
Code 542	R. A. Sprague	(1)
Code 772	J. A. Audia	(1)
Code 772	W. S. Bratt	(1)
Code 772	B. J. Satterlee	(1)
Code 833	G. Crane	(2)

Defense Technical Information Center
Alexandria, VA 22304–6145 (4)

NCCOSC Washington Liaison Office
Washington, DC 20363–5100

Center for Naval Analyses
Alexandria, VA 22302–0268

Navy Acquisition, Research and Development Information Center (NARDIC)
Arlington, VA 22244–5114

GIDEP Operations Center
Corona, CA 91718–8000

NCCOSC Division Detachment
Warminster, PA 18974–5000

Chief of Naval Operations
Washington, DC 20350–2000

Naval Research Laboratory
Washington, DC 20375–5320

Naval Security Agency
Ft. Meade, MD 20755 (3)

Naval Security Group Command
Washington, DC 20393–5100 (3)

Naval Computer & Telecommunications Command
Washington, DC 20390

Electromagnetic Compatibility Analysis Center
Annapolis, MD 21402–1187 (3)

Institute for Telecommunications Sciences
Boulder, CO 80303–3328 (3)

National Telecommunications & Information Administration
Annapolis, MD 21401

Naval Postgraduate School
Monterey, CA 93943–5100

USA Electronic Proving Ground
Fort Huachuca, AZ 85613–7110 (2)

Los Alamos National Laboratory
Los Alamos, NM 87545

CECOM
Fort Monmouth, NJ 07703 (3)

Voice of America
Washington, DC 20003 (2)

Lucas Consulting
Boulder, CO 80301

Hunsacker Consulting
Fairbanks, AK 99709

Southwest Research Institute
San Antonio, TX 78284

SRI International
Arlington, VA 22209